1997

Synthesis and characterization of novel Group VI metal (Mo, W) nitride and oxide compounds

Zhihong Zhang
Iowa State University

INFORMATION TO USERS

This manuscript has been reproduced from the microfilm master. UMI films the text directly from the original or copy submitted. Thus, some thesis and dissertation copies are in typewriter face, while others may be from any type of computer printer.

The quality of this reproduction is dependent upon the quality of the copy submitted. Broken or indistinct print, colored or poor quality illustrations and photographs, print bleedthrough, substandard margins, and improper alignment can adversely affect reproduction.

In the unlikely event that the author did not send UMI a complete manuscript and there are missing pages, these will be noted. Also, if unauthorized copyright material had to be removed, a note will indicate the deletion.

Oversize materials (e.g., maps, drawings, charts) are reproduced by sectioning the original, beginning at the upper left-hand corner and continuing from left to right in equal sections with small overlaps. Each original is also photographed in one exposure and is included in reduced form at the back of the book.

Photographs included in the original manuscript have been reproduced xerographically in this copy. Higher quality 6" x 9" black and white photographic prints are available for any photographs or illustrations appearing in this copy for an additional charge. Contact UMI directly to order.

UMI

A Bell & Howell Information Company
300 North Zeeb Road, Ann Arbor MI 48106-1346 USA
313/761-4700 800/521-0600

Synthesis and characterization of novel Group VI metal (Mo, W) nitride and oxide compounds

by

Zhihong Zhang

A dissertation submitted to the graduate faculty

in a partial fulfillment of the requirements for the degree of

DOCTOR OF PHILOSOPHY

Major: Inorganic Chemistry

Major Professor: Robert E. McCarley

Iowa State University

Ames, Iowa

1997

Graduate College
Iowa State University

This is to certify that the Doctoral dissertation of

Zhihong Zhang

has met the dissertation requirements of Iowa State University

Signature was redacted for privacy.

Major Professor

Signature was redacted for privacy.

For the Major Program

Signature was redacted for privacy.

For the Graduate College

TABLE OF CONTENTS

LIST OF FIGURES

GENERAL INTRODUCTION

CHAPTER 1.

CHAPTER 2.

CHAPTER 3.

CHAPTER 4.

APPENDIX C.

LIST OF TABLES

CHAPTER 3.

CHAPTER 4.

APPENDIX A.

APPENDIX B.

APPENDIX D.

GENERAL INTRODUCTION

Group VI metal compounds have been the subject of much research since the discovery of the elements. Applications of these compounds vary widely from use in the alloying of steel[1] and as refractory materials (*e.g.*, WC for cutting tools and Mo_2Si for resistance heaters) to the iron-molybdenum cofactor in nitrogenase and endogenous tungsten in bacterial enzymes.[2] The many applications and uses of molybdenum and tungsten materials and their relative availability (1.2 ppm in the earth's crust) make them ideal candidates for scientific inquiry. This dissertation focuses on two areas of research on the chemistry of these two elements, the binary tungsten nitrides and the reduced molybdenum oxide compounds.

Group VI Metal (Mo, W) Nitrides

Traditional methods of preparing solid state materials required high temperatures in order to obtain diffusion rates necessary for the completion of the reactions. Thus, the number and types of compounds that can be prepared were restricted. This is especially true for the syntheses of materials which are thermodynamically less favorable at high temperatures. Therefore, "turning down the heat"[3] has become a popular topic in current solid state research. Many new technologies involving low temperature reactions (with respect to the traditional high temperature solid state

reactions), including flux,[4] hydrothermal,[5] intercalation,[6] and molecular precursor methods,[7] have been developed.

Transition metal nitrides possess free energies of formation that are dramatically less favorable than the corresponding oxides, principally because of the tremendous strength of the N≡N bond (227 kcal mol^{-1}) relative to O=O (119 kcal mol^{-1}). As a consequence, the preparation of transition metal nitrides is often entropically disfavored at high temperatures, and the number and types of transition metal nitrides are much less than that of the oxides.

An examination of the Group VI elements indicates a paucity of binary nitrides prepared by the traditional high temperature synthetic techniques, even though a number of ternary Group VI metal nitride compounds have been discovered.[8-14] Thermodynamic studies on Mo_2N by Lyutaya and Lakhtin demonstrated that the Gibbs free energy change for the formation of Mo_2N increased with the increase of temperature.[15-16] Table 1 lists some known and possible binary Group VI metal nitrides. Although considerable synthetic efforts have been devoted to preparing these nitride compounds, the structures and properties of these nitrides have remained elusive.[17-18] Only two types of Group VI metal nitrides were observed as bulk solid phases, MN and M_2N (M = Mo, W), with the metals in their lower oxidation states. Other phases are either unknown or prepared as thin films and observed only with electron microscopy. No bulk phases of Group VI metal nitrides with the metals in

Table 1. Some known and possible binary Group VI metal nitrides

Nitride	Example	Preparation	Structure
M_2N	Mo_2N, W_2N	M + NH_3 (800°C)	metal fcc, N random
M_3N_2	unknown		
MN	MoN, WN	M + NH_3 (700°C)	WC-hexagonal or hexagonal superlattice
M_4N_5	unknown		
M_3N_4	unknown		
M_2N_3	Mo_2N_3, W_2N_3		thin film-hexagonal
M_3N_5	W_3N_5		thin film-hexagonal
M_4N_7	unknown		
MN_2	WN_2		thin film-trigonal

oxidation states higher than III have ever been reported. WN_2, for example, was only observed as a brown coating on W filaments.[19] Mo_2N_3, which was prepared by the chemical vapor deposition (CVD) of $Mo(NMe_2)_4$ in ammonia gas, was also observed as a thin film.[20]

The bulk solid phases of the molybdenum and tungsten nitrides, MN and M_2N (M = Mo, W) with the metals in oxidation states lower than III, were prepared by flowing

NH_3 over the metals at high temperature. The mononitrides were reported to have the hexagonal WC structure. In the structures of M_2N, the metals were reported to be fcc close packed, where the nitrogen atoms are randomly located in octahedral interstitial positions.[21]

Since the problems in traditional synthetic methodologies have limited the number and types of transition metal nitride compounds, new synthetic techniques of converting molecular precursors to the target products under more gentle conditions have been explored.[7] Parkin and co-workers attempted to convert metal halides to nitrides, which was successful for most early transition metals, but not for the Group VI metals.[22] They attempted to convert $MoCl_3$ and WCl_4 to the nitrides by reaction with magnesium or calcium nitride at 500 °C. However, only the metals were obtained.

Similarly, our synthetic strategy to produce binary Group VI metal nitrides involved the conversion of molecular precursors to the metal nitrides. However, our preferred molecular precursors are $MNCl_3$ (M = Mo, W), which can be prepared from the reaction of trimethylsilyl azide with $MoCl_5$ or WCl_6 in 1,1-dichloromethane or 1,2-dichloroethane, respectively. $MNCl_3$ represents a potential intermediate to the desired products MN_x ($x \geq 1$). Through metathesis or redox reactions, Cl atoms could be replaced by other ligands, such as N_3^-, N_2^{4-}, and N^{3-}, or removed by reduction reactions.

In this dissertation, new molecular precursors to tungsten nitrides are reported. Several new tungsten nitrides and carbide nitrides with novel structures, which were synthesized by metathetical reactions in a flux, thermal decomposition of the molecular precursors at relatively low temperatures, or by chemical vapor transport reactions, will be reported as well.

Ternary Reduced Molybdenum Oxides

Since the discovery of the reduced molybdenum oxide, $NaMo_4O_6$,[23] containing trans-edge-shared Mo_6 octahedra (Figure 1), ternary reduced molybdenum oxides have been studied extensively. A large number of compounds have been synthesized which contain various kinds of condensed Mo metal clusters.[24] Over the past several years, ternary reduced rare-earth molybdenum oxides have caused great interest, because these compounds may possess interesting electrical and magnetic properties. Many compounds have been discovered in this area, and most of them have been structurally characterized.[25-32]

One interesting family of ternary reduced rare-earth molybdenum oxides is the group of compounds containing Mo_8 bicapped octahedra. The Mo_8 bicapped octahedra could have three structural isomers (cis-, meta-, and trans-), which are shown in Figure 2. This structural feature may lead to an interesting crystal structure chemistry, because any combination of these isomers would generate a new crystal

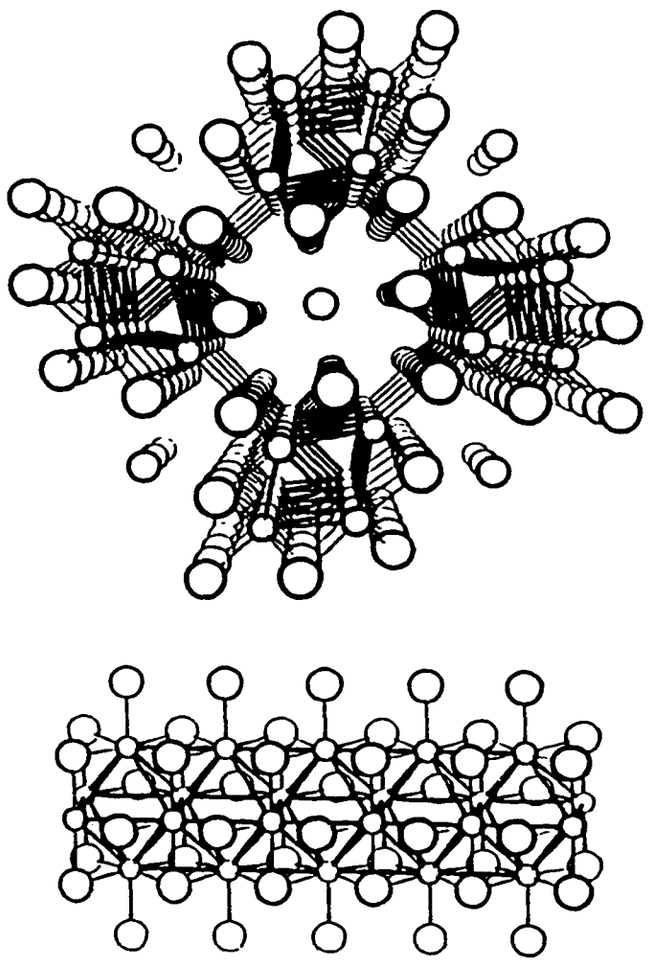

Figure 1. The structure of $NaMo_4O_6$ viewed down the tetragonal c axis and a segment of a single chain of trans-edge-shared Mo_6O_{12}-type clusters extended parallel to the c axis.

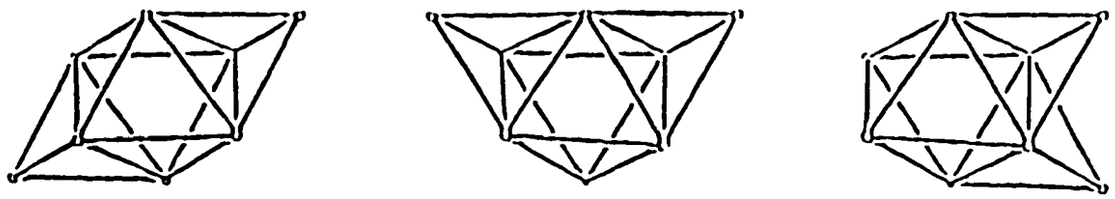

Trans- Meta- Cis-

Figure 2. The three structural isomers of Mo_8 bicapped octahedra.

structure type.

The first compound containing Mo_8 bicapped octahedra was synthesized by electrolysis in 1990.[33] This compound has a non-stoichiometric formula, $LaMo_{7.7}O_{14}$, and contains only cis-bicapped Mo_8 octahedra, in which the face-capping positions are only 85% occupied by the Mo atoms. Subsequently, a stoichiometric compound, $NdMo_8O_{14}$,[34] was discovered, in which the face-capping positions are fully occupied. These compounds exhibit paramagnetic behavior over the temperature range of 100-300K, and metallic character at room temperature.[35-36]

More recently, the $CeMo_8O_{14}$[37] and $PrMo_8O_{14}$[38] compounds, which contain 1:1 and 2:1 ratios of cis- to trans-bicapped Mo_8 octahedra, respectively, have been

prepared at extremely high temperatures by P. Gougeon and coworkers.

In this work, the $LnMo_8O_{14}$ compounds (Ln = rare-earth) containing Mo_8 bicapped octahedra have been systematically studied. The synthetic conditions, X-ray powder diffraction, single crystal structure determinations, electronic structure calculations, and properties of these interesting compounds will be discussed.

Dissertation Organization

This dissertation consists of four papers. Each paper is formatted for publication in a technical journal and the cited references are found at the end of each paper. GENERAL CONCLUSIONS follow the four papers. The references cited in the GENERAL INTRODUCTION are found at the end of the dissertation.

CHAPTER 1. SYNTHESIS, STRUCTURE, AND REACTIVITY OF THE MOLECULAR PRECURSOR $[WNCl_3 \cdot NCCH_3]_4 \cdot 2NCCH_3$

A paper to be submitted to Inorganic Chemistry

Zhihong Zhang and Robert E. McCarley

Abstract

An acetonitrile adduct of $WNCl_3$, $[WNCl_3 \cdot NCCH_3]_4 \cdot 2CH_3CN$, has been prepared from an acetonitrile solution of $WNCl_3$ at room temperature. The red-orange compound crystallizes in the triclinic space group $P\bar{1}$ with crystallographic data, a = 9.066(3) Å, b = 9.745(4) Å, c = 11.910(4) Å, α = 95.78(3)°, β = 108.82(3)°, γ = 109.93(3)°, V = 909(1) Å^3, Z = 1, R = 0.020, and Rw = 0.021. The molecular structure of $[WNCl_3 \cdot NCCH_3]_4$ consists of a W_4N_4 tetrameric core. Two significantly different types of W-N bonds are found. One can be assigned as a W≡N multiple bond with an average bond length of 1.705(5) Å. The other type can be designated as a W-N single bond with an average bond length of 2.075(5) Å. The IR spectrum of the tetramer shows strong W≡N stretching bands in the range of 1028-1075 cm^{-1}. $[WNCl_3 \cdot NCCH_3]_4 \cdot 2CH_3CN$ also reacts with solvent CH_3CN at reflux (81 °C). The dark blue amorphous product has a composition of $W(NH)Cl_3(CH_3CN)_2$, and is

soluble in acetonitrile. The tungsten atoms in $[WNCl_3 \cdot NCCH_3]_4 \cdot 2CH_3CN$ were reduced from VI to V during the reaction. The reduction was confirmed by oxidation state determinations, ESR, and magnetic susceptibility measurements.

Introduction

One fundamental objective of this research was to synthesize molecular precursors that could be converted to the desired high oxidation state metal nitrides of tungsten. $WNCl_3$ represents a potential intermediate to the desired products. For example, WN_2, which is a hypothetical compound, could be prepared by replacing three Cl^- anions with one N^{3-} anion.

$WNCl_3$ was initially prepared by K. Dehnicke and coworkers via the reaction of WCl_6 and chlorine azide (ClN_3) in CCl_4 at 30°C.[1] More recent studies have shown that ClN_3 can be replaced by trimethylsilyl azide and tris(trimethylsilyl)amine as nitriding reagents for the formation of $WNCl_3$.[2-4] The reaction of $W(CO)_6$ with ClN_3 in CCl_4 also provided a very efficient synthesis of $WNCl_3$.[5]

$WNCl_3$ was initially characterized by infrared spectroscopy, X-ray powder diffraction, and elemental analyses. Since then, the crystal structure of related compounds such as $[WNCl_3 \cdot OPCl_3]_4 \cdot 2OPCl_3$,[6] $[WNCl_3 \cdot 0.5HN_3]_4$,[7] and $[WNCl_3 \cdot NCPh]_4 \cdot 3CH_2Cl_2$,[8] which consist of molecular tetramers with multiple and

single W-N bonds arranged in an alternating fashion, have been characterized by single crystal X-ray diffraction methods. The crystal structure of $WNCl_3$ as a compound uncoordinated by other ligands was not reported in the literature until a tetrameric form was characterized by M. Close and R. E. McCarley using single crystal X-ray diffraction methods.[9]

In order to increase the utility of $WNCl_3$ as a soluble molecular precursor to tungsten nitrides, an acetonitrile adduct of $WNCl_3$ was prepared from acetonitrile solution, and characterized structurally by single crystal X-ray diffraction methods. In this section, the synthesis, structure, and reactivity of this $WNCl_3$-acetonitrile adduct will be discussed.

Experimental

Materials

The reagents are air and moisture sensitive. Therefore, all manipulations were performed under inert-atmosphere conditions using standard drybox, high vacuum manifold, and Schlenk techniques. Acetonitrile (MeCN) and 1,2-dichloroethane (DCE) were dried by standard methods using CaH_2 as a drying reagent. Tungsten hexachloride was obtained from Alfa Chemical Co. and sublimed under dynamic

vacuum at 120-160°C to remove the more volatile $WOCl_4$ impurity. Trimethylsilyl azide (TMSA) was obtained from Aldrich Chemical Co. and used as received.

Analytical Procedures

Tungsten analysis

Gravimetric determination of W was accomplished by conversion of samples to the trioxide via addition of an oxidizing solution in a tared crucible. Samples were initially treated with dilute (3M) nitric acid and then with concentrated nitric acid. The crucibles were gently heated (~100 °C) on a hot plate to slowly evaporate the solution. Once the solution was evaporated, the temperature of the hot plate was increased (~150 °C), and the crucibles were heated at this temperature until the samples became yellow. The crucibles were heated at 800 °C in a muffle furnace until constant weights were achieved.

Chlorine analysis

Chlorine was determined by the potentiometric titration of neutralized solutions of dissolved sample with a standardized $AgNO_3$ solution. Ag/AgCl was used as the working electrode and a silver electrode as the reference. Samples were dissolved in a basic solution (KOH) with 30 % H_2O_2, and gently heated on a hot plate. The clear

solutions were then neutralized with 3N nitric acid to pH ~ 6-7, and then titrated.

Nitrogen, carbon, and hydrogen analysis

The nitrogen, carbon, and hydrogen analyses were obtained from Galbraith Laboratories, Inc. and the ISU Chemistry Department Instrument Services.

Oxidation state analysis

A sample was dissolved in dilute NaOH solution under N_2 flow and then 6 M sulfuric acid was used to adjust the pH to 2. The Ce(IV) solution, which was prepared by dissolving reagent grade ammonium hexanitritocerate(IV) in 0.18 M sulfuric acid,[10] was added immediately. The solution was allowed to stand for 24 hours in an inert atmosphere glove bag. (It is better to directly dissolve the sample in Ce(IV) solution to avoid the oxidation of the sample by other oxidizing reagents, for example, oxygen. For this specific case, however, the sample was not soluble in the Ce(IV) solution, and the oxidation of tungsten took quite a long time. Thus the procedure described above was applicable.) A quantitative amount of freshly standardized Fe(II) ammonium sulfate solution was added to react with the excess Ce(IV). Titration of the excess Fe(II) with the cerium ammonium nitrate solution was then performed with a calomel reference electrode and a Pt indicating electrode.

Physical Measurements

Infrared spectroscopy

Infrared spectra were obtained on a Bomem MB-Series Fourier transform infrared spectrometer. The samples were prepared as Nujol mulls and pressed between CsI plates. The spectra were recorded in the range of 4000 to 185 cm^{-1}.

ESR spectroscopy

ESR spectra were obtained on a Bruker ER-200D X-band spectrometer. The samples were prepared by sealing 50 mg of material in a quartz tube (3mm ID, 4mm OD, and 28mm L) under dynamic vacuum. The spectra were recorded in the field range of 2000-5000 G at 9.49 x 10^9 Hz and 120 K.

Magnetic susceptibility measurements

Magnetic susceptibility was measured with a Quantum Design SQUID magnetosusceptometer. The samples were prepared by sealing 20-50 mg of material between two quartz rods (2.8-2.9mm D) in a quartz tube (3mm ID, 4mm OD, and 17mm L) under a helium atmosphere (less than 0.1 torr). The data were collected in the temperature range of 6-300 K at 3 tesla.

Synthetic Procedures

Preparation of $WNCl_3$

In a typical preparation, a solution of DCE (80 mL) and TMSA (9.68 mL, 70 mmol) was added dropwise (approximately 4 drops/s) to a refluxing solution of WCl_6 (28.0 g, 70 mmol) in DCE (270 mL). The mixture was refluxed for 2 days, and the solution color changed from dark purple to light purple, and a bright orange solid precipitated. The bright orange solid was isolated by filtration and purified by extraction with DCE to remove any unreacted WCl_6 and soluble silane. The solid was then dried under dynamic vacuum for a period of not less than 12 hours and isolated in a dry box. Then, the solid was heated at 160 °C under dynamic vacuum to remove the coordinated DCE. A typical yield was 15.0 g (70%). IR (Nujol, cm^{-1}): υ(W≡N), 1082 s, 1062 sh; υ(W-Cl), 389 sh, 378 s, 361 s, 356 sh, 331 s, 309 s. Anal. Calcd for $WNCl_3$: W, 60.43%; Cl, 34.96%; Cl:W, 3.00:1. Found: W, 60.32%; Cl, 34.60%; Cl:W, 2.99:1.

Preparation of $[WNCl_3 \cdot NCCH_3]_4 \cdot 2NCCH_3$

$WNCl_3$ (0.5 g) was loaded into a Pyrex tube in a drybox, and the tube sealed under dynamic vacuum. The bright orange sample was heated at 160-200 °C for 24 hours, and a brown solid was obtained. Extraction of the solid with CH_3CN gave a deep orange solution. The solution was allowed to stand at room temperature for 1

week, and orange single crystals were obtained. IR (Nujol, cm^{-1}): $\upsilon(N\equiv C)$, 2309 m, 2281 m; $\upsilon(W\equiv N)$, 1075 s. 1028 sh; υ(out-of-plane C-H bending), 936 s; υ(W-Cl), 378 sh, 357 s, 329 s.

Reaction of $[WNCl_3 \cdot NCCH_3]_4 \cdot 2CH_3CN$ with solvent CH_3CN

$WNCl_3$ (0.1 g) was loaded into a 100 mL reaction flask in a drybox, and ~60 mL of CH_3CN was then distilled onto the solid. A deep orange solution initially formed. The solution was heated to reflux under flowing N_2 for 2 days. A dark solution was then obtained. By removing solvent and drying under dynamic vacuum, a dark blue amorphous solid was produced. IR (Nujol, cm^{-1}): $\upsilon(N\equiv C)$, 2304 m, 2279 m ; υ(N-H), 3199; υ(W-Cl), 316 s. Anal. Calcd for $W(NH)Cl_3(CH_3CN)_2$: W, 47.48%; Cl, 27.47%; N, 10.85%; C, 12.40%; H, 1.81%. Found: W, 47.30%; Cl, 28.06%; N, 10.82%; C, 12.35%; H, 1.54%; Cl:W, 3.08:1; N:W, 3.00:1; C:W, 4.00:1; C:N, 1.33:1.

X-ray Structure Determination

A suitable orange single crystal with dimensions of 0.10 x 0.06 x 0.20 mm^3 was selected from material still in contact with the mother solution. The crystal was then encased in epoxy resin while in a glove bag under a nitrogen flow, attached to the tip of a glass fiber, and sealed in a glass capillary. All measurements were made on a Rigaku AFC6R diffractometer using graphite monochromated Mo Kα (λ = 0.71069

Å) radiation and a 12 kW rotating anode generator.

Cell constants and an orientation matrix for data collection were obtained from a least-squares refinement using the setting angles of 22 carefully centered reflections in the range $4.0 < 2\theta < 35.0$, and corresponded to a triclinic cell with dimensions: a = 9.066(3) Å, b = 9.745(4) Å, c = 11.910(4) Å, α = 95.78(3)°, β = 108.82(3)°, γ = 109.93(3)°, and V = 909(1) Å^3. The data were collected at -65 °C using the ω-2θ scan technique over the range $4° < 2\theta < 50°$ in the hemisphere ($\pm h$, $+k$, $\pm l$). Three standard reflections were monitored every 150 reflections and showed no intensity variation over the collection period. A total of 3436 reflections were collected, of which 3228 were unique (R_{int} = 0.026) and 2562 of which were observed with $I > 3.00\sigma(I)$. No Decay correction was applied. With an absorption coefficient for Mo Kα radiation of μ = 135.21 cm^{-1}, an empirical absorption correction using the ψ scan technique was applied after the structure solution. The data were corrected for Lorentz and polarization effects.

The triclinic space group was $P\bar{1}$ (#2) was chosen on the basis of systematic absences and intensity statistics. The structure was solved by the SHELXS direct methods[11a] which yielded the positions of the tungsten atoms. Successive Fourier electron difference maps yielded the positions of the chlorine, nitrogen and carbon atoms. The structure was then refined by full-matrix least-squares methods with anisotropic thermal parameters on all non-hydrogen atoms. Idealized hydrogen

positions were calculated and placed in the refinement with C-H distances equal to 1.04 Å, but their parameters were held constant during the subsequent cycles. The final cycle of full-matrix least-squares refinement was based on 2562 observed reflections and 172 variable parameters and converged with unweighted and weighted agreement factors of $R = 0.020$ and $Rw = 0.021$, respectively. The asymmetric unit was found to be $[WNCl_3 \cdot NCCH_3]_2 \cdot CH_3CN$. All calculations were performed using the TEXSAN[11b] crystallographic software package of Molecular Structure Corporation. The crystallographic data and refinement results are given in Table 1, and the positional parameters and isotropic equivalent temperature factors are given in Table 2. The anisotropic temperature factors are listed in Table 3.

Results and Discussion

Synthesis of $[WNCl_3 \cdot NCCH_3]_4 \cdot 2CH_3CN$

$WNCl_3$ may exist in two different solid state forms, namely, a polymeric form $[WNCl_3]_n$, and a tetrameric form $[WNCl_3]_4$. The $WNCl_3$ obtained from the reaction between WCl_6 and $(CH_3)_3SiN_3$ in dichloroethane at reflux may be the polymer $[WNCl_3]_n$, because this bright orange solid is not soluble in acetonitrile. However, when the bright orange solid was heated at 160-200°C in a sealed Pyrex tube, a deep

Table 1. Crystallographic data for $[WNCl_3 \cdot NCCH_3]_4 \cdot 2CH_3CN$

Empirical Formula	$C_{12}Cl_{12}H_{18}N_{10}W_4$
Formula Weight	1463.18
Crystal Size	0.10 x 0.06 x 0.20 mm^3
Crystal System	triclinic
Space Group	P1 (#2)
Lattice Parameters	a = 9.066(3) Å
	b = 9.745(4) Å
	c = 11.910(4) Å
	α = 95.78(3)°
	β = 108.82(3)°
	γ = 109.93(3)°
Volume	909(1) $Å^3$
Z Value	1
Calculated Density	2.671 g/cm^3
F_{000}	660.00
μ(MoKα)	135.21 cm^{-1}
Diffractometer	Rigaku AFC6R
Radiation	MoKα (λ = 0.71069Å)
Temperature	-65.0 °C
Two-theta Range	0-50°
Scan Mode	ω-2θ
No. of Reflections Collected	3228
No. Observations (I > 3.00σ(I))	2562
No. Variables	172
Max Shift/error in Final Cycle	0.00
Goodness of Fit[a]	1.39
Max. and Min. Peaks in the Final Diff. Map	0.73, -0.91 $e^-/Å^3$
Residuals[b]	R = 0.020, Rw = 0.021

[a] Goodness of Fit = $[\Sigma\omega\{|F_o| - |F_c|\}^2/\{N_{obs} - N_{parameters}\}]^{1/2}$

[b] $R = \Sigma \; | \; |Fo| - |Fc| \; | \; / \; \Sigma \; |Fo|$; $Rw = [(\Sigma \; w \; (|Fo| - |Fc|)^2 \; / \; \Sigma \; w \; Fo^2 \;)]^{1/2}$.

Table 2. Atomic coordinates and equivalent isotropic thermal parameters ($Å^2$) of the non-hydrogen atoms for $[WNCl_3 \cdot NCCH_3]_4 \cdot 2CH_3CN$

atom	x	y	z	B_{eq} [a]
W(1)	0.26657(3)	0.99225(3)	-0.20845(2)	1.270(6)
W(2)	0.25493(3)	0.82092(3)	0.08013(2)	1.151(6)
Cl(1)	0.3099(2)	0.7975(2)	-0.3026(2)	2.52(4)
Cl(2)	0.2864(2)	1.2287(2)	-0.1331(2)	2.58(4)
Cl(3)	-0.0094(2)	0.9141(3)	-0.3425(2)	3.19(5)
Cl(4)	0.2504(2)	0.6178(2)	-0.0608(2)	2.25(4)
Cl(5)	0.1897(2)	1.0123(2)	0.1310(2)	2.17(4)
Cl(6)	0.1968(2)	0.6933(2)	0.2049(2)	2.42(4)
N(1)	0.2431(6)	0.9133(6)	-0.0908(5)	1.2(1)
N(2)	0.5295(6)	1.0920(6)	-0.1319(5)	1.4(1)
N(3)	0.3377(8)	1.1013(8)	-0.3608(6)	2.6(2)
N(4)	-0.0374(7)	0.7075(6)	-0.0538(6)	1.9(1)
N(5)	0.289(1)	0.4577(10)	0.537(1)	6.8(3)
C(1)	0.3902(9)	1.1494(9)	-0.4286(7)	2.3(2)
C(2)	0.456(1)	1.205(1)	-0.5181(8)	3.7(2)
C(3)	-0.1764(9)	0.6584(8)	-0.1081(7)	2.0(2)
C(4)	-0.3618(10)	0.5909(10)	-0.1796(9)	3.9(2)
C(5)	0.186(1)	0.415(1)	0.5704(10)	3.9(2)
C(6)	0.051(1)	0.358(1)	0.6129(9)	4.4(3)

[a] $B_{eq} = 8/3\pi^2(U_{11}(aa^*)^2 + U_{22}(bb^*)^2 + U_{33}(cc^*)^2 + 2U_{12}aa^*bb^*\cos\gamma + 2U_{13}aa^*cc^*\cos\beta + 2U_{23}bb^*cc^*\cos\alpha)$

Table 3. Anisotropic thermal parameters[a] ($Å^2$) of the non-hydrogen atoms for $[WNCl_3 \cdot NCCH_3]_4 \cdot 2CH_3CN$

Atom	U_{11}	U_{22}	U_{33}	U_{12}	U_{13}	U_{23}
W(1)	0.0156(1)	0.0196(2)	0.0128(2)	0.0071(1)	0.0050(1)	0.0038(1)
W(2)	0.0151(1)	0.0120(2)	0.0165(2)	0.0049(1)	0.0063(1)	0.0035(1)
Cl(1)	0.037(1)	0.027(1)	0.032(1)	0.0114(9)	0.0176(9)	-0.0018(9)
Cl(2)	0.041(1)	0.028(1)	0.040(1)	0.0232(9)	0.0182(10)	0.0104(9)
Cl(3)	0.0213(9)	0.067(2)	0.023(1)	0.0154(9)	0.0007(8)	0.003(1)
Cl(4)	0.0356(10)	0.0186(9)	0.033(1)	0.0130(8)	0.0136(9)	0.0014(8)
Cl(5)	0.0329(9)	0.0248(10)	0.029(1)	0.0169(8)	0.0124(8)	0.0010(8)
Cl(6)	0.0334(10)	0.030(1)	0.032(1)	0.0098(8)	0.0167(9)	0.0181(9)
N(1)	0.011(3)	0.013(3)	0.021(3)	0.002(2)	0.007(2)	0.004(2)
N(2)	0.018(3)	0.019(3)	0.013(3)	0.007(2)	0.001(2)	0.008(2)
N(3)	0.033(4)	0.047(5)	0.023(4)	0.018(3)	0.010(3)	0.016(4)
N(4)	0.023(3)	0.018(3)	0.028(4)	0.005(3)	0.011(3)	0.007(3)
N(5)	0.072(6)	0.043(6)	0.14(1)	0.009(5)	0.056(7)	0.007(6)
C(1)	0.025(4)	0.048(5)	0.022(4)	0.020(4)	0.012(3)	0.013(4)
C(2)	0.046(5)	0.066(7)	0.040(6)	0.024(5)	0.026(5)	0.028(5)
C(3)	0.024(4)	0.012(4)	0.040(5)	0.007(3)	0.013(4)	0.009(4)
C(4)	0.023(4)	0.033(5)	0.071(7)	0.011(4)	-0.006(4)	0.013(5)
C(5)	0.043(5)	0.038(6)	0.062(7)	0.019(5)	0.016(5)	0.002(5)
C(6)	0.049(6)	0.067(7)	0.047(6)	0.024(5)	0.011(5)	0.007(6)

[a]The coefficients U_{ij} of the anisotropic temperature factor expression are defined as $\exp(-2\pi^2(a^{*2}U_{11}h^2 + b^{*2}U_{22}k^2 + c^{*2}U_{33}l^2 + 2a^*b^*U_{12}hk + 2a^*c^*U_{13}hl + 2b^*c^*U_{23}kl))$

orange solid which was soluble in acetonitrile was obtained. This deep orange solid is the tetrameric form of $WNCl_3$. Therefore, in order to obtain $[WNCl_3 \cdot NCCH_3]_4$, the starting $WNCl_3$ must be preheated at 160-200°C for 24 hours.

Structure of $[WNCl_3 \cdot NCCH_3]_4 \cdot 2CH_3CN$

$[WNCl_3 \cdot NCCH_3]_4 \cdot 2CH_3CN$ crystallizes in the triclinic space group $P\bar{1}$ with one $[WNCl_3 \cdot NCCH_3]_4$ molecule and two free CH_3CN molecules per unit cell. An ORTEP diagram of the unit cell is shown in Figure 1. The molecular structure of $[WNCl_3 \cdot NCCH_3]_4$ (Figure 2) consists of a W_4N_4 tetramer core, in which the four tungsten and four nitrogen atoms define a ring system. The selected bond distances and angles for $[WNCl_3 \cdot NCCH_3]_4 \cdot 2CH_3CN$ are listed in Tables 4 and 5, respectively. It is observed that there are essentially two significantly different types of W-N bonds in the W_4N_4 tetramer ring as previously found in $[WNCl_3]_4$ and related compounds. One type of bond has an average length of 1.705(5) Å, which can be assigned as a multiple bond. The other type of bond has an average length of 2.075(5) Å, which is a typical W-N single bond length. These two bond types are arranged in an alternating fashion to complete the tetramer ring system. The bond lengths and angles of $[WNCl_3 \cdot NCCH_3]_4$ are all quite similar to those of other tungsten nitride tetramers as shown by the comparison given in Table 6.

Each tungsten atom is coordinated by two nitrogen atoms, three chlorine atoms

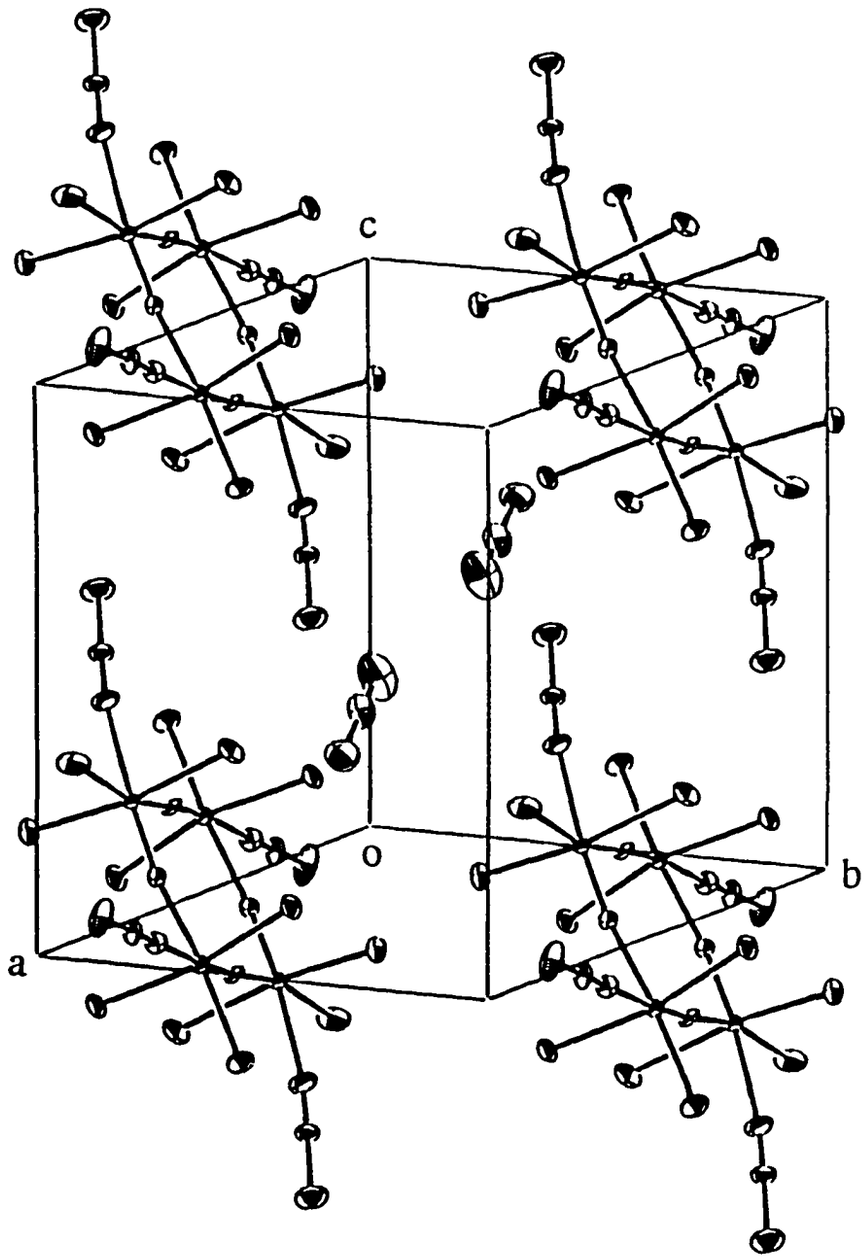

Figure 1. An ORTEP diagram of the unit cell for $[WNCl_3 \cdot NCCH_3]_4 \cdot 2CH_3CN$.

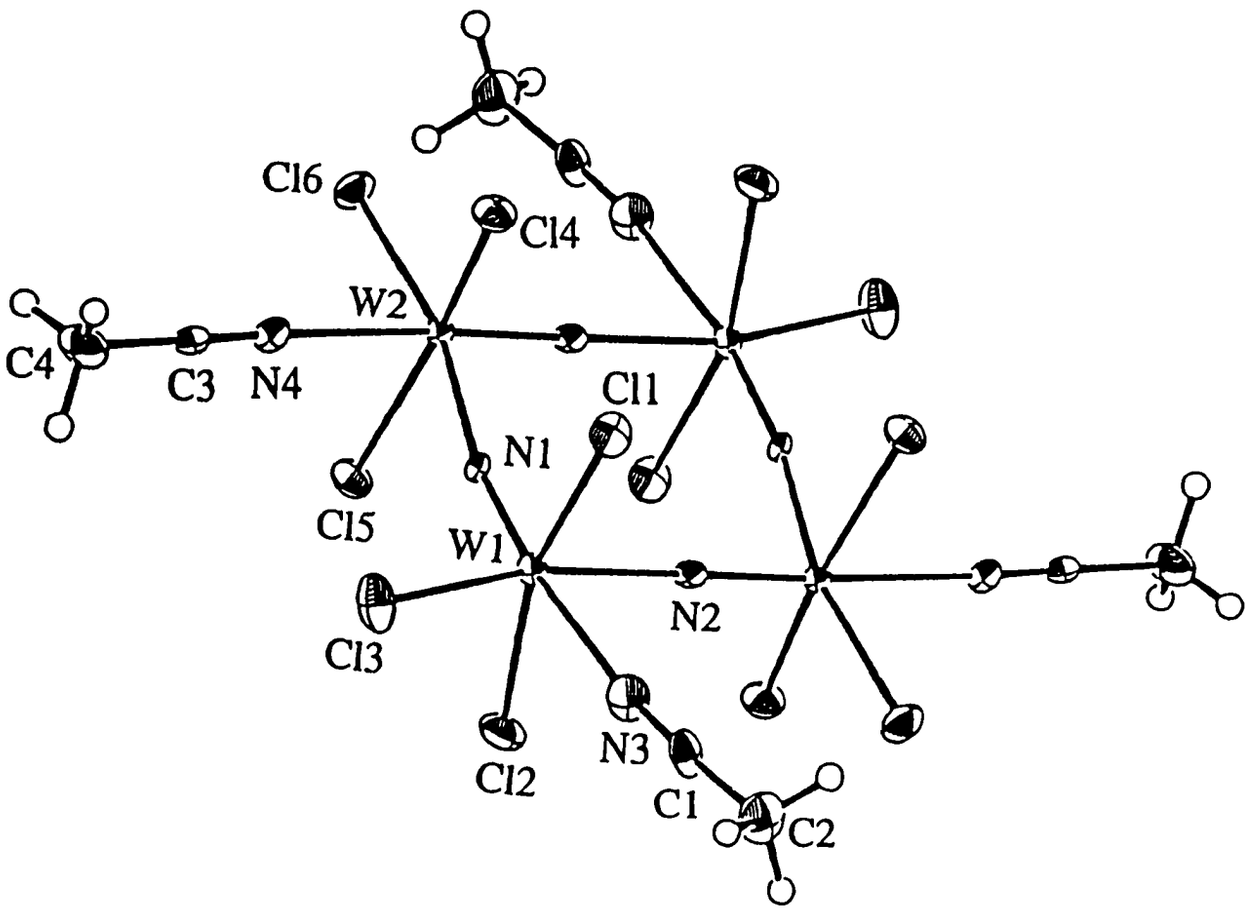

Figure 2. The molecular structure of $[WNCl_3 \cdot NCCH_3]_4$.

Table 4. Selected bond distances (Å) in $[WNCl_3 \cdot NCCH_3]_4 \cdot 2CH_3CN$

atom	atom	distance	atom	atom	distance
W(1)	Cl(1)	2.319(2)	W(1)	Cl(2)	2.312(2)
W(1)	Cl(3)	2.295(2)	W(1)	N(1)	1.703(5)
W(1)	N(2)	2.073(5)	W(1)	N(3)	2.348(6)
W(2)	Cl(4)	2.308(2)	W(2)	Cl(5)	2.302(2)
W(2)	Cl(6)	2.317(2)	W(2)	N(1)	2.078(5)
W(2)	N(2)	1.707(5)	W(2)	N(4)	2.338(6)
N(3)	C(1)	1.127(9)	N(4)	C(3)	1.112(9)
N(5)	C(5)	1.11(1)	C(1)	C(2)	1.45(1)
C(3)	C(4)	1.481(10)	C(5)	C(6)	1.43(1)

and one acetonitrile molecule to form a distorted octahedron (Figure 3). The acetonitrile molecules bound to the tungsten atoms are *trans* to the W-N multiple bonds. Because of the strong W-N multiple bond and the *trans* influence, the acetonitrile molecules are only weakly bound to the tungsten atoms. This is reflected by the relatively long average bond distance of W-$NCCH_3$, which is 2.343(6) Å. On the basis of the average W-Cl bond distance of 2.309 Å, we estimate that a normal W-N single bond distance should be ca. 2.02 Å, similar to the average W-N (nitride) distance of 2.076 Å.

Table 5. Selected bond angles (°) in $[WNCl_3 \cdot NCCH_3]_4 \cdot 2CH_3CN$

atom	atom	atom	angle	atom	atom	atom	angle
Cl(1)	W(1)	Cl(2)	162.70(7)	Cl(1)	W(1)	Cl(3)	93.85(9)
Cl(1)	W(1)	N(1)	94.4(2)	Cl(1)	W(1)	N(2)	83.9(2)
Cl(1)	W(1)	N(3)	81.7(2)	Cl(2)	W(1)	Cl(3)	93.99(9)
Cl(2)	W(1)	N(1)	99.0(2)	Cl(2)	W(1)	N(2)	83.9(2)
Cl(2)	W(1)	N(3)	83.6(2)	Cl(3)	W(1)	N(1)	102.2(2)
Cl(3)	W(1)	N(2)	161.9(2)	Cl(3)	W(1)	N(3)	85.2(2)
N(1)	W(1)	N(2)	95.9(2)	N(1)	W(1)	N(3)	171.9(2)
N(2)	W(1)	N(3)	76.7(2)	Cl(4)	W(2)	Cl(5)	163.06(7)
Cl(4)	W(2)	Cl(6)	94.63(7)	Cl(4)	W(2)	N(1)	84.6(2)
Cl(4)	W(2)	N(2)	96.5(2)	Cl(4)	W(2)	N(4)	81.8(2)
Cl(5)	W(2)	Cl(6)	92.29(7)	Cl(5)	W(2)	N(1)	84.9(2)
Cl(5)	W(2)	N(2)	97.7(2)	Cl(5)	W(2)	N(4)	83.2(2)
Cl(6)	W(2)	N(1)	166.0(1)	Cl(6)	W(2)	N(2)	98.9(2)
Cl(6)	W(2)	N(4)	86.0(2)	N(1)	W(2)	N(2)	95.0(2)
N(1)	W(2)	N(4)	80.0(2)	N(2)	W(2)	N(4)	174.9(2)
W(1)	N(1)	W(2)	170.7(3)	W(1)	N(2)	W(2)	176.2(4)
W(1)	N(3)	C(1)	170.9(6)	W(2)	N(4)	C(3)	177.6(6)
N(3)	C(1)	C(2)	177.8(9)	N(4)	C(3)	C(4)	179.1(8)
N(5)	C(5)	C(6)	179(1)				

Table 6. Comparison of bond lengths (Å) in selected $[WNCl_3 \cdot L]_4$ tetramers

Bond	$[WNCl_3 \cdot NCCH_3]_4$	$[WNCl_3]_4$	$[WNCl_3 \cdot 0.5HN_3]_4$	$[WNCl_3 \cdot NCPh]_4$	$[WNCl_3 \cdot OPCl_3]_4$
W(1)-N(1)	1.703(5)	1.705(7)	1.69(3)	1.65(2)	1.671(2)
W(1)-N(2)	2.073(5)	2.085(7)	2.11(3)	2.08(2)	2.169(3)
W(1)-Cl(1)	2.319(2)	2.276(2)	2.30(1)	2.280(6)	2.336(3)
W(1)-Cl(2)	2.312(2)	2.328(3)	2.28(1)	2.291(6)	2.318(3)
W(1)-Cl(3)	2.295(2)	2.276(2)	2.27(1)	2.270(6)	2.287(3)
W(1)-L(1)	2.348(6)	2.895(3)	2.44(2)	2.49(2)	2.379(2)
W(2)-N(1)	2.078(5)	2.077(7)	2.08(3)	2.11(2)	2.163(2)
W(2)-N(2)	1.707(5)	1.686(7)	1.68(3)	1.70(2)	1.648(3)
W(2)-Cl(4)	2.308(2)	2.265(2)	2.30(1)	2.315(6)	2.323(3)
W(2)-Cl(5)	2.302(2)	2.255(2)	2.26(1)	2.283(6)	2.318(2)
W(2)-Cl(6)	2.317(2)	2.387(2)	2.38(1)	2.324(6)	2.359(3)
W(2)-L(2)	2.338(6)	2.805(3)	2.80(2)	2.28(2)	2.316(3)

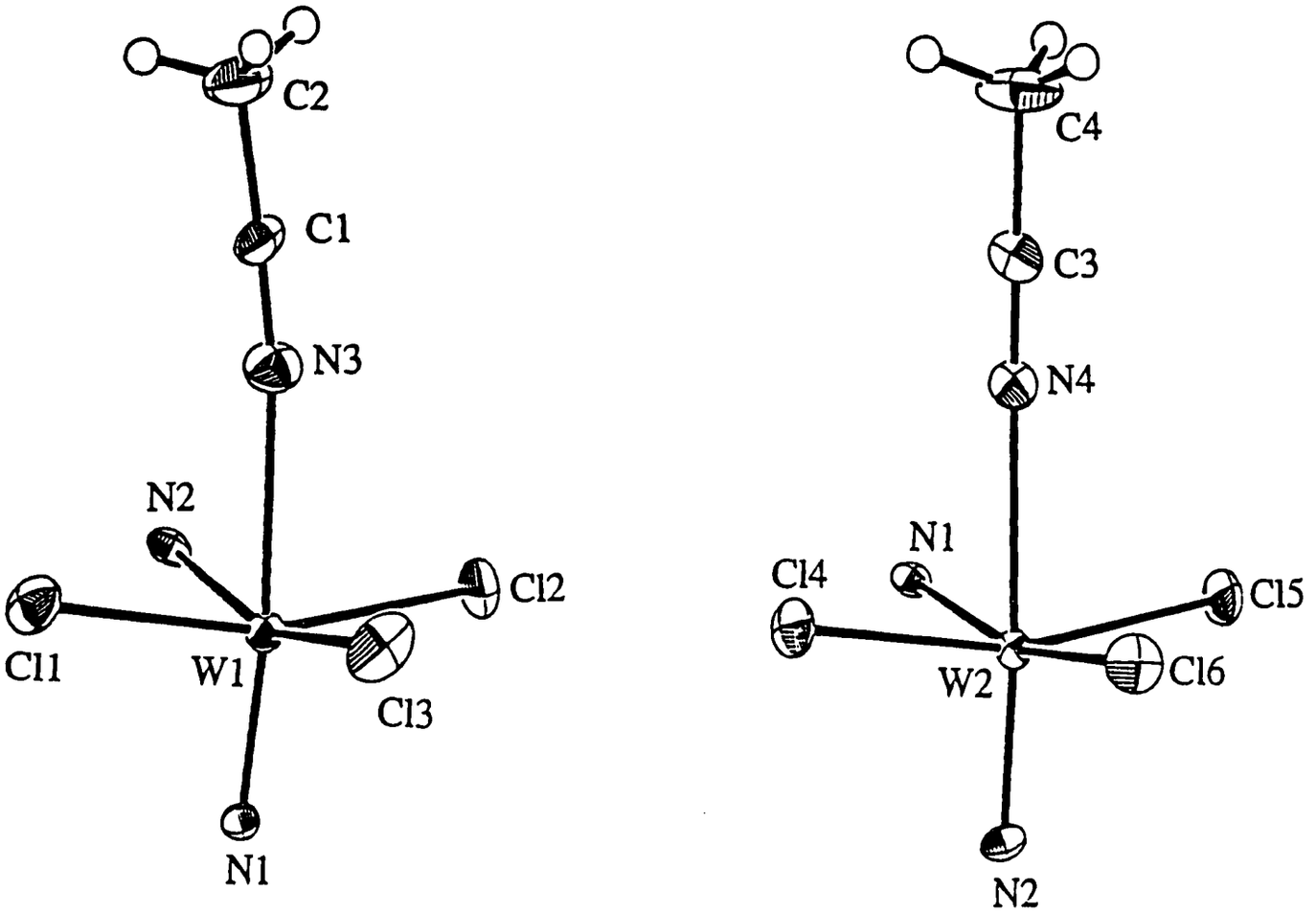

Figure 3. The coordination spheres of tungsten atoms in the structure of $[WNCl_3 \cdot NCCH_3]_4$.

Infrared spectroscopy

Infrared spectroscopy has been used extensively to characterize nitridometal chloride compounds. Its utility is based on the strong stretching mode of the M≡N multiple bonds and the sensitivity of the M-Cl stretching frequencies. Any reactions on nitrogen or chlorine will result in large changes in the IR spectra.

By examining the frequencies of the W≡N stretching vibrations (Table 7), it is noted that the relative intensities and frequencies of the W≡N multiple bond stretching modes are related to the W-N bonding types. The IR bands of W≡N multiple bonds in the W≡N-W bridging bonds exhibit stronger intensities and higher frequencies than that in the W≡N: terminal bonds. The W≡N asymmetric stretching frequencies in the W≡N-W bridging bonds, as shown in Table 7, are in the range of 1050-1090 cm^{-1}. In comparison, the W≡N asymmetric stretching frequencies in the W≡N: terminal bonds are in the range of 1000-1040 cm^{-1}. The IR spectrum of $[WNCl_3 \cdot NCCH_3]_4$ in this work shows a strong band at 1075 cm^{-1} (Figure 4), which can be assigned as υ(W≡N) modes. This observation further confirms that the relative intensities and frequencies of the W≡N multiple bond stretching modes in W≡N-W bridging bonds are stronger and higher. The W-Cl stretching frequencies are in the range of 270-400 cm^{-1}, which consist of two strong bands at 357 and 329 cm^{-1}, and two shoulders at 378 and 286 cm^{-1}. The bands at 2309 cm^{-1} and 2281 cm^{-1} are the characteristic C≡N stretching frequencies of coordinated acetonitrile.

Table 7. Frequencies (cm^{-1}) of W≡N stretching vibrations in compounds containing W≡N multiple bonds

Terminal type W≡N:	υ(W≡N:)	Bridging type W≡N-W	υ(W≡N)
$WNCl_3(Bipy)$[13]	1006	$[WNCl_3 \cdot POCl_3]_4$[6]	1074, 1087
$WNCl_3(Py)_3$[13]	1040	$[WNCl_3 \cdot NCPh]_4$[8]	1082
$AsPh_4[WNCl_4]$[12]	1036	$[WNCl_3 \cdot 0.5HN_3]_4$[7]	1050, 1082
		$[WNCl_3]_4$[9]	1076, 1086
		$[WNCl_3]_\infty$[12]	1068, 1086

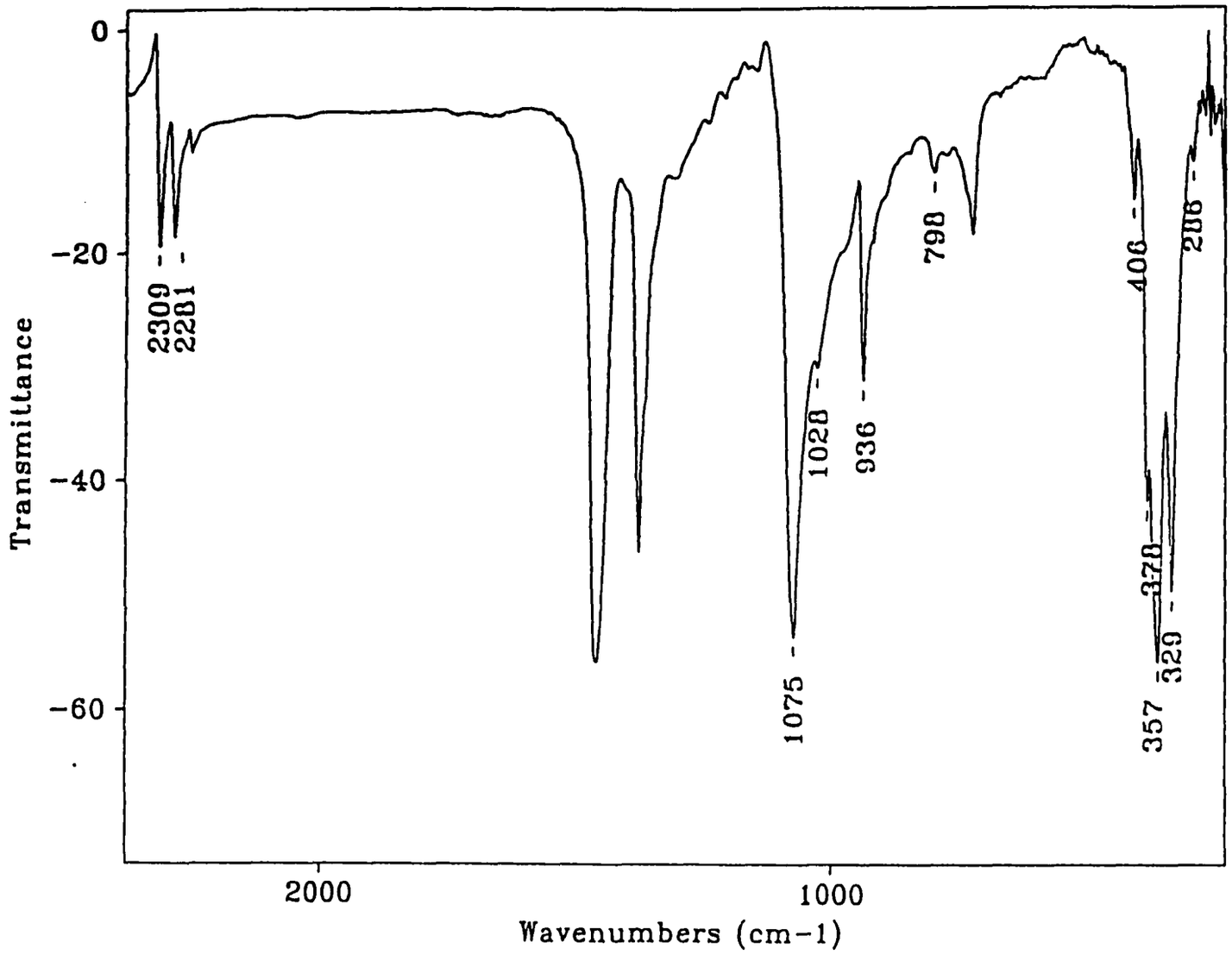

Figure 4. Infrared spectrum (Nujol) for $[WNCl_3 \cdot NCCH_3]_4$.

Reaction of $[WNCl_3 \cdot NCCH_3]_4$ with CH_3CN

Although $[WNCl_3 \cdot NCCH_3]_4$ is soluble in acetonitrile at room temperature, it reacts with CH_3CN at reflux. It is well known that alkyl cyanides react with high oxidation state transition metal halides. For example, the reactions of molybdenum and tungsten halides (MX_5, MX_6, M = Mo, W; X = Cl, Br) with alkyl cyanides (RCN, R = Me, Et, and n-Pr) were well studied by Fowles and coworkers.[14] The metals were reduced from M(V) or M(VI) to M(IV). The products were characterized as 6-coordinate complexes with the general formula $MX_4(RCN)_2$. The formation of hydrogen halides was also observed.

The product of $[WNCl_3 \cdot NCCH_3]_4$ with acetonitrile at reflux was a dark blue amorphous solid which was also soluble in acetonitrile. Chemical analyses of this product provided a composition of $WCl_{3.08}N_{2.99}C_{3.86}H_{6.34}$, which is close to that required for $W(NH)Cl_3(CH_3CN)_2$. This is a 6-coordinate complex. Therefore, the $[WNCl_3 \cdot NCCH_3]_4$ tetramers may be dissociated to $W(NH)Cl_3(CH_3CN)_2$ monomers due to the protonation of the bridging nitrogen atoms in the tetramers. The absence of the band at 1075 cm^{-1} in the IR spectrum shown in Figure 5 indicates that the W≡N-W bridging bonds are broken. The occurrence of the band at 3199 cm^{-1} indicates that the nitrogen atoms bonded to tungsten atoms may be protonated.

The tungsten oxidation state determination in $W(NH)Cl_3(CH_3CN)_2$ provided a value of 5.10, which is very close to 5. Therefore, it can be concluded that the W(VI)

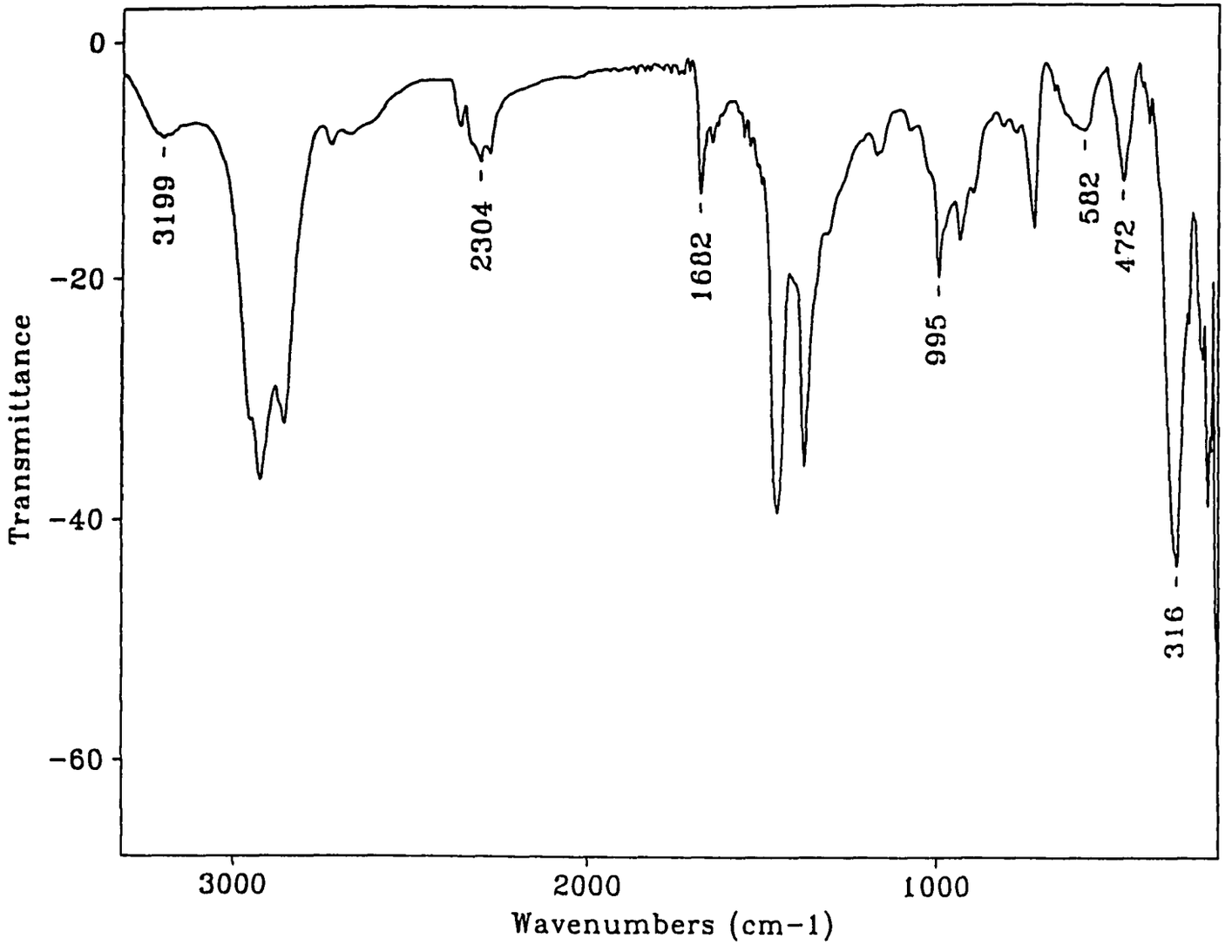

Figure 5. Infrared spectrum (Nujol) for $W(NH)Cl_3(CH_3CN)_2$.

in $[WNCl_3 \cdot NCCH_3]_4$ was reduced to W(V). The following ESR and magnetic susceptibility measurements confirm this conclusion as well.

The ESR spectrum of "$W_4Cl_{11}(NH)_4(CH_3CN)_8$" (Figure 6) shows a strong signal at H = 3860 G. The *g* factor of this material was then calculated to be 1.756, according to the equation $g = h\upsilon/\beta H$, where h is the Plank constant (6.6261×10^{-34} J·s); β is Bohr magneton (9.2740×10^{-24} J·T^{-1}); and υ is the frequency of the microwave radiation (9.495×10^{9} Hz). Based on this *g* factor, the material should have an effective magnetic moment, $\mu = g[s(s+1/2)]^{1/2}$, equal to 1.52. The small *g* factor indicates less delocalization of the single electron, which was also observed in many other compounds containing W(V) species.[15] For comparison, Table 8 lists the *g* factors of selected compounds containing W(V) species.

Figure 7 shows the molar susceptibility of $W(NH)Cl_3(CH_3CN)_2$ as a function of temperature. The susceptibility data in the range of 100-300 K were fitted to a modified Curie-Weiss relation, $\chi = C/(T - \theta) + \chi_o$, where C, θ, and χ_o refer to the Curie constant, the Weiss temperature, and temperature independent susceptibility, respectively. The values for C, θ, and χ_o are 0.2951, 21.95 K, and 2.144×10^{-2} emu/mol, respectively. An effective magnetic moment was then calculated to be 1.54 μ_B according to the equation $\mu = 2.83C^{-1/2}$. The calculated single electron spin-only moment based on the *g* factor obtained from ESR study was 1.52 μ_B. The consistency of these two values further confirmed that the tungsten atoms in the parent compound

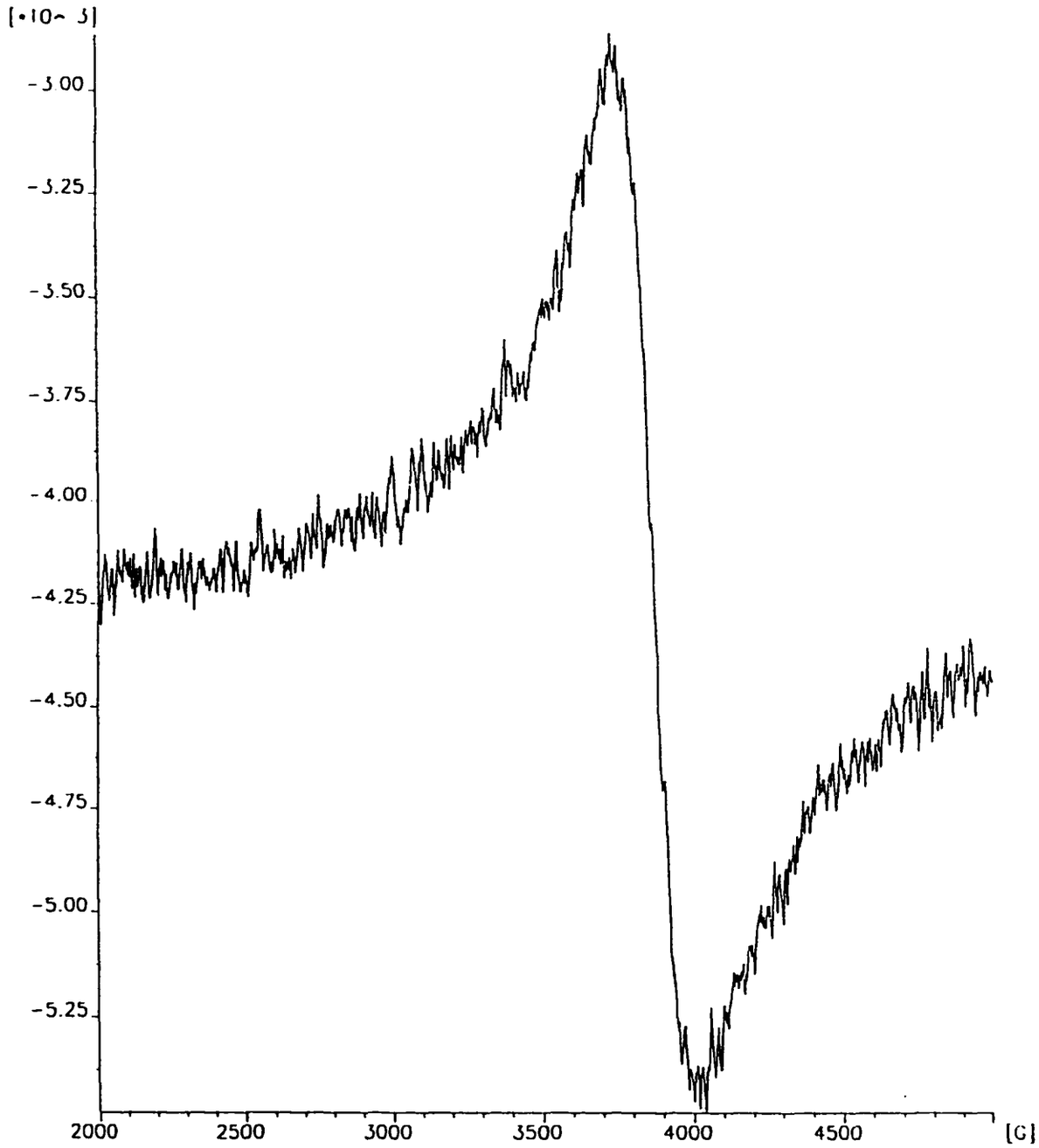

Figure 6. ESR spectrum for $W(NH)Cl_3(CH_3CN)_2$.

Table 8. The g factors of selected W(V) species

Species	g_{av}	$g_{\parallel}$	$g_{\perp}$
$[WOF_5]^{2-}$		1.589	1.767
$[WOCl_5]^{2-}$	1.773	1.804	1.758
$[WOBr_5]^{2-}$	1.830	1.940	1.775
$K_2[WO(NCS)_5]$	1.803	1.775	1.819
WCl_5			
in glycerol	1.754	1.79	1.757
in HCl	1.745	1.78	1.756
in C_2H_5OH	1.743	1.79	1.718

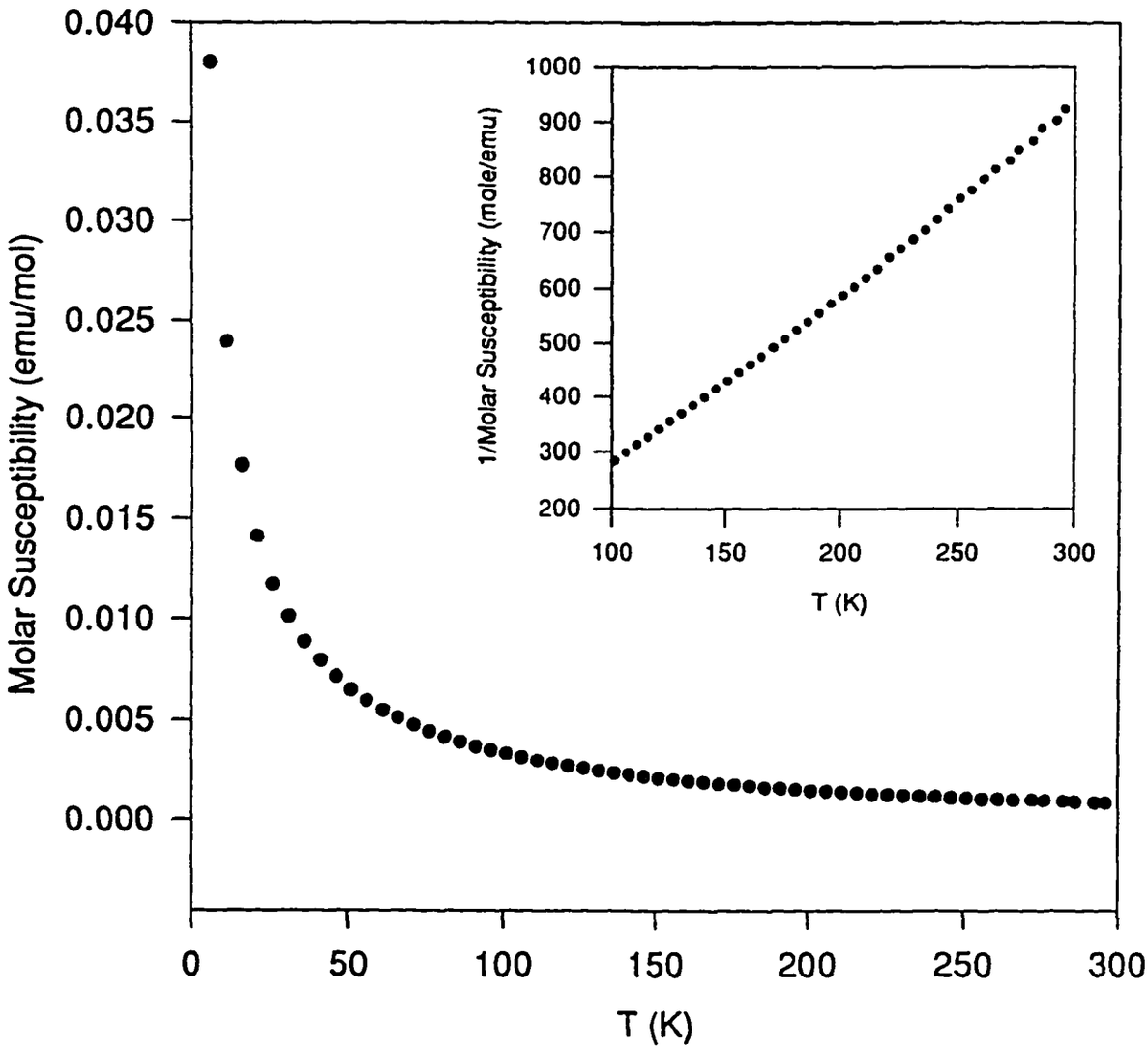

Figure 7. The molar susceptibility of $W(NH)Cl_3(CH_3CN)_2$ as a function of temperature. and reciprocal susceptibility vs. temperature (inset).

were reduced from W(VI) to W(V).

Although a single crystal structure would help to better understand this material, attempts to grow single crystals in many solvents, such as acetonitrile, propionitrile, pyridine, and THF, were not successful.

Conclusions

An acetonitrile adduct of $WNCl_3$ can be prepared from an acetonitrile solution of $WNCl_3$ at room temperature. $[WNCl_3 \cdot NCCH_3]_4 \cdot 2CH_3CN$ crystallizes in the triclinic space group $P\bar{1}$ with one $[WNCl_3 \cdot NCCH_3]_4$ molecule and two free CH_3CN molecules per unit cell. The molecular structure of $[WNCl_3 \cdot NCCH_3]_4$ consists of a W_4N_4 tetrameric core. Two significantly different types of W-N bonds are found. One can be assigned as a W≡N multiple bond with an average bond length of 1.705(5) Å. The other one can be designated as a W-N single bond with an average bond length of 2.075(5) Å.

Although $[WNCl_3 \cdot NCCH_3]_4 \cdot 2CH_3CN$ is soluble in acetonitrile at room temperature, it reacts with solvent CH_3CN at reflux (81 °C). The dark blue amorphous product has the composition of $W(NH)Cl_3(CH_3CN)_2$, and is soluble in acetonitrile as well. The tungsten atoms in $[WNCl_3 \cdot NCCH_3]_4 \cdot 2CH_3CN$ were reduced from W(VI) to W(V) during the reaction. The reduction was confirmed by oxidation state

determination, ESR, and magnetic susceptibility measurements.

References

1. Dehnicke, K.; Strähle, J. *Z. Anorg. Allg. Chem.* **1965**, *339*, 171.
2. Chatt, J.; Dilworth, J. R. *J. Chem. Soc. Chem. Commun.* **1974**, 157.
3. Schweda, E.; Strähle, J. *Z. Naturforsch.* **1980**, *35B*, 1146.
4. Godemeyer, T.; Berg, A.; Gross, H.-D.; Müller, U.; Dehnicke, K. *Z. Naturforsch.* **1985**, *40B*, 999.
5. Görge, A.; Dehnicke, K.; Fenske, D. *Z. Naturforsch.* **1988**, *43B*, 677.
6. Musterle, W.; Strähle, J.; Liebelt, W.; Dehnicke, K. *Z. Naturforsch.* **1979**, *34B*, 942.
7. Walker, I.; Strähle, J. *Z. Anorg. Allg. Chem.* **1982**, *487*, 26.
8. Ergezinger, C.; El-Kholi, A.; Müller, U.; Dehnicke, K. *Z. Anorg. Allg. Chem.* **1989**, *568*, 55.
9. Close, M. R.; McCarley, R. E. *Inorg. Chem.* **1994**, *33*, 4198.
10. Banks, C. V.; O'Laughlin, J. W. *Anal. Chem.* **1956**, *28*, 1338.
11. (a) Sheldrick, G. M. *Crystallographic Computing 3*, Eds Sheldrick G. M.; Kruger, C.; Goddard, R., Oxford University Press, 175.

(b) Crystal Structure Analysis Package, Molecular Structure Corporation (1985 & 1992).

12. Dehnicke, K.; Strähle, J. *Angew. Chem. Int. Ed. Engl.* **1981**, *20*, 413.
13. Dehnicke, K.; Prinz, H.; Kafitz, W.; Kujanek, R. *Liebigs Ann. Chem.* **1981**, 20.
14. Allen, E. A.; Brisdon, B. J.; Fowles, G. W. A. *J. Chem. Soc.* **1964**, 4531.
15. Goodman B. A.; Raynor, J. B. *Advances in Inorganic Chemistry and Radiochemistry*, Emeleus, H. J.; Sharpe, A. G. Eds. Academic Press, **1970**, *13*, 135.

CHAPTER 2. SYNTHESIS AND CHARACTERIZATION OF MOLECULAR PRECURSORS TO TUNGSTEN NITRIDES AND THEIR THERMAL DECOMPOSITION STUDIES

A paper to be submitted to Chemistry of Materials

Zhihong Zhang and Robert E. McCarley

Abstract

Three molecular precursors to tungsten nitrides, $WN(N_3)_3 \cdot xCH_3CN$, $WN_{10}C_5H_{7.5}$, and $WN(N_3)Cl_2 \cdot 2Py$ have been prepared. The explosive compound $WN(N_3)_3 \cdot xCH_3CN$ was prepared from the reaction of $WNCl_3$ and NaN_3 in acetonitrile at room temperature. The IR spectrum of this compound indicated that the W≡N multiple bond (1050 cm^{-1}) still remained, and the chloride was completely replaced by azide. The reaction of $WNCl_3$ and NaN_3 in refluxing acetonitrile, however, produced a complex with a composition of $WN_{10}C_5H_{7.5}$. The XPS study indicated that the tungsten atom in this complex was in an oxidation state lower than +6. The reaction of $WNCl_3$ and NaN_3 in refluxing pyridine yielded a complex with a composition of $WN(N_3)Cl_2(Py)_2$. The substitution of chloride by azide was not complete in this reaction. By replacement of CH_3CN with Py in $WN(N_3)_3 \cdot xCH_3CN$, the thermal decomposition of $WN(N_3)_3 \cdot xPy$ was attempted in refluxing 1,2-

dichlorobenzene (b.p. 186°C). However, the azide did not decompose completely as noted by a strong band at ~2030 cm^{-1} in the IR spectrum of the product. Further thermal treatments produced an amorphous phase (500°C) and a hexagonal WN phase (750°C). The amorphous phase had a composition close to WN_2 based on the tungsten analysis.

Introduction

Due to the thermodynamic instability of transition metal nitrides with respect to the corresponding metal elements and molecular nitrogen, traditional methods involving high temperature reactions were found to restrict the number and types of transition metal nitrides.[1-2] Therefore, "turning down the heat"[3] is one important strategy to the metal nitride synthesis. Low temperature reactions of precursor compounds with appropriate nitriding reagents in polar organic solvents may be a good direction to investigate.[4]

$WNCl_3$[5] was considered as a potential intermediate to the desired tungsten nitrides in our research. It has been known that $WNCl_3$ in the presence of acetonitrile exists in the form of a tetrameric molecule $[WNCl_3 \cdot NCCH_3]_4$ at room temperature.[6] Therefore, the chloride could be replaced by other nitriding reagents, such as N^{3-}, N_3^-, N_2^{4-}, in an acetonitrile solution. The replacement of chloride in metal halides by N_3^-

has been reported. For example, the explosive compounds $MoN(N_3)_3(bpy)$ and $MoN(N_3)_3(py)_2$ can be prepared from the reactions of excess trimethylsilyl azide with $MoCl_4(bpy)$ and $MoCl_4(py)_2$, respectively.[7]

In this paper, the reactions between $WNCl_3$ and NaN_3 in acetonitrile and pyridine will be discussed. Furthermore, thermal decomposition studies of the reaction products are examined.

Experimental

Materials

Most materials used in this study are air and moisture sensitive. Manipulations of oxygen- and water-sensitive materials were performed under inert-atmosphere conditions using standard drybox, high vacuum manifold, and Schlenk techniques.

Acetonitrile, pyridine, and dichlorobenzene were dried with CaH_2, and distilled onto 4Å molecular sieves. Tungsten hexachloride was obtained from Alfa Chemical Co. and sublimed under dynamic vacuum at 120-160°C to remove the more volatile $WOCl_4$ impurity. Trimethylsilyl azide and NaN_3 were obtained from Aldrich Chemical Company, Inc., and used as received. $WNCl_3$ was prepared as described.[5]

Analytical Procedures

Tungsten analysis

Gravimetric determination of W was accomplished by conversion of samples to the trioxide via addition of an oxidizing solution in a tared crucible. Samples were initially treated with dilute (3M) nitric acid and then with concentrated nitric acid. The crucibles were gently heated (~100°C) on a hot plate to slowly evaporate the solution. Once the solution was evaporated, the temperature of the hot plate was increased (~150 °C), and the crucibles were heated at this temperature until the samples became yellow. The crucibles were heated at 800°C in a muffle furnace until constant weights were achieved.

Chlorine analysis

Chlorine was determined by the potentiometric titration of neutralized solutions of dissolved sample with a standardized $AgNO_3$ solution. Ag/AgCl was used as the working electrode and a silver electrode as the reference. Samples were dissolved in a basic solution (KOH) with 30 % H_2O_2, and gently heated on a hot plate until H_2O_2 completely decomposed. The clear solutions were then neutralized with 3N nitric acid to pH ~ 6-7.

Nitrogen, carbon, and hydrogen analysis

The nitrogen, carbon, and hydrogen analyses were obtained from Galbraith Laboratories, Inc. and the ISU Chemistry Department Instrument Services.

Physical Measurements

Infrared spectroscopy

Infrared spectra were obtained on a Bomem MB-Series Fourier transform infrared spectrometer. The samples were prepared as Nujol mulls and pressed between CsI plates. The spectra were recorded in the range of 4000 to 185 cm^{-1}.

X-ray powder diffraction

X-ray powder diffraction data were obtained from a Phillips ADP3520 X-ray powder diffractometer using Cu $K\alpha_1$ radiation (λ = 1.54056 Å).

X-ray photoelectron spectroscopy

XPS spectra were collected at room temperature with a Physical Electronics Industries 5500 multitechnique surface analysis system. This system was equipped with a hemispherical analyzer, a toroidal monochromator, and multichannel detector which sampled a 2 mm^2 area. The samples were pressed onto an indium substrate and

loaded into an air-sensitive sample holder in the drybox. The sample holder was then transferred to the chamber of the spectrometer. After the system was completely evacuated, the sample holder was opened and the sample was excited with monochromatic Mg K_α radiation (1253.6 eV) at a power of 300 W. The photoelectron binding energies (BE's) were calibrated with C 1s BE = 284.6 eV.

Synthetic Procedures

Caution. The following preparations involve explosive materials, azides. Care should be taken to do the reactions on a small scale (less than one gram of reactant mixture) with adequate safety precautions.

Preparation of $WN(N_3)_3 \cdot xNCCH_3$

A typical preparation involved placing 0.5 g (0.164 mmol) of $WNCl_3$ and 0.33 g (0.508 mmol) of NaN_3 into a 100 mL reaction flask. Approximately 50 mL acetonitrile was distilled onto the mixture, and a deep orange solution formed. The solution was stirred under flowing N_2 at room temperature for 36 hrs, and an orange solid and a red solution were separated by filtration. The solid was examined by X-ray powder diffraction, and indicated mainly NaCl and a trace of NaN_3. The orange color was due to a small amount of the main product mixed with NaCl. Attempts to

obtain this azidotungsten nitride by the removal of acetonitrile solvent were not successful due to the extremely explosive nature of the product. Yet, a small amount (~1.0 mg) of this azidotungsten nitride was obtained for an IR study. IR (Nujol, cm^{-1}): υ(C≡N), 2303 w, 2282 w; υ(N-N-N), 2071 s; υ(W≡N), 1050 s.

Preparation of $WN_{10}C_5H_{7.5}$

The preparation was conducted with 0.5 g (0.164 mmol) of $WNCl_3$ and 0.33 g (0.508 mmol) of NaN_3 placed into a 100 mL reaction flask, followed by distilling 50 mL acetonitrile onto the mixture. The reaction was carried out under flowing N_2 at reflux (81°C) for 48 h. A dark brown solid and black solution were separated by filtration. The solid was examined by X-ray powder diffraction, and indicated mainly NaCl and a trace of NaN_3. By removal of solvent from the filtrate, ~0.6 g of black solid was obtained. IR (Nujol, cm^{-1}): υ(N-N-N), 2089 s. Anal. Calcd for $WN_{10}C_5H_{7.5}$: W, 46.98%; N, 35.77%; C, 15.33%; H, 1.92%. Found: W, 46.50%; N, 34.88%; C, 14.92%; H, 1.96%; Cl < 0.7%; N:W = 9.85; C:W = 4.92; H:W = 7.71.

Preparation of $WN(N_3)Cl_2 \cdot 2Py$

A typical preparation involved placing 0.5 g (0.164 mmol) of $WNCl_3$ and 0.33 g (0.508 mmol) of NaN_3 into a 100 mL flask, and the addition of 50 mL pyridine by distillation onto the mixture. The solution was heated to reflux (115°C) under flowing

N_2 for 48 h. A brown solid and deep red solution were separated by filtration. The solid was examined by X-ray powder diffraction, which indicated NaCl and NaN_3. By removal of solvent from the filtrate, a deep red solid was obtained (yield: 85%). Anal. Calcd for $WN(N_3)Cl_2 \cdot 2Py$: W, 39.21%; Cl, 15.14%; N, 17.92%; C, 25.60%; H, 2.13%. Found: W, 37.96%; Cl, 15.04%; N, 15.49%; C, 25.01%; H, 2.54%. Cl:W, 2.05:1; N:W, 5.36:1; C:W, 10.09; H:W, 12.30:1. IR (Nujol, cm^{-1}): υ(N-N-N), 2076 s; υ(C-C, C-N, ring stretching), 1602 m; υ(in-plane C-H deformation), 1216 m, 1154 w, and 1064 sh; υ(in-plane ring bend), 1026 w; υ(W≡N), 998 m; υ(out-of-plane C-H deformation), 936 w; υ(W-Cl), 395 m, 287 m.

Thermal decomposition of $WN(N_3)_3 \cdot xNCCH_3$

A general procedure for the thermal decomposition of the azidotungsten nitride $WN(N_3)_3 \cdot xNCCH_3$ is as follows. Before removing the acetonitrile solvent from the reaction flask, 5 mL of pyridine was added by syringe, and then the solvents were removed at room temperature *in vacuo*. In order to completely remove the acetonitrile, 10 mL of pyridine was added again, and a deep red solution was obtained. The deep red solution was then re-evaporated, and a dark red solid was obtained. To the flask containing the dark red solid, 40 mL of 1,2-dichlorobenzene was added by syringe. The mixture was then heated at reflux for 48 h. A black solid was obtained by filtration, washed with 1,2-dichloroethane to remove any residual 1,2-dichlorobenzene,

and then dried under dynamic vacuum overnight. Anal. Found: W, 64.8%; Cl < 1.0%. IR (Nujol, cm^{-1}): υ(N-N-N), 2026 s; υ(C-C, C-N, ring stretching), 1600 w; υ(in-plane C-H deformation), 1216 w, 1153 w, and 1064 sh; υ(in-plane ring bend), 1011 sh; υ(out-of-plane C-H deformation), 936 w.

Results and Discussion

Reactions of $WNCl_3$ with NaN_3 in different solvents

In acetonitrile at room temperature. A general reaction for the preparation of $WN(N_3)_3 \cdot xNCCH_3$ can be expressed as follows,

$$WNCl_3 + 3NaN_3 \xrightarrow{CH_3CN} WN(N_3)_3 + 3NaCl$$

In order to avoid the reaction between $WNCl_3$ and CH_3CN,[6] the reaction was run at room temperature. The main product was quite soluble in acetonitrile. The solid phase was basically the NaCl by-product which was identified by X-ray powder diffraction. By removing the acetonitrile solvent from the filtrate, a red solid was obtained. However, it is impossible to recover this red solid in a large yield because of the extremely explosive nature of the compound.

In acetonitrile at reflux (81°C). Three reactions appear to take place under reflux conditions: the expected substitution reaction of Cl^- by N_3^-; the reaction between $WNCl_3$ and acetonitrile;[6] and a nucleophilic attack by azide on the carbon atoms of the nitrile groups in $[WNCl_3 \cdot NCCH_3]_4$. Therefore, the reaction of $WNCl_3$ and NaN_3 in acetonitrile at reflux was much more complicated than the reaction at room temperature. The nucleophilic attack by the azide can be catalyzed by a acid.[8] For example, BF_3, a Lewis acid, catalyzed the formation of 5-substituted tetrazoles through nucleophilic attack of azide on the carbon atoms of the nitrile groups. For the reaction of $WNCl_3$ and NaN_3 in refluxing acetonitrile, $WNCl_3$ acts as a Lewis acid, where the coordination of $WNCl_3$ with the acetonitrile nitrogen generates a $+\delta$ charge on the nitrile carbon and facilitates the nucleophilic attack of the azide on the carbon atom of the nitrile group. A single crystal structure and NMR study would help to better understand this reaction, however, the product was not soluble in any of the common organic solvents such as acetonitrile, 1,1-dichloromethane, THF, and methanol. Chemical analyses on the black product provided a composition close to $WN_{10}C_5H_{7.5}$, and only a trace of chlorine was found. These results indicated that the replacement of chloride by azide was complete.

In pyridine at reflux (115°C). Solvent effects play an important role in the structural form of $WNCl_3$. It was reported that $WNCl_3$ existed as a $WNCl_3(Py)_3$

monomer instead of a tetramer.[9] The reactivity of this $WNCl_3(Py)_3$ monomer is quite different from the $[WNCl_3 \cdot NCCH_3]_4$ tetramer. When the substitution reaction of chloride by azide was carried out in refluxing pyridine, a deep red, soluble product was obtained. Chemical analyses of the main product provided a composition of $WCl_{2.05}N_{5.36}C_{10.09}H_{12.30}$, which is close to that expected for $WN(N_3)Cl_2 \cdot 2(C_5H_5N)$. The insoluble by-products were identified by X-ray powder diffraction as NaCl and NaN_3. Therefore, only one chlorine can be replaced by azide, and the reaction is then expressed as follows:

$$WNCl_3 + NaN_3 \xrightarrow{Py} WN(N_3)Cl_2 + NaCl$$

Infrared spectroscopy

Infrared spectroscopy has been used extensively to characterize nitridometal chloride compounds. Its utility is based on the strong stretching mode of the M≡N multiple bonds and the sensitivity of the M-Cl stretching frequencies. Any reactions on nitrogen or chlorine will result in large changes in the IR spectra.

The IR spectrum of $WN(N_3)_3 \cdot xNCCH_3$ is shown in Figure 1. A strong band at 2071 cm^{-1} can be assigned to the N-N-N stretching mode. Another strong band at 1050 cm^{-1} can be assigned to the W≡N stretching mode. This observation indicates that the W≡N-W bridging bonds may remain after the replacement of Cl^- by N_3^-, and the tetrameric core W_4N_4 may remain as well. The weak bands at about 2300 cm^{-1}

are due to the coordinated acetonitrile. A strong band at 419 cm^{-1}, which is not observed in the IR spectrum of $[WNCl_3 \cdot NCCH_3]_4$, may be due to the W-N stretching mode. The absence of bands corresponding to W-Cl vibrations (~350 cm^{-1}) indicate that the reaction undergoes complete replacement of chloride by azide.

Figure 2 shows the IR spectrum of "$WN_{10}C_5H_{7.5}$". A strong band at 2089 cm^{-1} can be assigned to the N-N-N stretching mode. The absence of bands corresponding to the W≡N (1000-1900 cm^{-1}) and the W-Cl vibrations (~350 cm^{-1}) indicated that the W≡N multiple bond was broken and the chloride was completely replaced by azide. The breaking of the W≡N multiple bond may be due to its direct involvement in the reaction between $WNCl_3$ and acetonitrile.[6]

The IR spectrum of $WN(N_3)Cl_2 \cdot 2Py$ is shown in Figure 3. A strong azide (N-N-N) stretching band was observed at 2076 cm^{-1}. The W-Cl vibration bands were found in the 400-280 cm^{-1} range, which indicated that the chloride was only partially replaced by azide. A medium sharp band at 998 cm^{-1} may be due to the W≡N: terminal bond vibration.[6]

X-ray photoelectron spectrum of "$WN_{10}C_5H_{7.5}$"

XPS was used to obtain W and N binding energies and provide further information about the possible oxidation states of tungsten. The W4f and N1s XPS spectra of "$WN_{10}C_5H_{7.5}$" are shown in Figure 4. There is only one type of tungsten

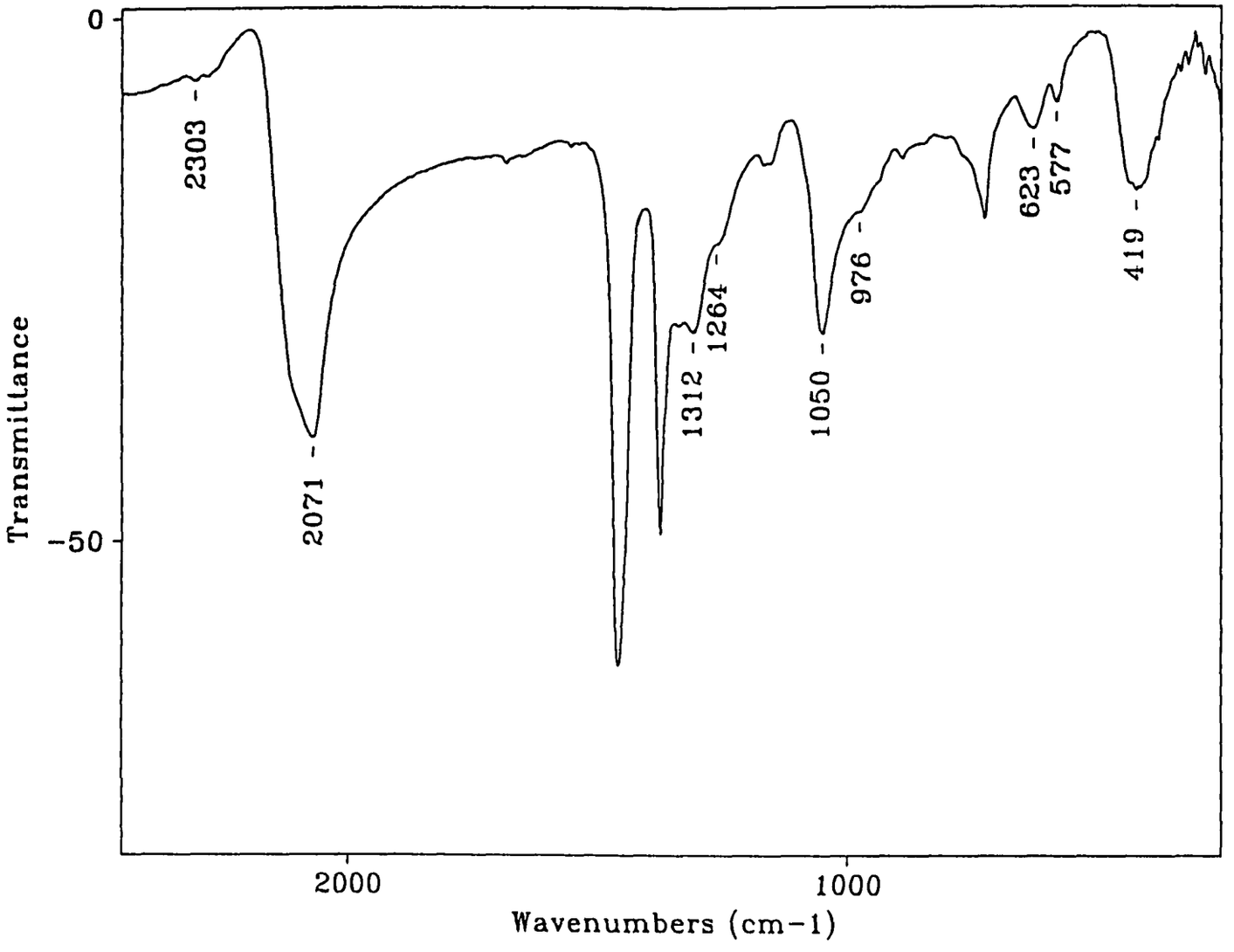

Figure 1. Infrared spectrum (Nujol) for $WN(N_3)_3 \cdot xNCCH_3$.

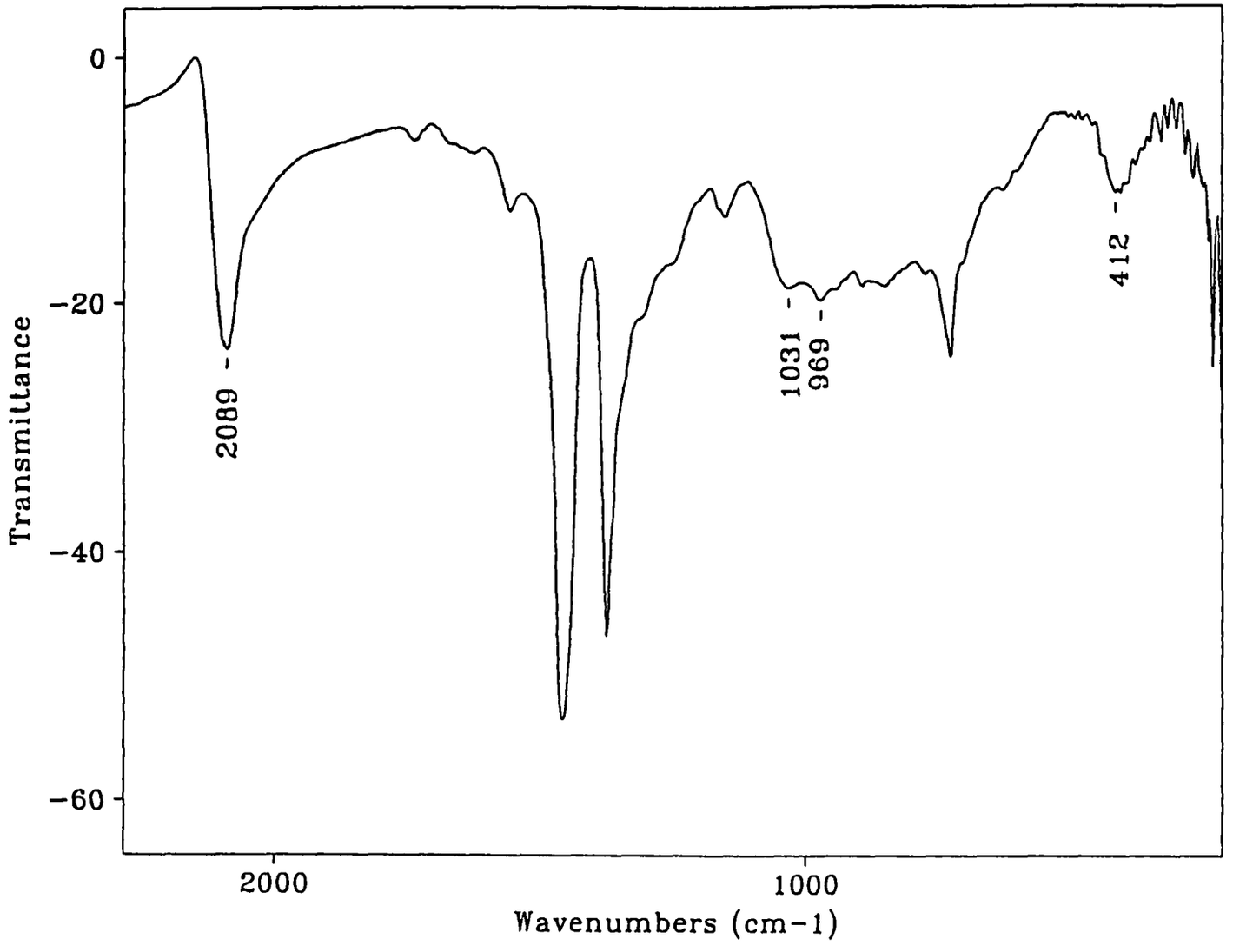

Figure 2. Infrared spectrum (Nujol) for "$WN_{10}C_5H_{7.5}$".

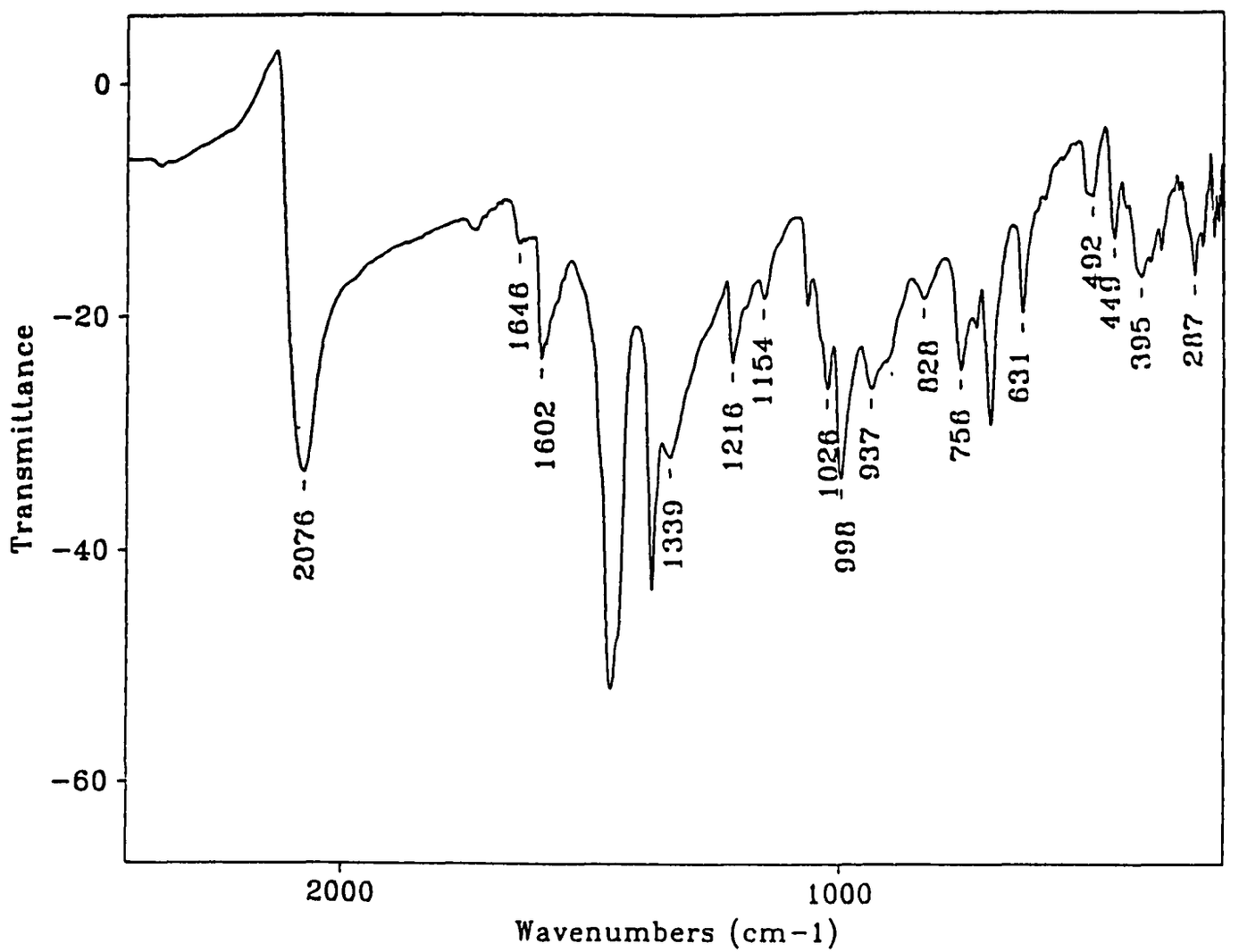

Figure 3. Infrared spectrum (Nujol) for $WN(N_3)Cl_2 \cdot 2Py$.

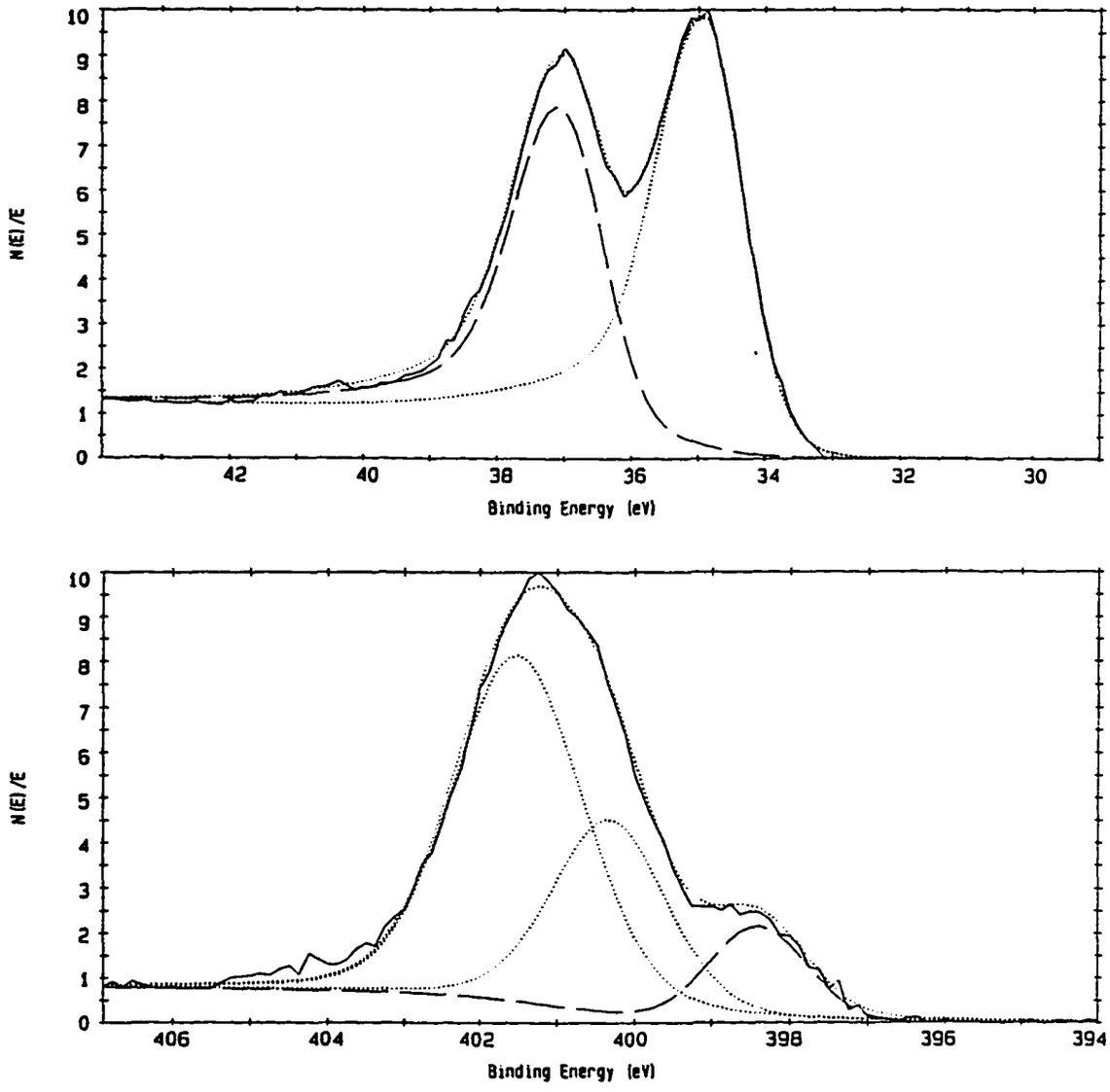

Figure 4. XPS spectra of "$WN_{10}C_5H_{7.5}$", (a) W4f and (b) N1s.

Table 1. XPS binding energies (eV) of $WNCl_3$ and "$WN_{10}C_5H_{7.5}$"

Compound	$W4f_{7/2}$	$W4f_{5/2}$	N1s
$WNCl_3$	34.7	36.8	397.5
"$WN_{10}C_5H_{7.5}$"	33.5	35.7	397.0, 398.9, 400.1

observed in the W4f XPS spectrum. The calibrated binding energies of $W4f_{7/2}$ and $W4f_{5/2}$ are 33.5 and 35.7 eV , respectively. Three types of nitrogen were necessary to fit the N1s XPS spectrum, and the calibrated binding energies of N1s were 397.0, 398.9, and 400.1 eV.

For comparison, Table 1 lists the W4f and N1s binding energies of $WNCl_3$. It is noted that the W4f binding energies of "$WN_{10}C_5H_{7.5}$" are about 1.0 eV lower than the values of $WNCl_3$. This result indicates that the tungsten atom in "$WN_{10}C_5H_{7.5}$" is in an oxidation state lower than +6. The value of 397.0 eV is typical for the N1s binding energy of a nitride (N^{3-}).[10] The N1s binding energy of the bridging nitrogen in azide ($N\text{-}N^{*}\text{-}N$) is always higher than that of the terminal nitrogen atoms ($N^{*}\text{-}N\text{-}N^{*}$). Therefore, the band at 400.1 eV can be assigned as the bridging nitrogen in azide, and the band at 398.9 eV assigned to the terminal nitrogen atoms in azide. The band at 398.9 eV may also be the binding energy of the nitrogen atom in a nitrile by comparison to the binding energy of PhCN (399.2 eV).[10]

Thermal decomposition of $WN(N_3)_3 \cdot xNCCH_3$

Since it was very difficult to recover $WN(N_3)_3 \cdot xNCCH_3$ from the reaction vessels, attempts to thermally decompose this azidotungsten compound in solution seemed like a reasonable idea. However, if the acetonitrile molecules were still coordinated to tungsten, the reaction would not proceed cleanly. Therefore, the acetonitrile must be either removed or replaced by a more unreactive molecule, before conducting the thermal decomposition reaction. Pyridine was chosen to replace acetonitrile. Moreover, the thermal decomposition should be carried out in a more inert solvent with high boiling point.

An attempt to thermally decompose $WN(N_3)_3 \cdot xPy$ in chlorobenzene (b.p. 131°C) was not successful. The azidotungsten nitride was only slightly soluble in chlorobenzene, and thus most of the materials remained in the solid state. *Once the temperature increased, an explosion occurred!*

Fortunately, the azidotungsten nitride pyridine adduct was quite soluble in 1,2-dichlorobenzene (b.p. 186°C). Thermal decomposition of this explosive material was successful in dichlorobenzene, and a black solid was obtained. Both the chlorine and tungsten analyses were obtained on this black solid. The results corresponded to 64.8% tungsten, and less than 1.0% for chlorine. An IR spectrum of the black product is shown in Figure 5. A N-N-N stretching band at 2026 cm^{-1} was observed, which indicated the presence of end-on azide ligand. Therefore, the azide did not completely

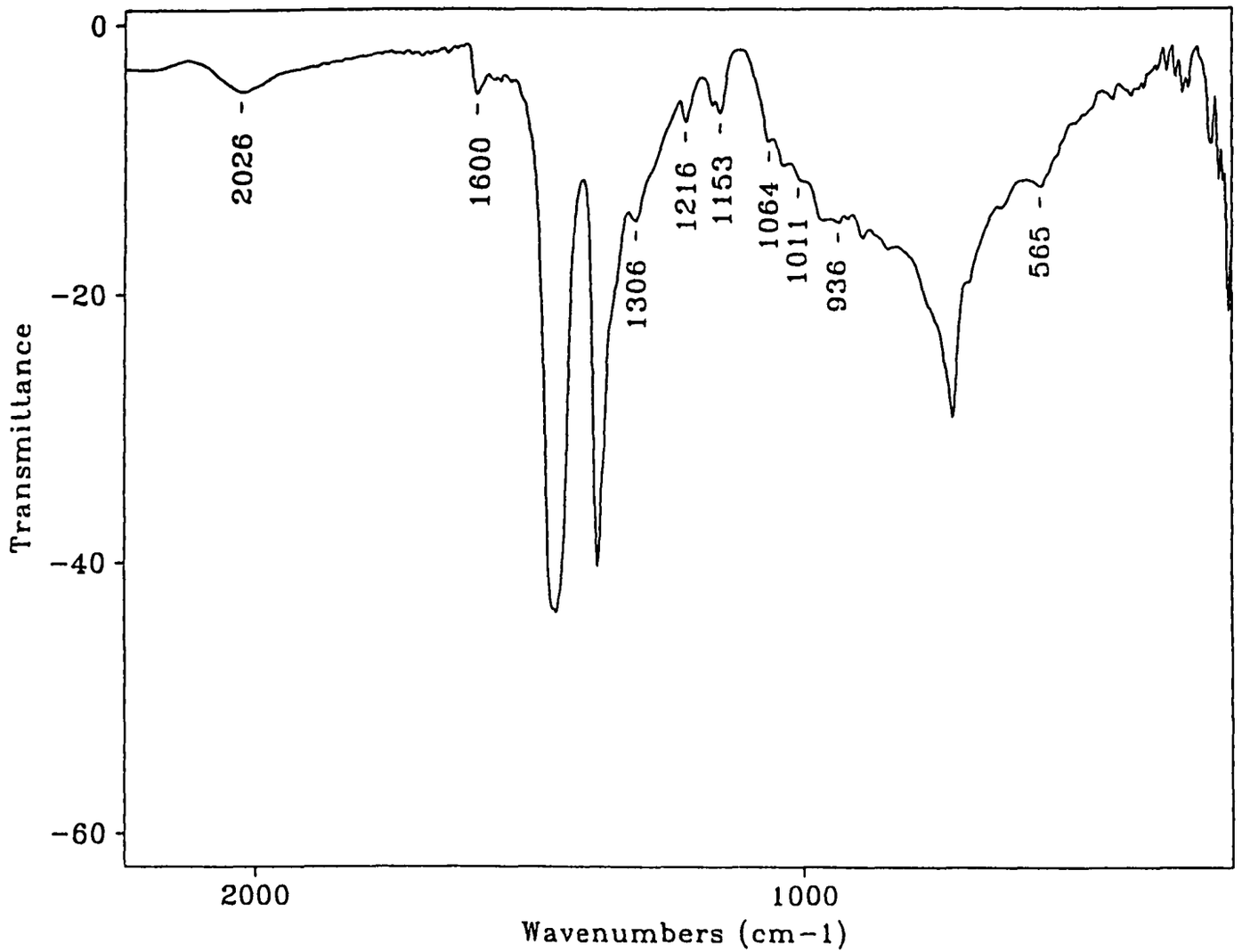

Figure 5. Infrared spectrum (Nujol) for the product from thermal decomposition of $WN(N_3)_3 \cdot xPy$ in 1,2-dichlorobenzene.

Table 2. Results of tungsten analyses for the samples prepared by heating the black solid (obtained from thermal decomposition of $WN(N_3)_3 \cdot xPy$ in 1,2-dichlorobenzene) under dynamic vacuum (5×10^{-3} torr) at different temperatures

Temperature (°C)	Time (h)	W%	Phase
250	4	69.47	amorphous
350	5	74.90	amorphous
500	12	86.1	amorphous
750	12	92.8	Hexagonal WN

decompose in this thermal decomposition reaction. Some bands attributed to coordinated pyridine were also observed (1600, 1216, 1153, 1064, 1011 and 936 cm^{-1}).

In order to decompose the azide completely, and to obtain pure nitride compounds, thermal treatments of the black solid were carried out under dynamic vacuum in a programmable tube furnace. Table 2 lists the thermal decomposition results. The X-ray powder patterns for samples from 500 °C and 750 °C are shown in Figures 6 and 7, respectively.

From Table 2, one can see that the sample from the 750 °C treatment contained 92.8 % of W, which is very close to the calculated value for WN, 92.92%. The X-ray powder pattern of this sample indicated that the sample contained mainly hexagonal WN (or perhaps WN_xC_{1-x}). The sample from the 500 °C treatment contained 86.1%

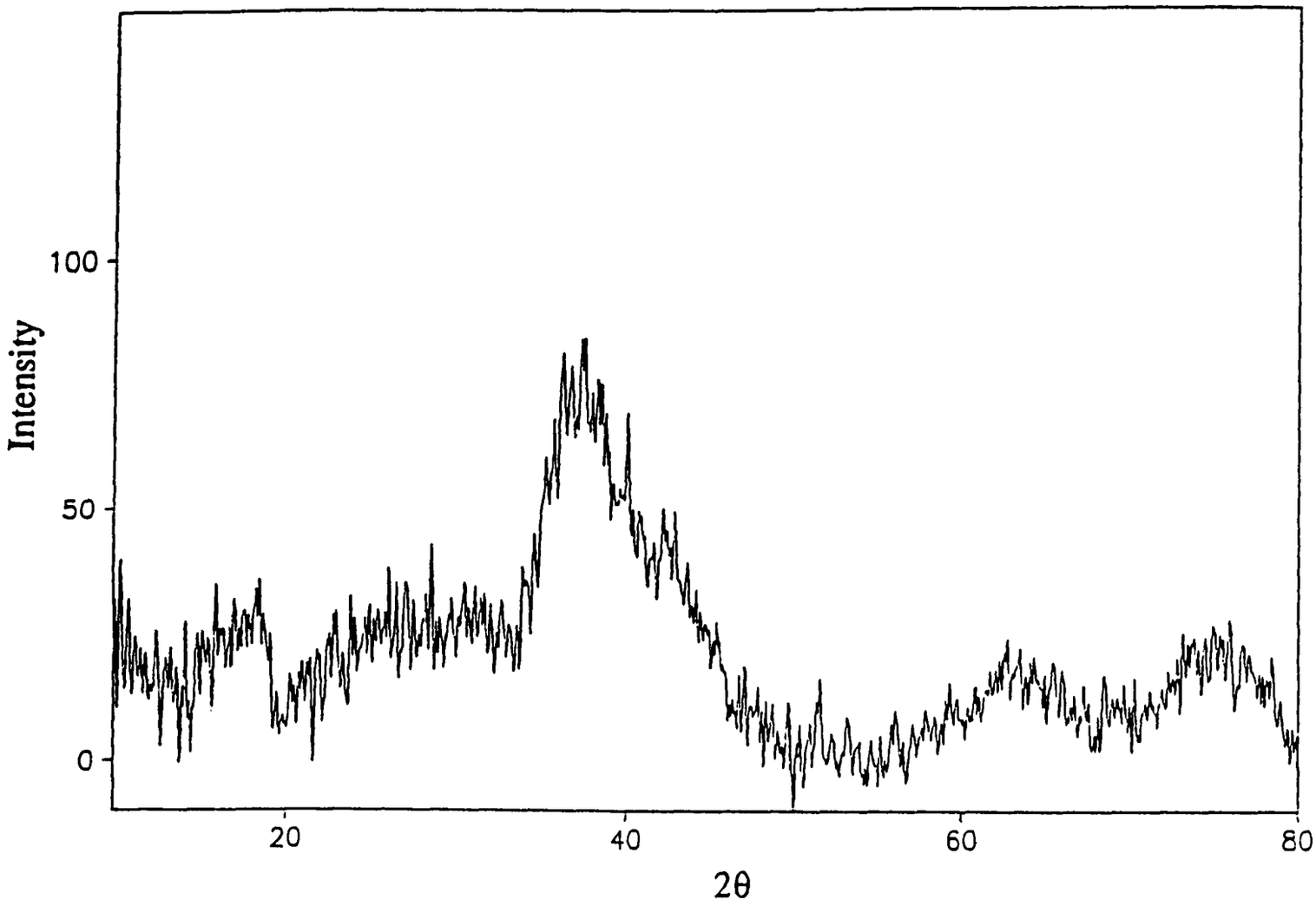

Figure 6. X-ray powder diffraction pattern of the sample prepared by heating the black solid (obtained from thermal decomposition of $WN(N_3)_3 \cdot xPy$ in 1,2-dichlorobenzene) under dynamic vacuum (5×10^{-3} torr) at 500°C.

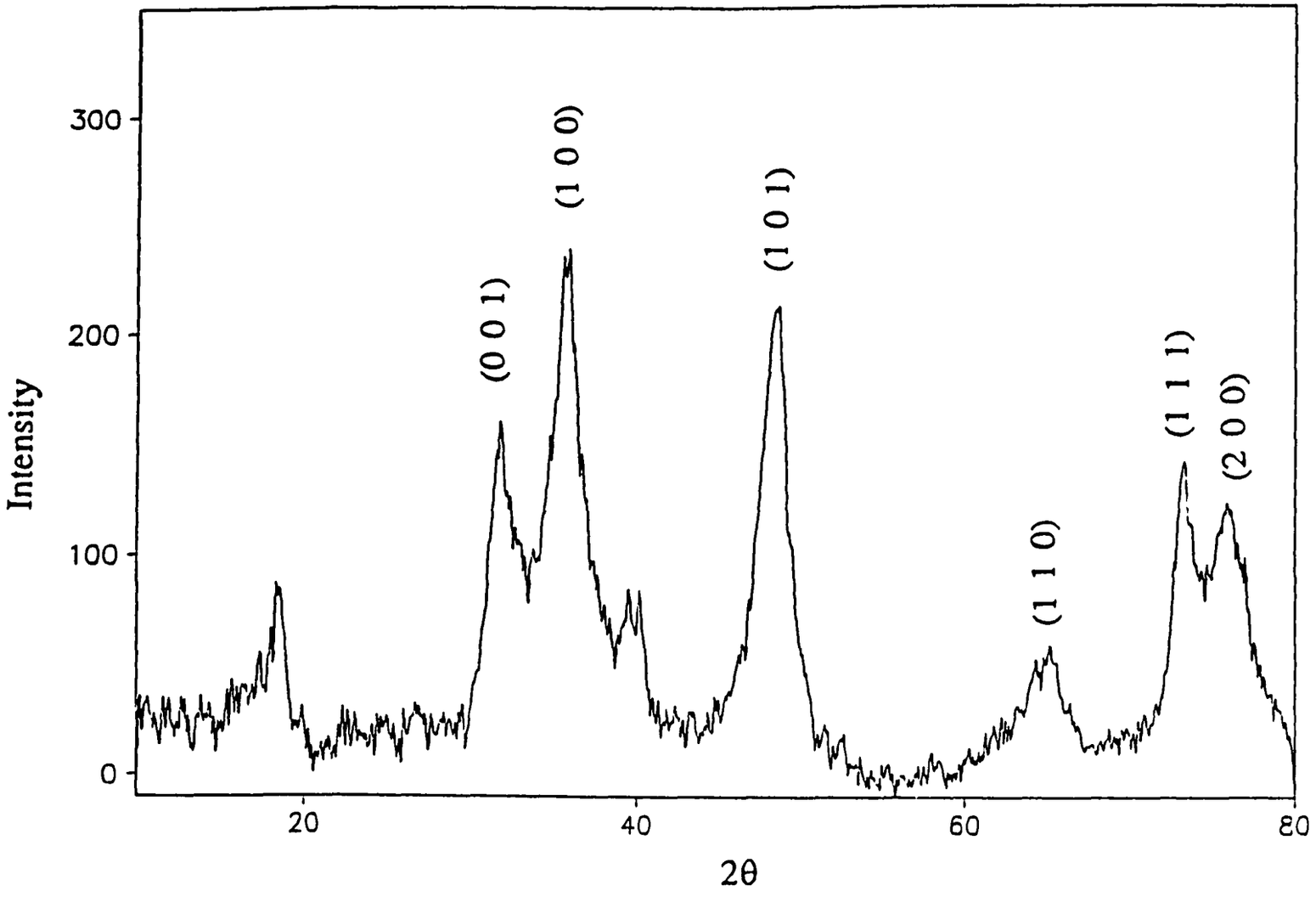

Figure 7. X-ray powder diffraction pattern of the sample prepared by heating the black solid (obtained from thermal decomposition of $WN(N3)_3 \cdot xPy$ in 1,2-dichlorobenzene) under dynamic vacuum (5×10^{-3} torr) at 750°C.

of W, which is very close to the calculated value for WN_2, 86.78%. However, this is an amorphous material as indicated by its X-ray powder diffraction pattern.

Conclusions

This paper describes the preparation and characterization of three molecular precursors to tungsten nitrides, $WN(N_3)_3 \cdot xCH_3CN$, $WN_{10}C_5H_{7.5}$, and $WN(N_3)Cl_2 \cdot 2Py$. The most interesting compound $WN(N_3)_3 \cdot xCH_3CN$ was prepared from the reaction of $WNCl_3$ and NaN_3 in acetonitrile at room temperature. The IR spectrum of this compound indicated that the W≡N multiple bond still remained, and the chloride was completely replaced by azide. However, this compound is extremely explosive, and it can not be isolated from the acetonitrile solution in a large yield.

The reaction of $WNCl_3$ and NaN_3 in refluxing acetonitrile, however, produced a complex with a composition of $WN_{10}C_5H_{7.5}$. The XPS study indicated that the tungsten atom in this complex was in an oxidation state lower than +6.

The reaction of $WNCl_3$ and NaN_3 in refluxing pyridine yielded a complex with a composition of $WN(N_3)Cl_2(Py)_2$. The substitution of chloride by azide was not complete in this reaction.

By replacement of CH_3CN with Py in $WN(N_3)_3 \cdot xCH_3CN$, the thermal decomposition of $WN(N_3)_3 \cdot xPy$ was successful in refluxing 1,2-dichlorobenzene (b.p.

186°C). However, the azide did not decompose completely as noted by a band at ~2030 cm^{-1} in the IR spectrum of the product. Further thermal treatments were carried out under dynamic vacuum in a programmable tube furnace on the product obtained from refluxing 1,2-dichlorobenzene. An amorphous phase was produced at 500°C. This amorphous phase had a composition close to WN_2 based on the tungsten analysis. Furthermore, a hexagonal WN phase was observed in the product obtained at 750°C.

References

1. Toth, L. E. *Transition Metal Carbides and Nitrides*, Academic Press, NY, **1971**.
2. Brese, N. E.; O'Keeffe, M. *Structure and Bonding*, **1992**, *79*, 307.
3. Stein, A.; Keller, S. W.; Mallouk, T. E. *Science*, **1993**, *259*, 1558.
4. (a) Baxter, D. V.; Chisholm, M. H.; Gama, G. J.; DiStasi, V. F.; Hector, A. L.; Parkin, I. P. *Chem. Mater.* **1996**, *8*, 1222.

   (b) Holl, M. M. B.; Wolczanski, P. T.; Proserpio, D.; Bielecki, A.; Zax, D. B. *Chem. Mater.* **1996**, *8*, 2468.
5. Close, M. R.; McCarley, R. E. *Inorg. Chem.* **1994**, *33*, 4198.

6. Zhang, Z. *Ph. D. Dissertation*, Iowa State University, **1997**.

7. Dehnicke, K.; Strähle, J. *Angew. Chem. Int. Ed. Engl.* **1981**, *20*, 413.

8. Finnegan, W. G.; Henry, R. A.; Lofquist, R. *J. Amer. Chem. Soc.* **1958**, *80*, 3908.

9. Dehnicke, K.; Prinz, H.; Kafitz, W.; Kujanek, R. *Liebigs Ann. Chem.* **1981**, 20.

10. (a) Moulder, J. F.; Stickle, W. F.; Sobol, P. E.; Bomben, K. D. *Handbook of X-ray Photoelectron Spectroscopy*, Chastain, J. Ed,; Perkin-Elmer Corp.: Eden Prairies, MN, **1992**.

    (b) Colton, R. J.; Rabalais, J. W. *Inorg. Chem.* **1976**, *15*, 236.

CHAPTER 3. SYNTHESIS AND CHARACTERIZATION OF NOVEL TUNGSTEN NITRIDES AND CARBIDE NITRIDES

A paper to be submitted to Chemistry of Materials

Zhihong Zhang and Robert E. McCarley

Abstract

A new bulk solid phase of tungsten nitride W_3N_5 has been prepared through solid state reactions between $WNCl_3$ and Zn_3N_2 in sealed Pyrex tubes at 400 °C. The XPS study indicated that the oxidation state of tungsten in this amorphous phase was +5. Heating W_3N_5 at 600°C in sealed quartz tubes yielded a cubic tungsten mononitride phase (WN) with rock salt structure (a = 4.171 Å). Heating W_3N_5 at 800 °C in sealed quartz tubes produced the hexagonal WN phase and tungsten metal. At the same time, a few golden crystals were also obtained, which were grown via a chemical vapor transport reaction. The golden compound $W_2N_2(C_2N_2)$ crystallizes in the monoclinic system, space group *I2/a* (#15, nonstandard setting) with a = 5.6521(9) Å, b = 4.889(1) Å, c = 9.576(1) Å, β = 90.20(1)°, V = 264.6(1) Å^3, Z = 4, R = 0.035, and Rw = 0.042. The structure of $W_2N_2(C_2N_2)$ consists of W_2 dimers, hydrazido ligands N_2^{4-}, and 1,4-diazabutenido ligands represented by three resonance structures, $[N\text{-}C{=}C\text{-}N]^{6-}$, $[N{=}C\text{-}C\text{-}N]^{6-}$, and $[N\text{-}C\text{-}C{=}N]^{6-}$. The metal to hydrazido nitrogen bond distances fall

in the range 1.97(4) to 2.19(4) Å, and the metal-diazabutenido nitrogen distances show a more limited range from 2.01(4) to 2.07(3) Å. The hydrazido N-N distance is 1.43(5) Å, and the diazabutenido C-C distance is 1.59(4) Å. The W-W single bond distance is 2.767(2) Å. The magnetic susceptibility measurements over the range 6-300 K indicated that the cubic WN was basically diamagnetic and not a superconductor above 6 K. The electronic structure calculations suggested, however, that this cubic phase might exhibit superconductivity because of the high density of states at the Fermi level.

Introduction

The binary nitride compounds of Group VI elements are characterized by thermodynamic instability towards dissociation to N_2 and the N-saturated element at high temperatures.[1] Thermodynamic studies on Mo_2N indicated that the Gibbs free energy change of formation of Mo_2N increased with the increase of temperature.[2-3] Therefore, only a few binary nitrides of Group VI metals have ever been found, even though considerable synthetic efforts using high temperature solid state reactions have been devoted to preparing these binary nitrides.[1,4]

As for binary tungsten nitrides, although a number of hexagonal tungsten nitrides with the metal in oxidation states higher than +3 have been reported, these binary

nitrides can only be prepared as thin films and observed by electron microscopy. For example, WN_2 with a hexagonal supercell (a = 2.89 Å and c = 16.4 Å) was observed as a brown coating on W filaments.[5] W_3N_5 was also observed as a thin film,[6] and has a hexagonal supercell with a = 2.89 Å and c = 10.8 Å. No bulk tungsten nitride phases with oxidation states of the metal higher than +3 have ever been prepared using high temperature solid state synthesis.

The bulk solid phases of molybdenum and tungsten nitrides, MN and M_2N (M = Mo, W) with the metals in oxidation states +3 or lower than +3, were prepared by flowing NH_3 over metals at high temperatures.[7] For example, tungsten mononitride (WN) was reported to have a hexagonal WC structure type with a = 2.893 Å and c = 2.826 Å.

It has been known that most early transition metal mononitrides with rock salt structure exhibit superconductivity.[8] For example, NbN shows superconductivity at 17.3K. However, cubic molybdenum and tungsten mononitrides with rock salt structure, which may exhibit superconductivity,[8-9] have not yet been reported. Cubic MoN with rock salt structure was predicted to be a superconductor with the value of T_c as high as 29K,[9] even though this compound is unknown.

Recently, new synthetic techniques of converting molecular precursors to the target products under more gentle conditions have been explored.[10-11] Parkin and co-workers attempted to convert metal halides to nitrides, which was successful for most

early transition metals, but not for the Group VI metals. They attempted to convert $MoCl_3$ and WCl_4 to the nitrides by reaction with magnesium or calcium nitride at 500 °C. However, only the metals were obtained.[11] Our synthetic strategy to prepare binary tungsten nitrides involved the conversion of molecular precursor $WNCl_3$ and related compounds to nitrides through metathetical reactions with other metal nitrides at relatively low temperatures.

In this paper, a bulk solid tungsten nitride phase W_3N_5, which was prepared by a solid state metathetical reaction between $WNCl_3$ and Zn_3N_2 at relatively low temperature, will be reported. A cubic tungsten mononitride phase and a tungsten carbide nitride $W_2N_2(N_2C_2)$ with a novel three dimensional network structure will be reported as well.

Experimental

Materials

Most reagents are air and moisture sensitive. Manipulations of oxygen- and water-sensitive materials were performed under inert-atmosphere conditions using standard drybox, high vacuum manifold, and Schlenk techniques.

Acetonitrile (MeCN) and 1,2-dichloroethane (DCE) were dried by standard

methods using CaH_2 as a drying reagent. Zn_3N_2 was obtained from Alfa Chemical Co, and was used as received. Trimethylsilyl azide was obtained from Aldrich Chemical Company, Inc., and used as received. $WNCl_3$ was prepared as described in literature.[12]

Analytical Procedures

Tungsten analysis

Gravimetric determination of W was accomplished by conversion of samples to the trioxide via addition of an oxidizing solution in a tared crucible. Samples were initially treated with dilute (3M) nitric acid and then with concentrated nitric acid. The crucibles were gently heated (~100 °C) on a hot plate to slowly evaporate the solution. Once the solution was evaporated, the temperature of the hot plate was increased (~150 °C), and the crucibles were heated at this temperature until the samples became yellow. The crucibles were heated at 800 °C in a muffle furnace until constant weights were achieved.

Chlorine analysis

Chlorine was determined by the potentiometric titration of neutralized solutions of dissolved sample with a standardized $AgNO_3$ solution. Ag/AgCl was used as the working electrode and a silver electrode as the reference. Samples were dissolved in

a basic solution (KOH) with 30 % H_2O_2, and gently heated on a hot plate. The clear solutions were then neutralized with 3N nitric acid to pH ~ 6-7.

Physical Measurements

X-ray powder diffraction

X-ray powder diffraction data were obtained from a Phillips ADP3520 X-ray powder diffractometer using Cu $K\alpha_1$ radiation (λ = 1.54056 Å).

X-ray photoelectron spectroscopy

XPS spectra were collected at room temperature with a Physical Electronics Industries 5500 multitechnique surface analysis system. This system was equipped with a hemispherical analyzer, a toroidal monochromator, and multichannel detector which sampled a 2 mm^2 area. The samples were pressed on to an indium substrate and loaded into an air-sensitive sample holder in the drybox. The sample holder was then transferred to the chamber of the spectrometer. After the system was completely evacuated, the sample holder was opened and the sample was excited with monochromatic Mg K_α radiation (1253.6 eV) at the power of 300 W. The photoelectron binding energies (BE's) were calibrated with C 1s emission, BE = 284.6 eV.

Magnetic susceptibility measurements

Magnetic susceptibilities were measured with a Quantum Design SQUID magnetosusceptometer. The samples were prepared by sealing 20-50 mg of material in a quartz tube (3mm ID, 4mm OD, and 17mm L) under a helium atmosphere (less than 0.1 torr). The data were collected over the temperature range of 4-300 K at 3 tesla.

Synthetic Procedures

Caution. The following preparations are exothermic, and involve releasing nitrogen gas. Care should be taken to do reactions with adequate safety precautions. It is important to calculate the pressure generated by the nitrogen gas byproduct before performing any reactions, since high gas pressure can lead to explosions. It is also important to use a programmable furnace, and increase reaction temperature slowly (1-2°/min) when conducting any reactions.

Preparation of W_3N_5

In a typical preparation of W_3N_5, 0.288 g (0.95 mmol) of $WNCl_3$ and 0.106 g (0.473 mmol) of Zn_3N_2 were mixed in the drybox (in order to avoid explosion, $ZnCl_2$ (50%, weight) can be added into the reaction mixture, if it is necessary), and loaded into a Pyrex tube (8 mm ID, 10 mm OD, 100 mm length). The tube was then sealed

under dynamic vacuum, and placed into a programmable tube furnace. The temperature was increased at a rate of 2 °C/min to 400 °C, and held at 400 °C for 48 hours. A black solid mixed with some white solid ($ZnCl_2$) was obtained. The white solid was removed by washing the solid mixture with acetonitrile. Chlorine analyses indicated that less than 0.5% remained in the samples. Tungsten analysis was obtained on the black solid and found to match the tungsten nitride with a composition of W_3N_5. Anal. Calcd for W_3N_5: W, 88.73%. Found: W, 88.85%.

Preparation of cubic WN

0.25 g of W_3N_5 was loaded into a quartz tube (8-mm OD, 6-mm ID, and 150-mm long) in the drybox. The tube was then sealed under dynamic vacuum, and placed into a tube furnace. The reaction was fired at 600 °C for 2 days. A black solid was obtained. Anal. Calcd for WN: W, 92.92%. Found: W, 92.26%.

Single crystal growth of $W_2N_2(N_2C_2)$

0.1 g of W_3N_5 was weighed in a drybox and transferred into a quartz tube (10 mm OD, 8 mm ID, and 80mm length). The tube was sealed under dynamic vacuum ($< 5.0 \times 10^{-3}$ torr), and then placed into a programmable tube furnace. The temperature was increased at a rate of 5 °C/min to 800 °C, and held there for 3-4 days. A few golden crystals were found in the cool zone of the tube. The residual black

powder, examined by X-ray powder diffraction, contained tungsten metal and hexagonal tungsten mononitride (WN).

Electronic Structure Calculations

All electronic structure calculations were of the extended Hückel tight-binding type.[13] The observed lattice parameters of cubic WN were obtained by X-ray powder diffraction. Atomic orbital parameters for all atoms, listed in Table 1, and charge iteration parameters for W and N were taken from standard sources.[14] DOS and COOP curves were evaluated using 465 k-points sets.

Table 1. Atomic Parameters Used in the Extended Hückel Calculations

atom	orbital	H_{ii}(eV)	ζ_1	C_1	ζ_2	C_2
W	6s	-8.26	2.34			
	6p	-5.17	2.31			
	5d	-10.37	4.98	0.6683	2.070	0.5422
N	2s	-26.00	1.95			
	2p	-13.40	1.95			

X-ray Structure Determination

A suitable golden single crystal with dimensions of 0.10 x 0.06 x 0.01 mm^3 was selected from the transported reaction product. The crystal was then encased in epoxy

resin while in a glove bag under a nitrogen flow, attached to the tip of a glass fiber, and sealed in a glass capillary. All measurements were made on a Rigaku AFC6R diffractometer with graphite monochromated Mo Kα (λ = 0.71069 Å) radiation and a 12 KW rotating anode generator.

Cell constants and an orientation matrix for data collection, obtained from a least-squares refinement using the setting angles of 19 carefully centered reflections in the range $11.0 < 2\theta < 30.0$, corresponded to monoclinic cell with cell parameters: a = 5.6521(9) Å, b = 4.889(1) Å, c = 9.576(1) Å, β = 90.20(1)°, and V = 264.6(1) Å^3. The data were collected at room temperature using the ω-2θ scan technique over the range $4° < 2\theta < 65°$ in the hemisphere ($\pm h$, $+k$, $\pm l$). Three standard reflections were monitored every 150 reflections and showed no intensity variation over the collection period. A total of 2121 reflections were collected, of which 1064 were unique (R_{int} = 0.104) and 148 of which were observed with $I > 3.00\sigma(I)$. No Decay correction was applied. With an absorption coefficient for Mo Kα radiation of μ = 885.1 cm^{-1}, an empirical absorption correction using the ψ scan technique was applied after the structure solution. The data were corrected for Lorentz and polarization effects.

The monoclinic space group was *I2/a* (#15, non-standard setting) was chosen on the basis of systematic absences and intensity statistics. The structure was solved by the SHELXS direct methods[15a] which yielded the positions of the tungsten atoms. Successive Fourier electron difference maps yielded the positions of the nitrogen

atoms. The structure was then refined by full-matrix least-squares methods with anisotropic thermal parameters on all non-hydrogen atoms. The final cycle of full-matrix least-squares refinement was based on 148 observed reflections and 19 variable parameters and converged with unweighted and weighted agreement factors of R = 0.044 and Rw = 0.054, respectively. The asymmetric unit was found to be WN_2.

However, the maximum peak in the final difference Fourier map was still relatively large (5.48e$^-$/Å^3). By refining this maximum peak as a carbon atom, isotropic refinement was successful. An empirical absorption correction using the DIFABS program[15b] was then applied, resulting in relative transmission factors ranging from 0.78 to 1.16. The final cycle of full-matrix least-squares refinement was based on 148 observed reflections and 23 variable parameters and converged with unweighted and weighted agreement factors of R = 0.035, and Rw = 0.042, and the maximum peak in the final difference Fourier map decreased to 2.69e$^-$/Å^3. The asymmetric unit was then WCN_2. All calculations were performed using the TEXSAN[15c] crystallographic software package of Molecular Structure Corporation.

The crystallographic data and refinement results are given in Table 2, Positional parameters and isotropic equivalent temperature factors are given in Table 3. The anisotropic temperature factors are listed in Table 4.

Table 2. Crystallographic data for $W_2N_2(N_2C_2)$

Empirical Formula	$W_2N_4C_2$
Formula Weight	447.75
Crystal Size	0.10 x 0.03 x 0.01 mm^3
Crystal System	monoclinic
Space Group	I2/a (#15, non-standard setting)
Lattice Parameters	a = 5.6521(9) Å
	b = 4.889(1) Å
	c = 9.576(1) Å
	β = 90.20(1)°
Volume	264.6(1) $Å^3$
Z Value	4
Calculated Density	11.237 g/cm^3
F_{000}	752
μ(MoKα)	885.11 cm^{-1}
Diffractometer	Rigaku AFC6R
Radiation	MoKα (λ = 0.71069Å)
Temperature	23 °C
Two-theta Range	0-65°
Scan Mode	ω-2θ
No. of Reflections Collected	1064
No. Observations (I > 3.00σ(I))	148
No. Variables	23
Max Shift/error in Final Cycle	0.03
Goodness of Fit[a]	1.64
Max. and Min. Peaks in the Final Diff. Map	2.69, -3.13 $e^-/Å^3$
Residuals[b]	R = 0.035, Rw = 0.042

[a] Goodness of Fit = $[\Sigma\omega\{|F_o| - |F_c|\}^2/\{N_{obs} - N_{parameters}\}]^{1/2}$

[b] $R = \Sigma \; | \; |Fo| - |Fc| \; | \; / \; \Sigma \; |Fo|$; $Rw = [(\Sigma \; w \; (|Fo| - |Fc|)^2 \; / \; \Sigma \; w \; Fo^2)]^{1/2}$.

Table 3. Atomic coordinates and equivalent isotropic thermal parameters ($Å^2$) of the atoms for $W_2N_4C_2$

atom	x	y	z	B_{eq}[a]
W	0.3987(2)	0.2421(4)	0.1151(1)	0.27(5)
N1	0.668(3)	0.471(8)	0.056(2)	0.1(3)
N2	0.402(4)	0.441(6)	0.305(2)	0.3(4)
C	0.655(4)	0.299(7)	0.301(3)	0.4(4)

[a] $B_{eq} = 8/3\pi^2(U_{11}(aa^*)^2 + U_{22}(bb^*)^2 + U_{33}(cc^*)^2 + 2U_{12}aa^*bb^*\cos\gamma + 2U_{13}aa^*cc^*\cos\beta + 2U_{23}bb^*cc^*\cos\alpha)$

Table 4. Anisotropic thermal parameters[a] ($Å^2$) of the atoms for $W_2N_2(N_2C_2)$[b]

Atom	U_{11}	U_{22}	U_{33}	U_{12}	U_{13}	U_{23}
W	0.0034(6)	0.0030(7)	0.0037(6)	0.002(1)	-0.0003(3)	0.001(1)
N1	0.001(4)					
N2	0.003(4)					
C	0.005(5)					

[a] The coefficients U_{ij} of the anisotropic temperature factor expression are defined as $\exp(-2\pi^2(a^{*2}U_{11}h^2 + b^{*2}U_{22}k^2 + c^{*2}U_{33}l^2 + 2a^*b^*U_{12}hk + 2a^*c^*U_{13}hl + 2b^*c^*U_{23}kl))$

[b] Thermal parameters for N1, N2, and C only refined isotropically.

Results and Discussion

Synthesis of W_3N_5

Metathetical reactions between Group VI metal chlorides and Group II metal nitrides at elevated temperature (> 500 °C) were attempted by Hector and Parkin.[11] In both cases, however, no metal nitrides were obtained. Instead, pure metals were the products. The reactions indicated that the Group VI metal nitrides could not be prepared by metathetical solid state reactions at reaction temperature higher than 500 °C. Therefore, reactions between $WNCl_3$ and Zn_3N_2 at a relatively lower temperature range (300-500 °C) were attempted in sealed pyrex tubes.

The intended reaction was

$$2WNCl_3 + Zn_3N_2 \xrightarrow{400°C} 2WN_2 + 3ZnCl_2$$

However, due to the instability of the tungsten nitride compounds, WN_2 was not formed; instead, an amorphous compound W_3N_5 was produced. The composition of W_3N_5 was derived from the tungsten analysis. A pressure build-up was noted inside the reaction tube after the reaction, which indicated that N_2 was released during the reaction. Therefore, the reaction can be expressed as

$$6WNCl_3 + 3Zn_3N_2 \xrightarrow{400°C} 2W_3N_5 + N_2 + 9ZnCl_2$$

Other nitriding reagents, such as Mg_3N_2, Ca_3N_2, Cu_3N and AlN, were also attempted, however, the reactions were not successful.

Synthesis of cubic WN

The thermal treatment of W_3N_5 in sealed, evacuated quartz tube at 600 °C resulted in the thermal decomposition of W_3N_5 to a cubic phase. Again pressure built-up was noted inside the reaction tube. The tungsten analysis gave a result of 92.6%, which is very close to the composition of WN. The thermal decomposition reaction can be expressed as

$$W_3N_5 \xrightarrow{600°C} 3WN + N_2$$

With respect to hexagonal WN and elemental W, the cubic WN is a metastable phase. Upon annealing the cubic WN at 800 °C, the cubic phase partially transformed to the hexagonal phase, and partially decomposed to elemental tungsten.

Synthesis of $W_2N_2(N_2C_2)$ via chemical transport reaction

The thermal treatment of W_3N_5 in a sealed, evacuated quartz tube at 800 °C resulted in the thermal decomposition of W_3N_5 to hexagonal WN as well as W metal. The products were identified by X-ray powder diffraction. The X-ray powder pattern is shown in Figure 1. The pressure also built up inside the reaction tube after the

reaction. Therefore, the reaction of thermal decomposition of W_3N_5 at 800 °C could be expressed as

$$W_3N_5 \xrightarrow{800°C} 3WN + N_2$$

$$W_3N_5 \xrightarrow{800°C} 3W + 5/2N_2$$

When annealing W_3N_5 in the sealed quartz tube at 800 °C, a few golden crystals were formed in the cool zone of the tube. The temperature difference between the hot and cool zone was about 50 °C. It is believed that this temperature difference caused the formation of the golden crystals via a chemical transport reaction, even though the mechanism of the chemical transport reaction has not yet been understood. The golden crystal was characterized as $W_2N_2(N_2C_2)$ by X-ray single crystal diffraction.

The reaction was repeatable. More than 20 reactions were conducted. The yield of the golden compound, however, was always low (a few crystals). In order to improve the yield of the golden compound, $W_2N_2(N_2C_2)$, several different reactions were attempted. For example, the additions of carbon, cyanides, ethylenediamine, and dichloroethane, to the reaction mixture were explored. However, the yield could not be improved. Additions of NH_3, NH_4Cl, and $WNCl_3$ as transport reagents were also attempted, but unfortunately, the yield was not improved either.

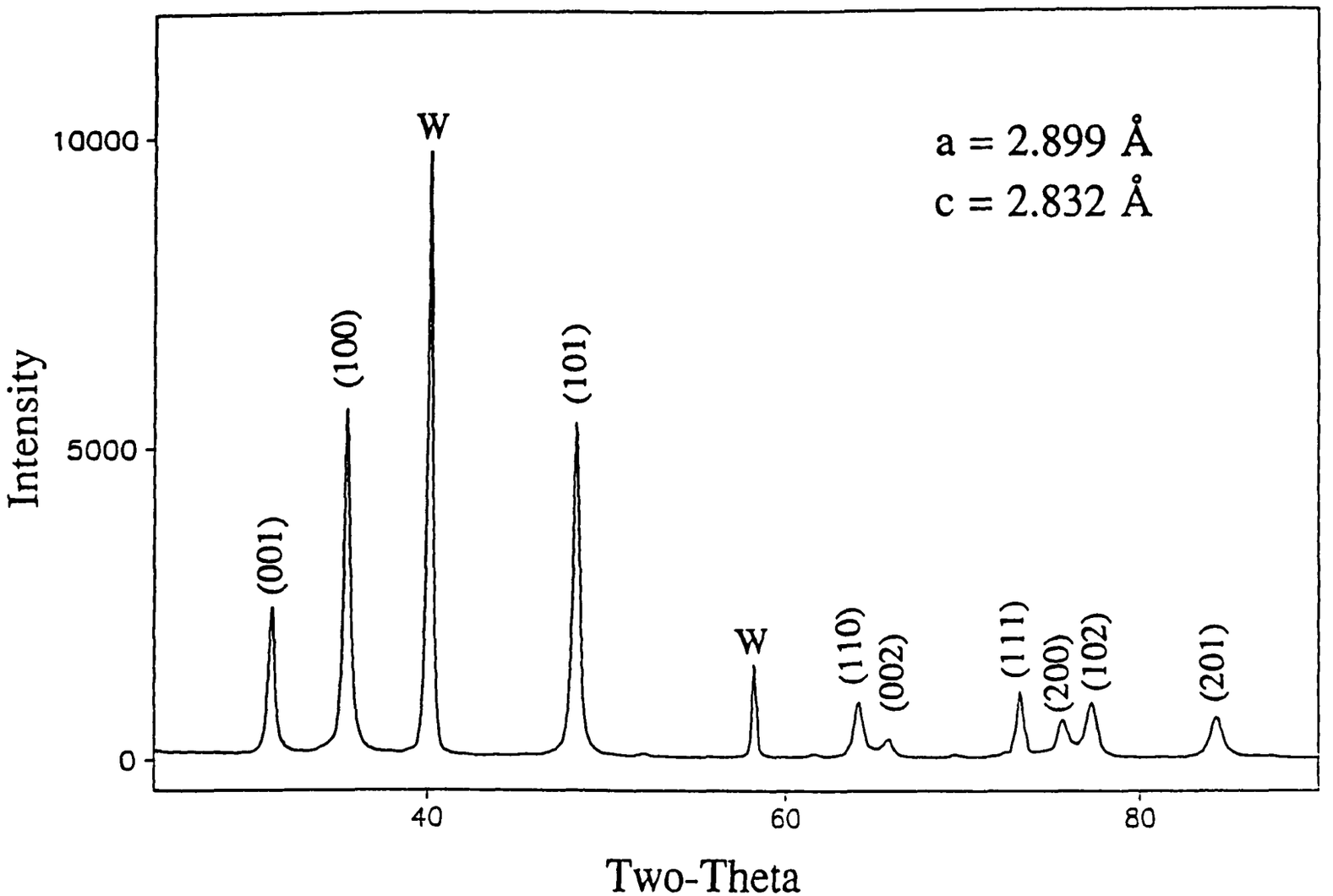

Figure 1. X-ray powder diffraction pattern of WN and W mixture obtained from the reaction of annealing W_3N_5 at 800°C.

X-ray powder diffraction of cubic WN

The X-ray powder diffraction pattern of the cubic phase WN is shown in Figure 2. The broad reflection peaks may be due to either the small sizes of particles or poor crystallization of the sample. The indexed lines of the powder diffraction pattern are given in Table 5. The cubic phase, WN, has the NaCl structure with a = 4.171 Å, which is smaller than the cell of the known cubic WC superconductor phase (a = 4.266 Å)[16]. For comparison, the calculated d spacings of cubic WN and the observed d spacings of cubic WC are also listed in Table 5.

Table 5. X-ray powder diffraction data for cubic WN (a = 4.171 Å) and WC (a = 4.266 Å) with NaCl structure

	WN		WC
h k l	d_{obv}	d_{cal}	d_{cal}
1 1 1	2.408	2.408	2.463
2 0 0	2.082	2.086	2.133
2 2 0	1.472	1.475	1.508
3 1 1	1.256	1.258	1.286
2 2 2	1.207	1.204	1.231

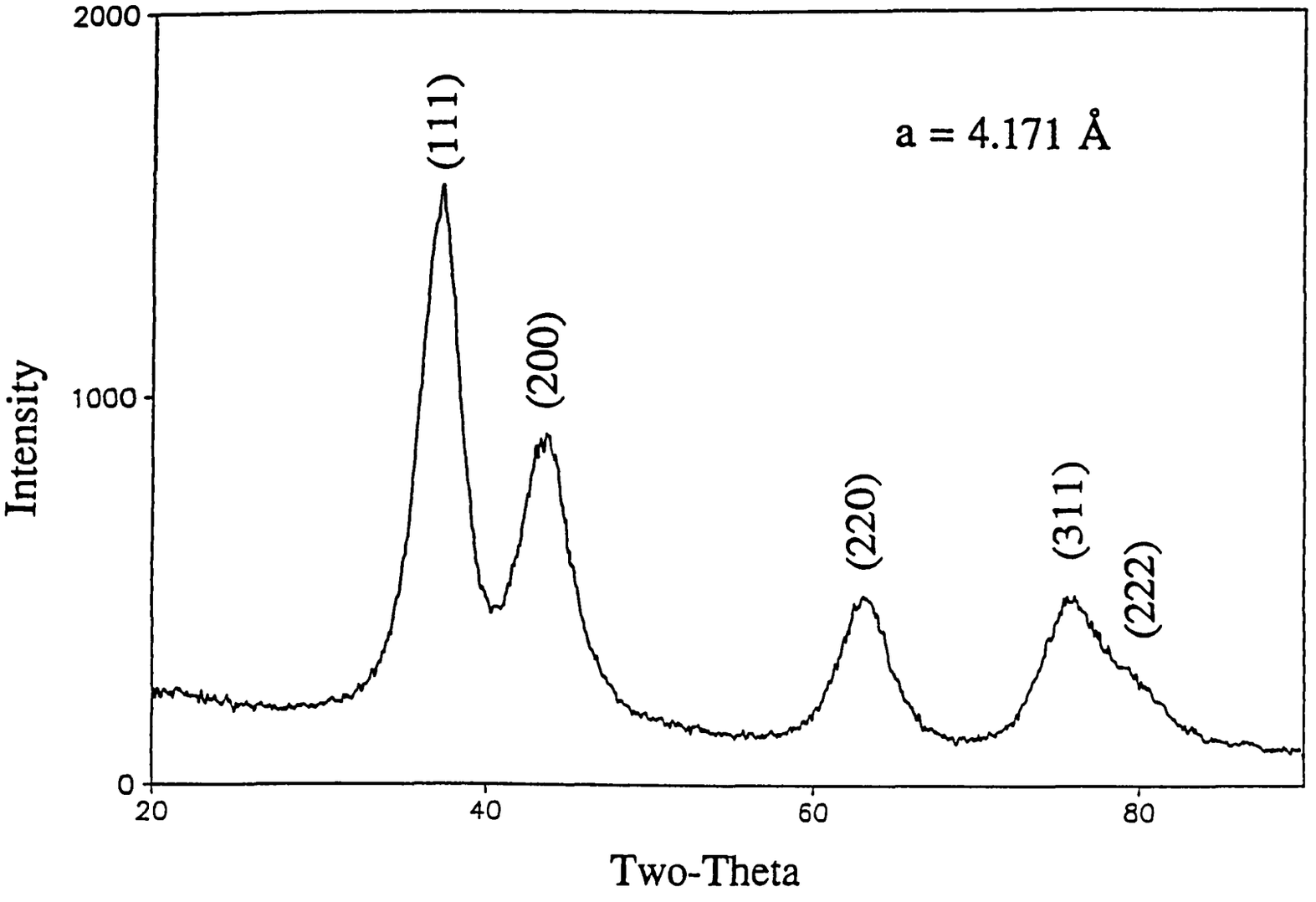

Figure 2. X-ray powder diffraction pattern of cubic WN with NaCl structure.

Structure description of $W_2N_2(N_2C_2)$

An ORTEP drawing of the structure of $W_2N_2(N_2C_2)$ projected along the b axis is shown in Figure 3. It is seen that the structure consists of a network of dimers $W_2(N_2)_{3/3}(N_{3/3}C_{2/2}C_{2/2}N_{3/3})$, where the two bonded W atoms (d = 2.768(2) Å) are bridged by a N-N (N1) group in a μ-η^2,η^2 manner. Each N atom (N1) of the bridging N-N group also is bonded to one W atom of a neighboring dimer. The other N atom (N2) binds to a tungsten atom in each of three different dimers, while the C atom only binds to a tungsten atom in each of two different dimers. The N2 and C atoms form a N-C-C-N group. The two W atoms of any two neighboring dimers are bridged by a C-N (N2) group in a μ-η^2,η^2 manner as well. The dimers are linked together by the N-N and N-C-C-N groups to form a 3-dimensional network. Figure 4 shows the coordination environment of the W_2 dimer core in $W_2N_2(N_2C_2)$.

In the $W_2N_2(N_2C_2)$ structure, the W-W bond length is 2.768(2) Å, which is a typical W-W single bond distance. Therefore, the tungsten atoms in the structure are probably in the oxidation state of V. The bond length of N-N in bridging N-N group is 1.43(3) Å, which is a typical N-N single bond distance. Thus, the bridging N-N group can be considered as a hydrazido ligand, N_2^{4-}. The N-C-C-N group then can be considered as a 1,4-diazabutenido ligand with bonding represented by three resonance structures, $[N\text{-}C{=}C\text{-}N]^{6-}$, $[N{=}C\text{-}C\text{-}N]^{6-}$, and $[N\text{-}C\text{-}C{=}N]^{6-}$.

Figure 5 shows the coordination sphere of the tungsten atom (W1). Selected

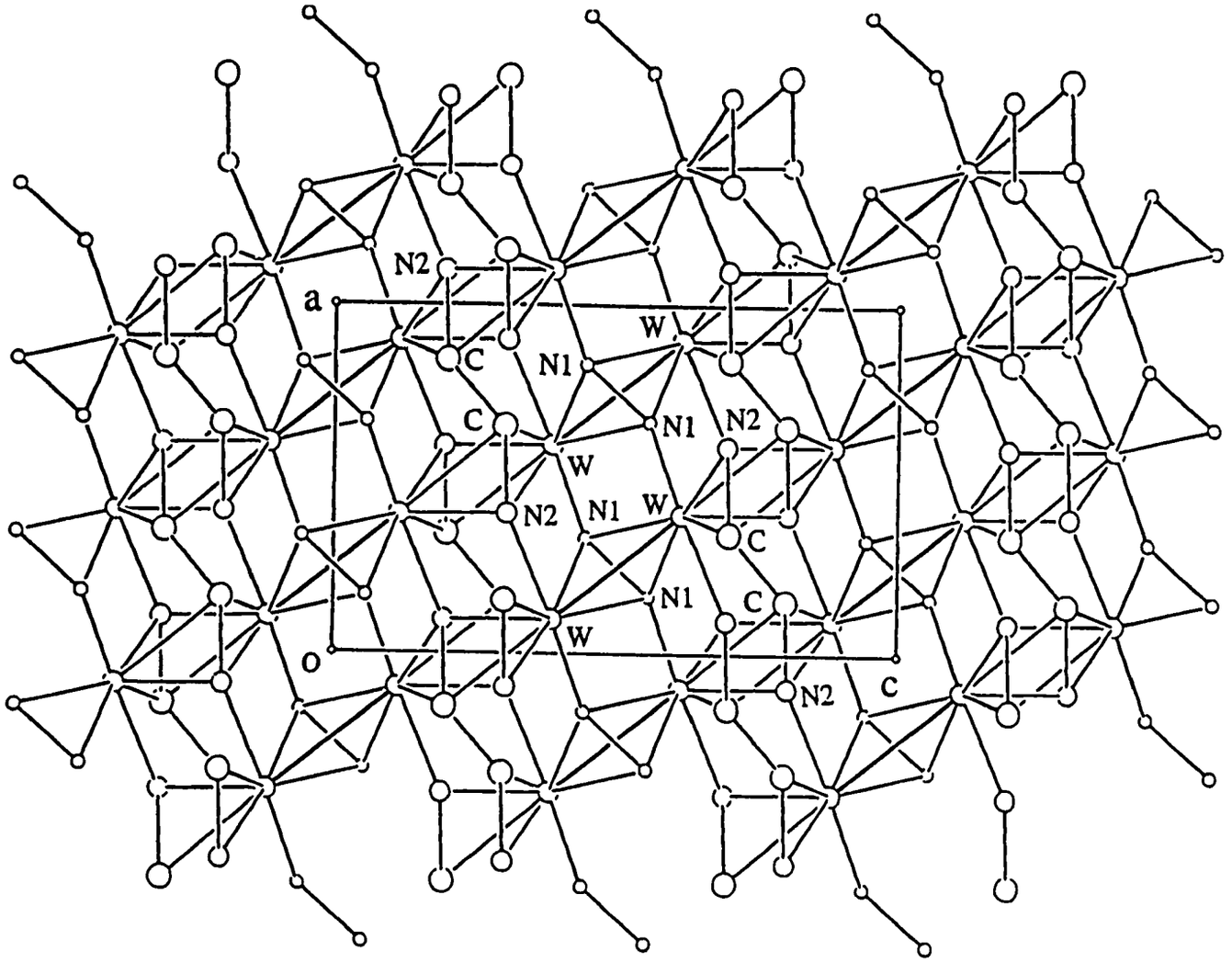

Figure 3. The ORTEP diagram of $W_2N_2(C_2N_2)$ viewed down the b axis.

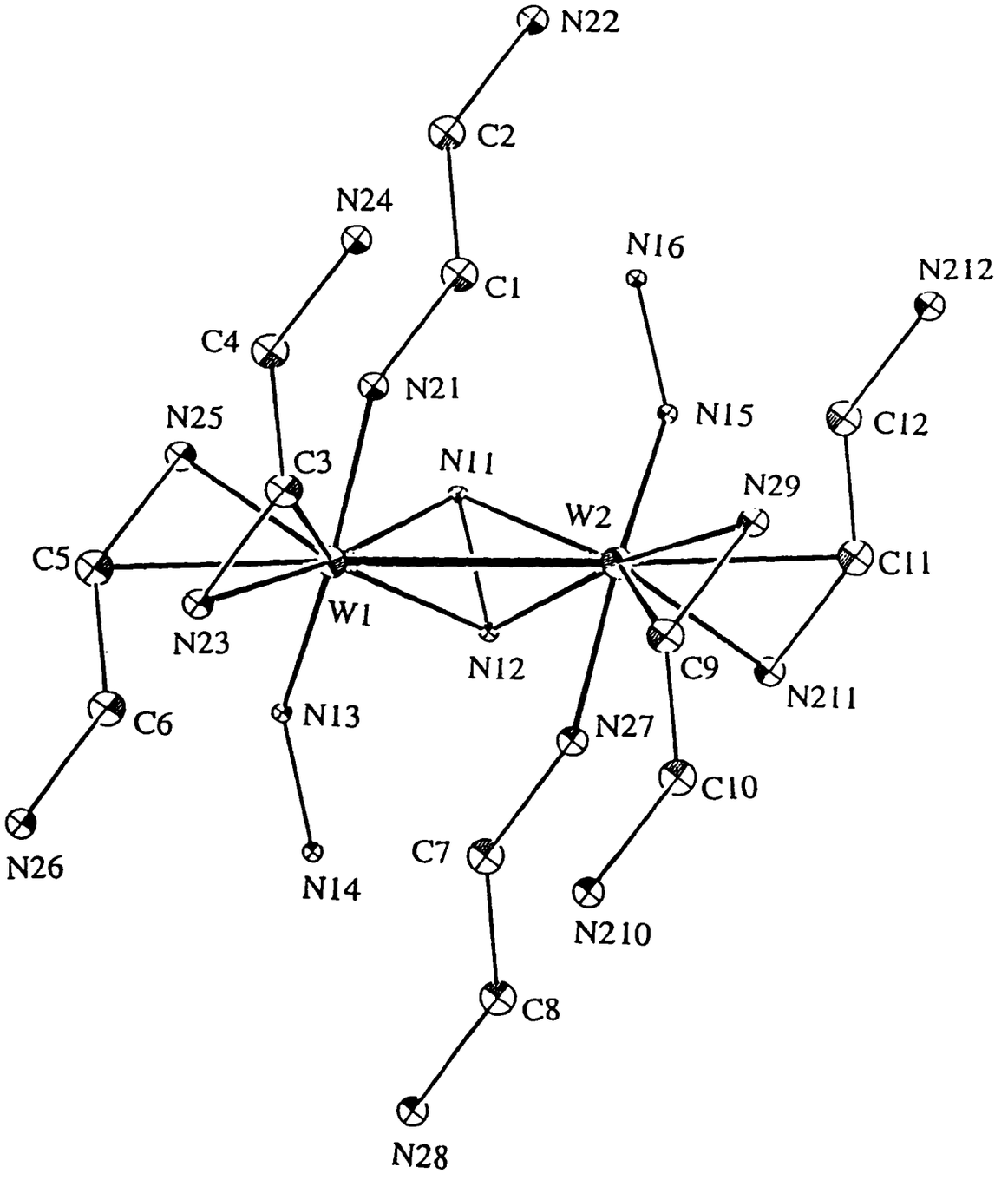

Figure 4. The coordination environment of a W_2 dimer core in $W_2N_2(N_2C_2)$.

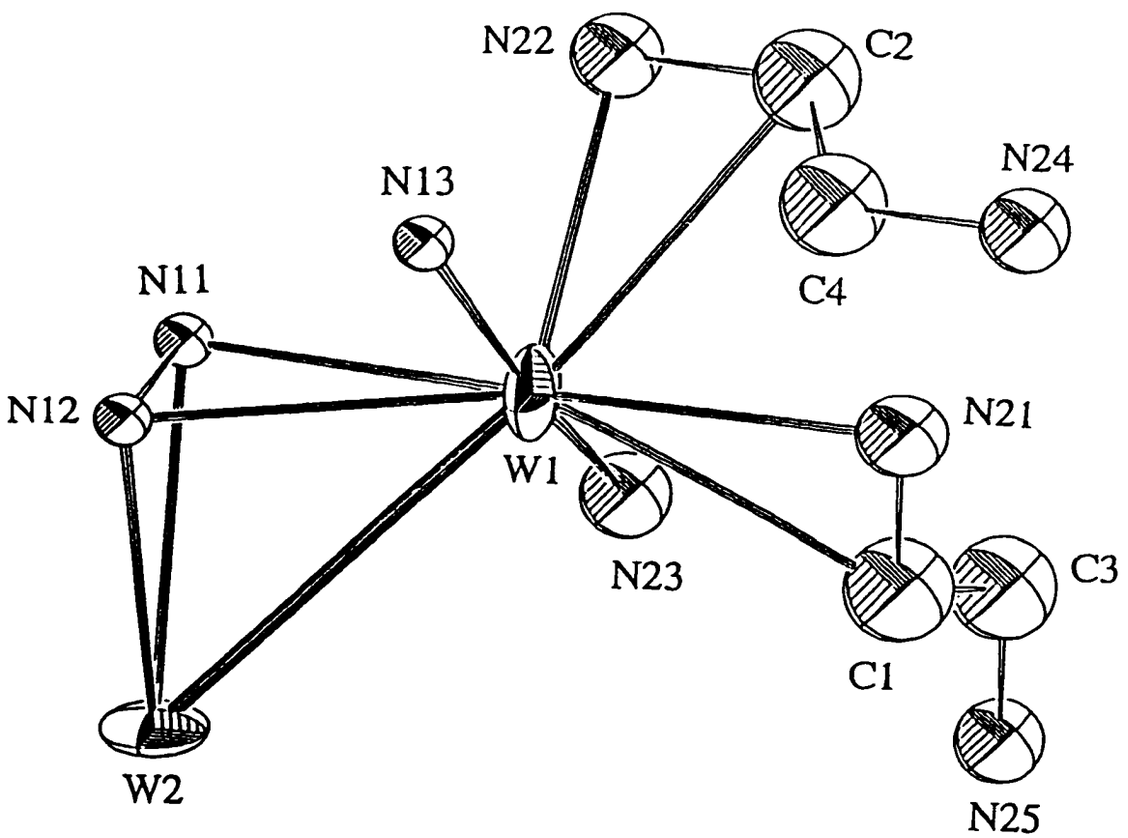

Figure 5. The coordination sphere of the tungsten atom (W1) in $W_2N_2(N_2C_2)$.

bond lengths and bond angeles are given in Tables 6 and 7, respectively. Without considering the W2 atom, the W1 atom is coordinated by three N1 atoms (N11, N12, and N13), three N2 atoms (N21, N22, and N23), and two C atoms (C1, and C2). If the centroids of N11-N12, N21-C1, and N22-C2 are considered as groups coordinated to W1, the coordination configuration of W1 can be viewed as a distorted square pyramid. N11-N12, N13, N21-C1, and N23 form the square planar base, and the N22-C2 group occupies the apex position of the square pyramid.

Table 6. Selected bond distances (Å) in $W_2N_4C_2$

atom	atom	distance	atom	atom	distance
W1*	W2*	2.768(2)	W1	N11	2.00(3)
W1	N12	2.19(3)	W1	N13	1.97(3)
W1	N21	2.01(3)	W1	N22	2.06(2)
W1	N23	2.07(2)	W2	N11	2.19(3)
W2	N12	2.00(3)	W1	C1	2.33(4)
W1	C2	2.31(3)	N11	N12	1.43(4)
N21	C1	1.59(4)	C1	C2	1.52(5)

* W1 and W2 are symmetry related tungsten atoms.

Table 7. Selected bond angles (°) in $W_2N_4C_2$

atom	atom	atom	angle	atom	atom	atom	angle
W2	W1	N11	51.8(7)	W2	W1	N12	45.7(7)
W2	W1	N13	103.9(6)	W2	W1	N21	130.1(7)
W2	W1	N22	134.9(6)	W2	W1	N23	78.4(6)
W2	W1	C1	101.3(6)	W2	W1	C2	172.8(9)
N11	W1	N12	39.5(6)	N11	W1	N13	91.5(8)
N11	W1	N21	171.9(6)	N11	W1	N22	85.4(7)
N11	W1	N23	82.6(7)	N11	W1	C1	131.6(8)
N11	W(1)	C2	122.7(8)	N12	W1	N13	63.5(1)
N12	W1	N21	148.4(6)	W1	N11	W2	82.6(6)
W1	N11	N12	78(1)	W2	N11	N12	63(1)
W1	N12	W2	82.6(1)	W1	N12	N11	63(1)
W2	N12	N11	78(1)	W1	N21	C1	79.9(1)
W1	N22	C2	77.2(1)	W1	C1	N21	57.9(2)
W1	C1	C3	127.3(2)	N21	C1	C3	141.9(2)
W1	C2	N22	60.5(1)	W1	C2	C4	85.0(1)
N22	C2	C4	141.9(1)	C1	C3	N25	142(3)
C2	C4	N24	142(3)				

The coordination sphere of the N1 atom (N11) is shown in Figure 6. The N11 atom is tetrahedrally coordinated by three tungsten atoms (W1, W2, and W3) and one nitrogen atom (N12) to form a distorted tetrahedron.

Figure 7 shows the coordination sphere of the N2 atom (N21). The N21 atom is coordinated by three W atoms (W1, W3, and W4) and one C atom (C1). Since the sum of the angles of W1-N21-W3, W1-N21-W4, and W3-N21-W4 is almost 360°, the coordination geometry of the N2 atom can be considered as a distorted triangular pyramid. W1, W3, and W4 resides in the triangular basal plane, and C1 occupies the apex position of the triangular pyramid.

The coordination sphere of the C atom is irregular (Figure 8). It is coordinated by two W atoms (W1, W4), one N atom (N21), and one C atom (C3).

Although the structural refinement results are satisfactory, several weak intermolecular interactions were found in the structure which are much longer than normal bonding distances, but shorter than the van der Waals interactions. For instance, the bond distances of N12-N13 (2.20(4) Å) and N23-C1 (1.89(4) Å) (see Figure 5) are much shorter than the van der Waals distance (~3.20 Å), but they are much longer than the normal N-N and C-N single bond distances (1.45 Å and 1.47 Å, respectively).

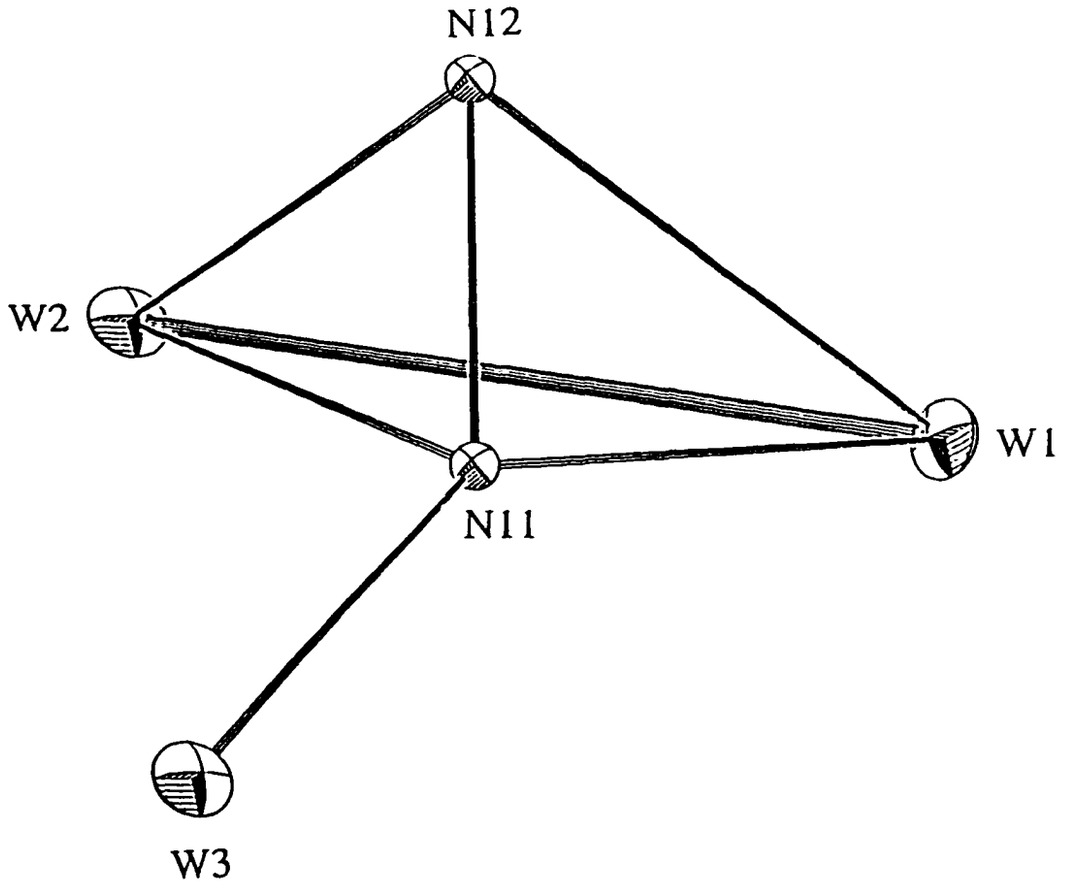

Figure 6. The coordination sphere of the N1 atom (N11) in $W_2N_2(N_2C_2)$. Selected bond distances (Å) and bond angles (°) are as follows: N11-W1, 2.00(3); N11-W2, 2.19(3); N11-W3, 1.97(3); N11-N12, 1.43(4); W1-N11-W2, 82.5(1); W1-N11-W3, 145.4(2); W2-N11-W3, 116.5(1); N12-N11-W1, 76.6(2); N12-N11-W2, 62.4(1); N12-N11-W3, 136(1).

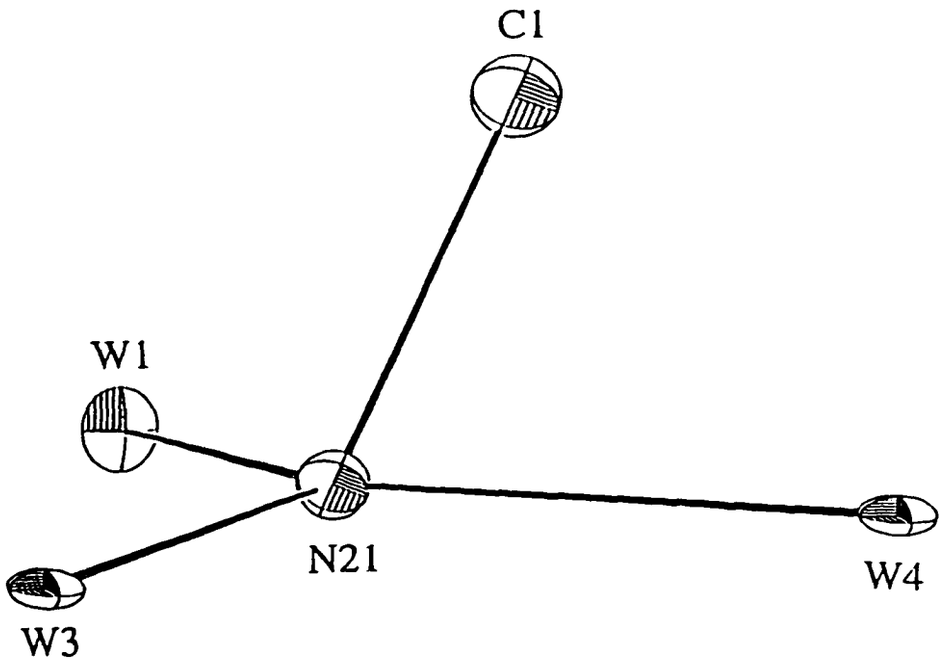

Figure 7. The coordination sphere of the N2 atom (N21) in $W_2N_2(N_2C_2)$. Selected bond distances (Å) and bond angles (°) are as follows: N21-W1, 2.01(3); N21-W3, 2.07(3); N21-W4, 2.06(2); N21-C1, 1.59(4); W1-N21-W3, 129.4(7); W1-N21-W4, 133.3(7); W3-N21-W4, 96.8(1); C1-N21-W1, 79.8(1); C1-N21-W3, 124.1(1); C1-N21-W4, 77.1(1).

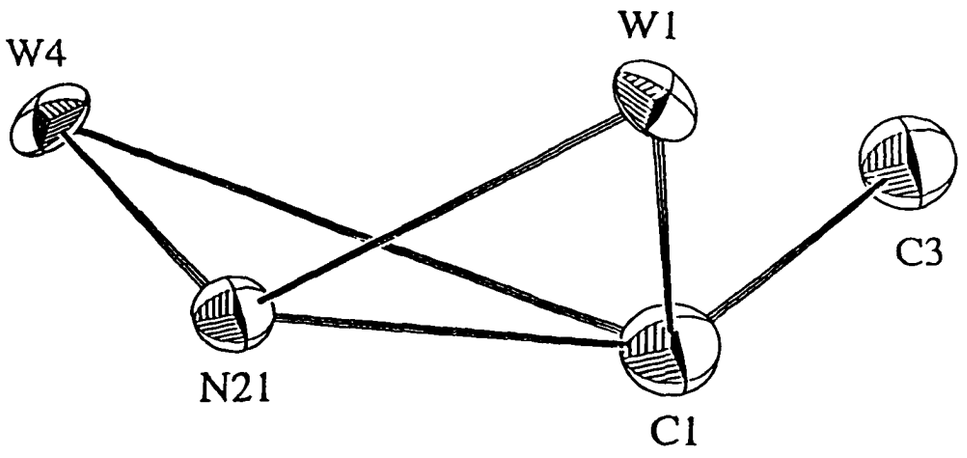

Figure 8. The coordination sphere of the C atom (C1) in $W_2N_2(N_2C_2)$. Selected bond distances (Å) and bond angles (°) are as follows: C1-W1, 2.33(4); C1-W4, 2.31(3); C1-N21, 1.59(4); C1-C3, 1.52(5); W1-C1-C3, 127.3(2); W1-C1-N21, 57.8(6); W4-C1-C3, 85.0(1); W4-C1-N21, 60.5(1); W1-C1-W4, 107.2(4); N21-C1-C3, 141.8(7).

X-ray photoelectron spectroscopy

XPS was used to obtain W and N binding energies and provide further information about the possible oxidation states of tungsten. The W4f XPS spectra of W_3N_5, cubic WN, and the product mixture (hexagonal WN and W metal) from annealing W_3N_5 at 800 °C are shown in Figure 9. Only one type of tungsten is necessary to fit the XPS spectra of W_3N_5 and cubic WN. The calibrated binding energies of $W4f_{7/2}$ and $W4f_{5/2}$ are 32.8 and 34.9 eV for W_3N_5, and 32.0 and 34.2 eV for WN, respectively. Two types of tungsten are necessary to fit the spectrum of the product mixture (hexagonal WN and W metal) from annealing W_3N_5 at 800 °C. One type of W has calibrated binding energies of $W4f_{7/2}$ and $W4f_{5/2}$ at 31.3 and 33.4 eV, which are typical W4f binding energies for tungsten metal. The other type of W has calibrated binding energies of $W4f_{7/2}$ and $W4f_{5/2}$ at 32.3 and 34.4 eV, which can be assigned to the tungsten atoms in hexagonal WN.

For comparison, Table 8 lists the binding energies of WO_2, $WNCl_3$, and WO_3. It can be observed that the binding energies of W_3N_5 are higher than the binding energies of WO_2; however, they are lower than the binding energies of $WNCl_3$ and WO_3, which indicates that the oxidation state of tungsten in W_3N_5 is evidently +5. The binding energies of cubic and hexagonal WN are lower than the binding energies of WO_2, but higher than the binding energies of tungsten metal, indicating that the

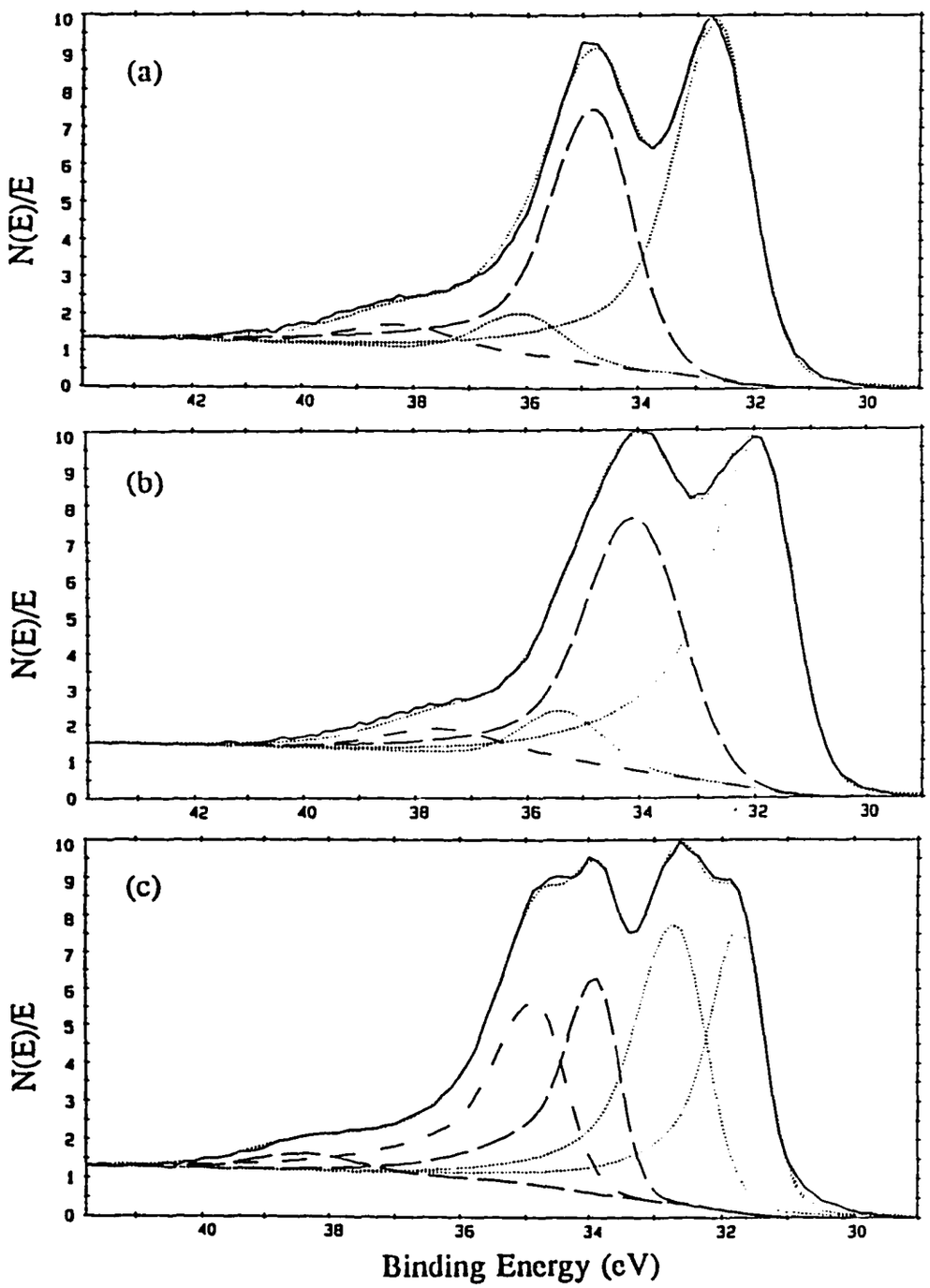

Figure 9. W4f XPS spectra of (a) W_3N_5, (b) cubic WN, and (c) product mixture (hexagonal WN and W metal) from annealing W_3N_5 at 800 °C.

Table 8. W4f XPS binding energies (eV) of tungsten and related compounds

Compound	$W4f_{7/2}$	$W4f_{5/2}$	N1s
W[a]	31.4	33.5	
WO_3[a]	35.5	37.6	
WO_2[a]	32.5		
$WNCl_3$	34.7	36.8	397.5
W_3N_5	32.8	34.9	397.4
WN[b]	32.0	34.2	397.6
WN[c]	32.3	34.4	398.2
W	31.3	33.4	

[a] Reference 17 [b] Cubic WN. [c] Hexagonal WN.

oxidation state of tungsten is +3. The N 1s binding energies for all compounds are in the range 396.2-398.2 eV, which is characteristic of transition metal nitrides (N^{3-})[17a].

Electronic structure calculations

Cubic phases of molybdenum and tungsten mononitrides with the rock salt structure were predicted to exhibit superconductivity.[8-9] The qualitative correlation

arising between T_c and the density of states (DOS) at the Fermi level, $N(E_F)$, is given in equation A

$$kT_c = 1.13\hbar\omega \exp(-1/N(E_F)V) \qquad \text{(A)}$$

where V is a measure of the electron-phonon interaction and ω is a characteristic phonon frequency whose magnitude is similar to the Debye frequency.[18] According to this expression, large values of either $N(E_F)$ or V (or both) would lead to high T_c values. The electronic structure calculations on cubic MoN with the rock salt structure (a = 4.250 Å) have shown a large value of the density of states at the Fermi level.[9] Therefore, it would be interesting to know the electronic structure of the cubic WN with rock salt structure.

The total DOS curve (Figure 10a) for cubic WN with rock salt structure (a = 4.171 Å) was obtained by sampling 465 uniformly distributed K points in the *fcc* Brillouin zone. The contribution of the tungsten 6s-6p bands is not included in this curve. The Fermi level falls in the manifold of the t_{2g} bands which are the combinations of tungsten $5d_{xy}$, $5d_{xz}$, $5d_{yz}$, and nitrogen 2p interactions. The e_g bands raised above the t_{2g} bands are mainly the combinations of tungsten $5d_{x2-y2}$, $5d_{z2}$, and nitrogen 2p interactions. The crystal orbital overlap population (COOP) for the W-N and W-W interactions are shown in Figures 11. In both cases, the e_g and t_{2g} bands show antibonding characteristic due to the interactions between the tungsten 5d and nitrogen 2p orbitals. The 2p bands, which are the combinations of the tungsten 5d and

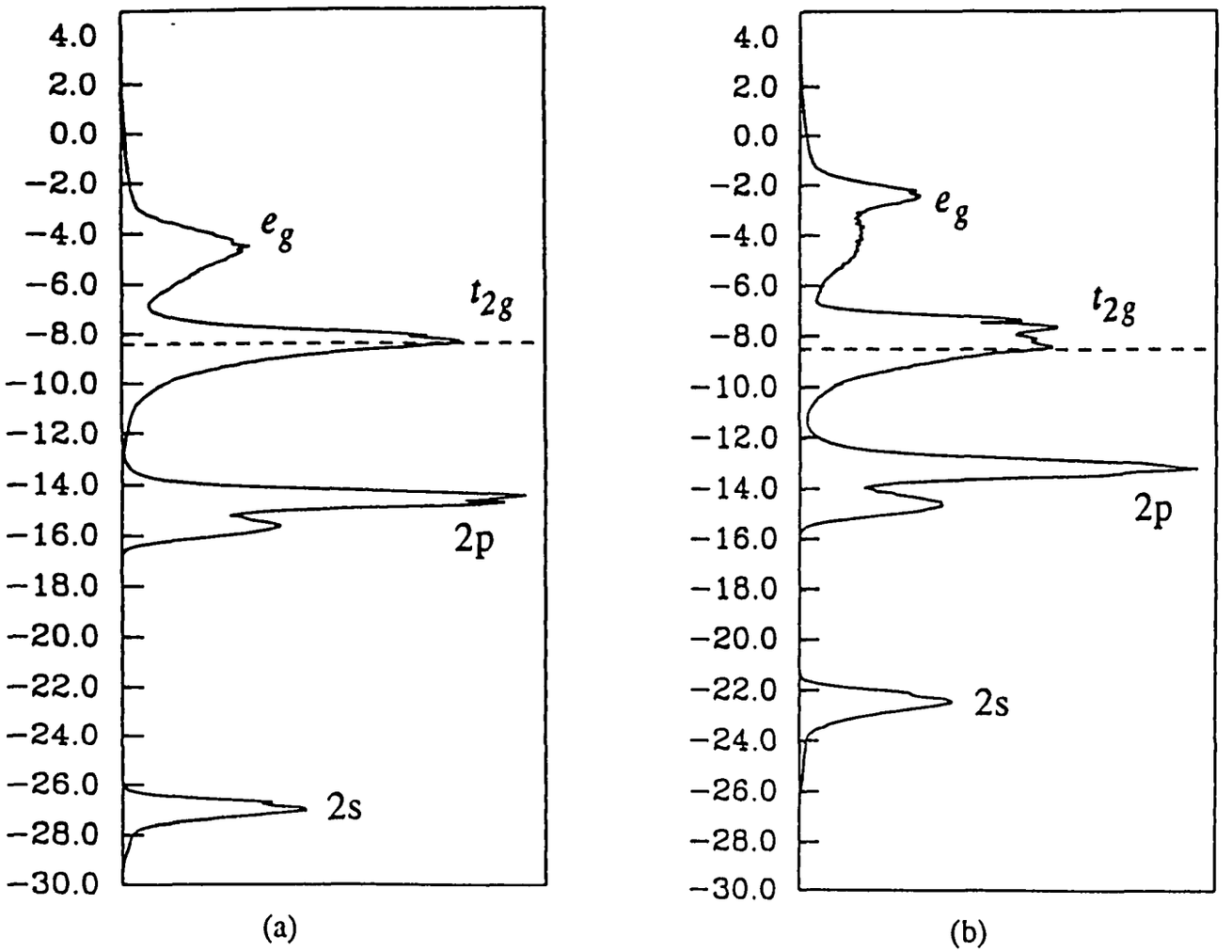

Figure 10. The total DOS curve for (a) cubic WN (a = 4.178 Å) and (b) cubic WC (a = 4.266 Å) with NaCl structure. The Fermi levels noted by dashed lines are at -8.41 eV for cubic WN, and -8.50 eV for cubic WC.

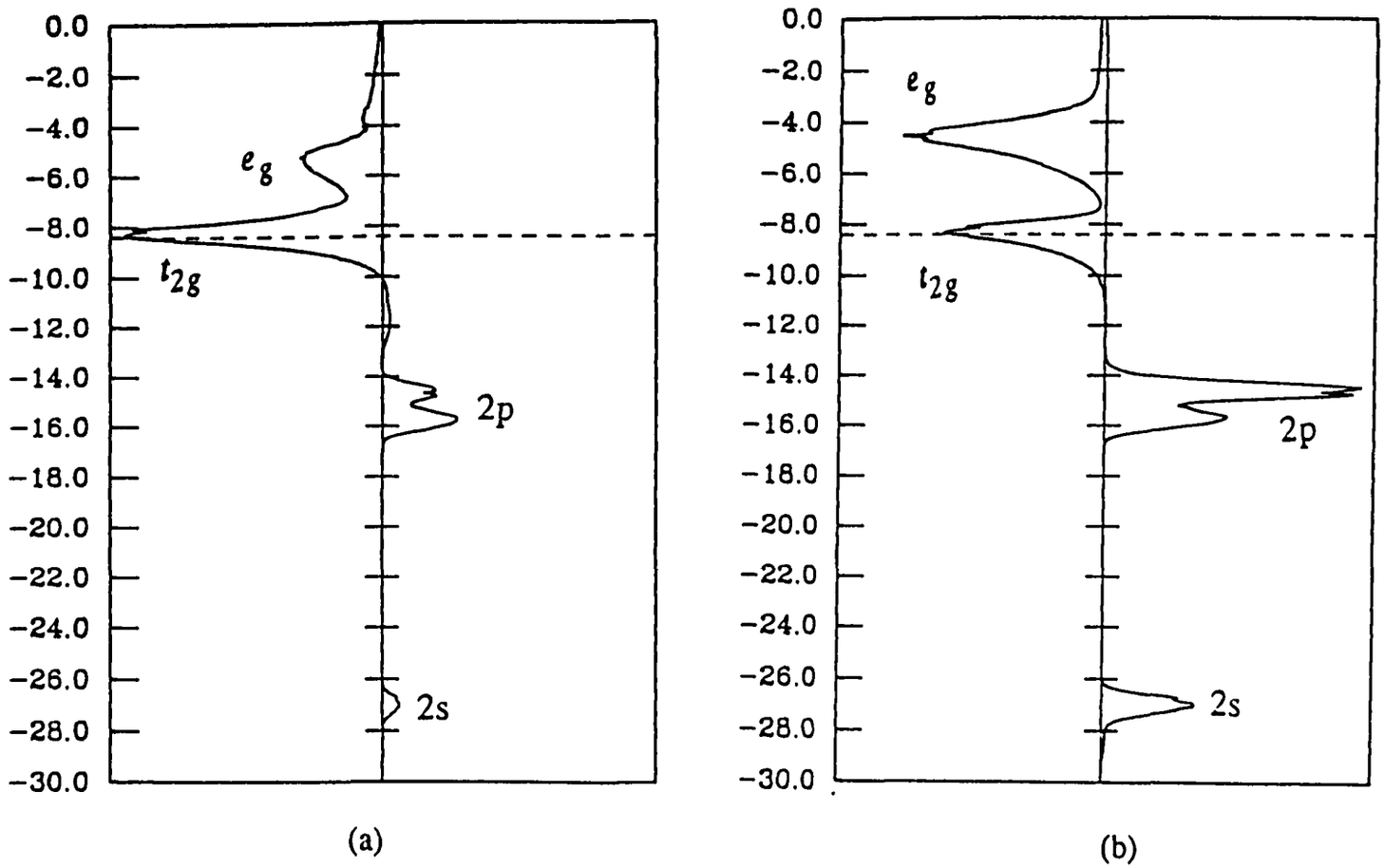

Figure 11. The crystal orbital overlap population (COOP) for (a) the W-N and (b) the W-W interactions. The Fermi level at -8.41 eV is noted by dashed lines.

nitrogen 2p interactions, show a bonding character. The 2s bands, however, are mainly composed of nitrogen 2s orbitals, and show a bonding character as well.

Clearly, the total DOS curve shows cubic WN to be an electrical conductor. By comparison to the total DOS curve (Figure 10b) for cubic WC with rock salt structure (a = 4.266 Å)[16] which was obtained by the same calculation method, it was found that the $N(E_F)$ for the cubic WN was about 1.34 times higher than that for the cubic WC. According to equation A, the T_c for the cubic WN may be estimated to be higher than 10K, which was the value of T_c for cubic WC.

Magnetic properties

The molar magnetic susceptibilities of W_3N_5 and cubic WN as a function of temperature are shown in Figures 12 and 13. The susceptibility data in the range 100-300 K were fit to a modified Curie-Weiss relationship, $\chi = C/(T - \theta) + \chi_o$, where C, θ, and χ_o refer to the Curie constant, the Weiss temperature, and temperature independent susceptibility. The results of nonlinear fitting of the observed data are given in Table 9.

A very small effective moment (0.13 BM) in the 100-300 K temperature range was observed for W_3N_5. Similarly, a very small effective moment (0.088 BM) in the 100-300 K temperature range was observed for the cubic WN phase as well. Using the assumption that spin 1/2 ions are the sources of the Curie-Weiss behavior, the

Table 9. Parameters derived from the non-linear magnetic fitting results of observed magnetic data for W_3N_5 and cubic WN with NaCl structure

Compound	C(emu·K/mole)	θ(K)	χ_o(emu/mole)	μ(BM)
W_3N_5	2.10×10^{-3}	-10.9	-1.60×10^{-4}	0.13
cubic WN	7.91×10^{-4}	-56.3	-2.75×10^{-5}	0.088

concentration of the paramagnetic carriers estimated from the corresponding Curie constant (C) was less than 0.1%, suggesting that the moments may be due to impurities. Therefore, both W_3N_5 and cubic WN are diamagnetic materials.

The electronic structure calculations have indicated that the cubic WN with NaCl structure is a conductor, and might be a superconductor. However, the magnetic susceptibility measurements of this cubic WN did not show any evidence of superconductivity in the temperature range 6-300 K .

Based on the XPS data of W_3N_5, the oxidation state of tungsten in this compound is +5. Therefore, each tungsten atom in this compound possesses one single electron. The diamagnetic behavior of W_3N_5 thus suggests that the electron are paired by W-W bond formation, and thus this material should be an insulator.

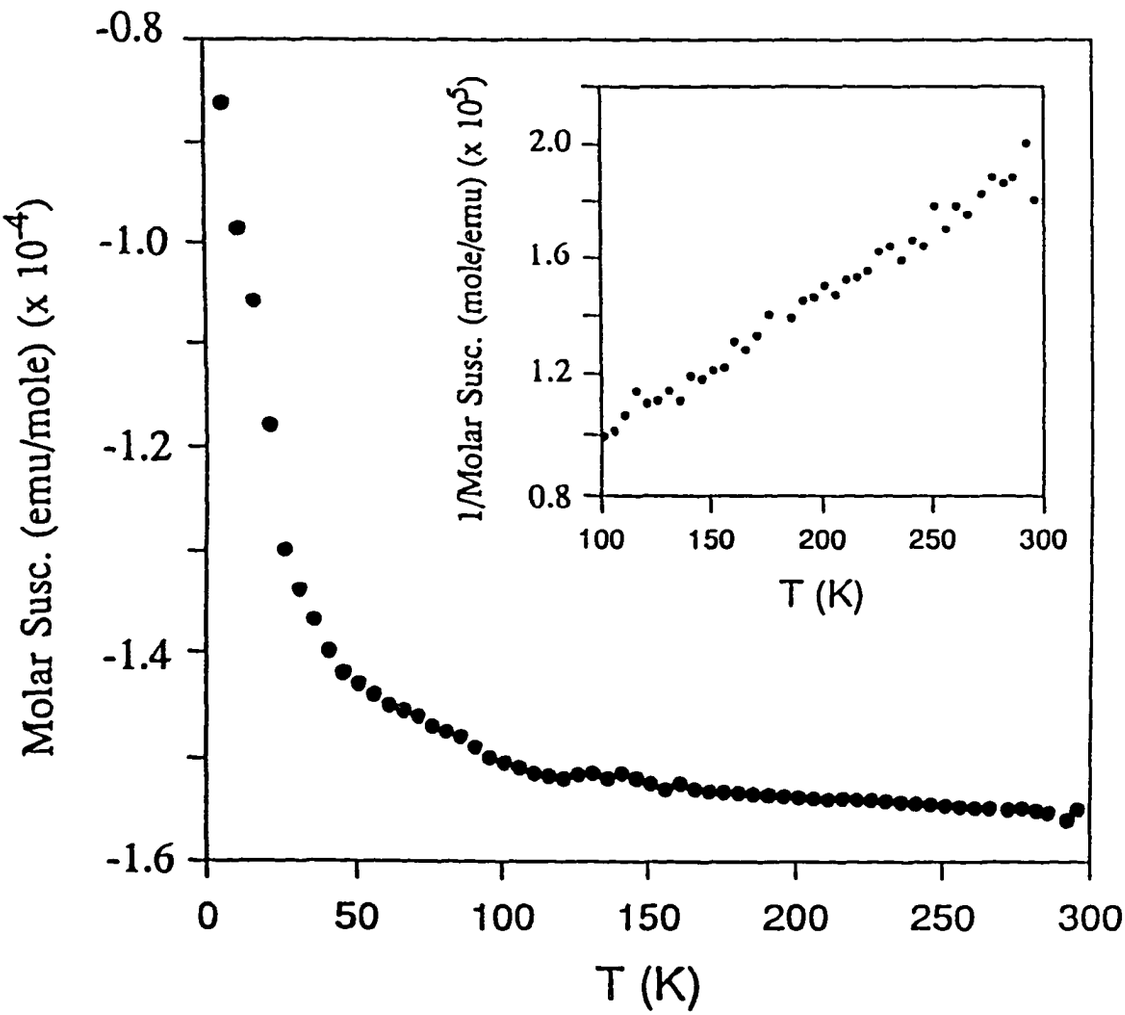

Figure 12. The molar magnetic susceptibility of W_3N_5 as a function of temperature, and reciprocal susceptibility vs. temperature (inset).

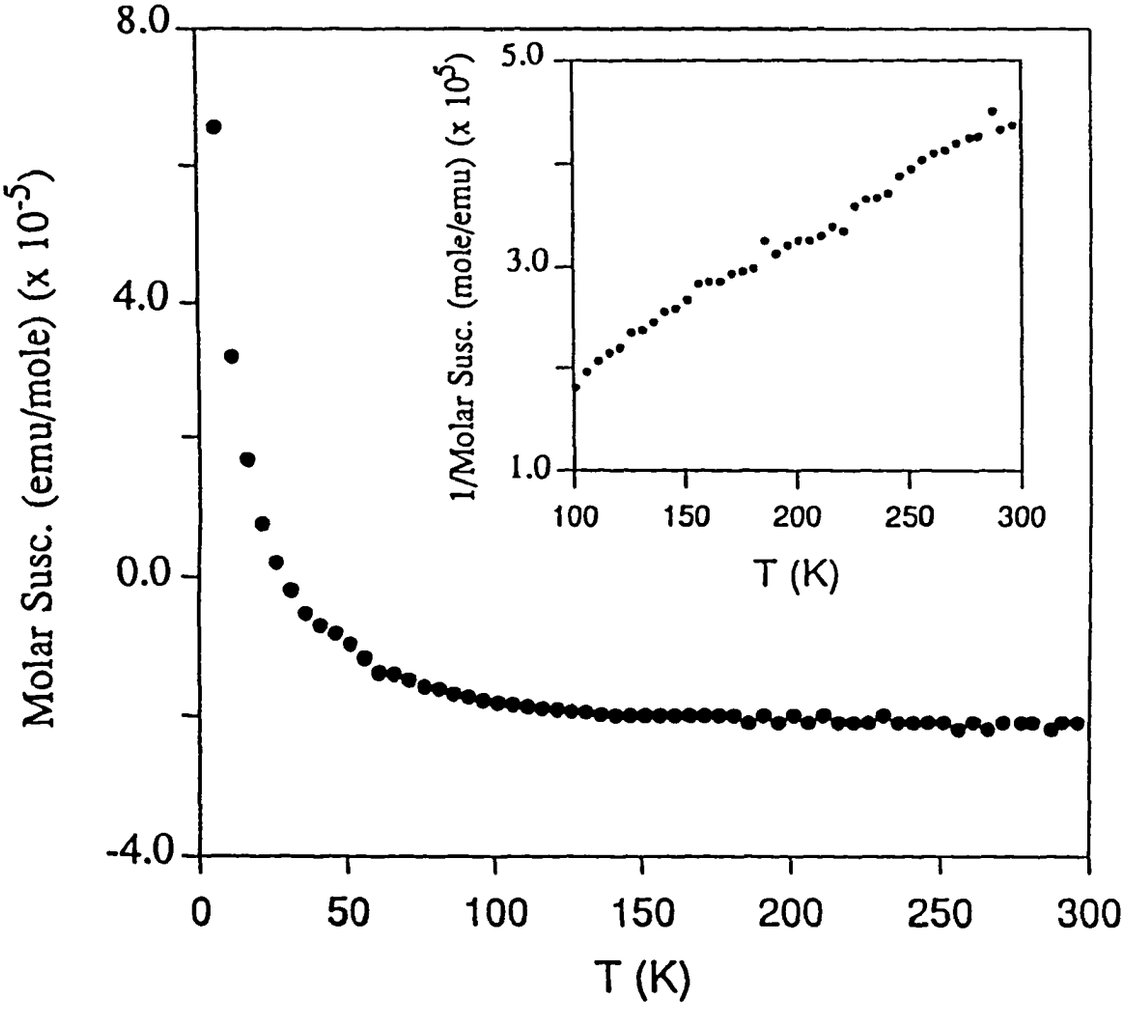

Figure 13. The molar magnetic susceptibility of cubic WN with NaCl structure as a function of temperature, and reciprocal susceptibility vs. temperature (inset).

Conclusions

This paper describes the preparation and characterization of new tungsten nitride and carbide nitride compounds. A bulk solid phase of tungsten nitride W_3N_5 was prepared through a solid state reaction between $WNCl_3$ and Zn_3N_2 in sealed Pyrex tubes at 400 °C. The XPS study indicated that the oxidation state of tungsten in this amorphous phase was +5. Therefore, each tungsten atom in this W_3N_5 compound possesses one single electron. The magnetic susceptibility measurements showed that W_3N_5 was diamagnetic in the temperature range 6-300 K. This result suggests that the single electron possessed by the tungsten atom in W_3N_5 is paired through W-W bond formation.

Heating W_3N_5 at 600°C in sealed quartz tubes yielded a cubic tungsten mononitride phase (WN) with rock salt structure (a = 4.171 Å). Heating W_3N_5 at 800 °C in sealed quartz tubes produced hexagonal WN phase and tungsten metal. At the same time, a few golden crystals were also obtained, which were grown via a chemical vapor transport reaction.

The golden $W_2N_2(C_2N_2)$ compound crystallizes in the monoclinic space group *I2/a* (#15, nonstandard setting) with crystallographic data, a = 5.6521(9) Å, b = 4.889(1) Å, c = 9.576(1) Å, β = 90.20(1)°, V = 264.6(1) Å^3. The structure of $W_2N_2(C_2N_2)$ consists of W_2 dimers, hydrazido ligands N_2^{4-}, and 1,4-diazabutenido ligands represented by three resonance structures, $[N\text{-}C{=}C\text{-}N]^{6-}$, $[N{=}C\text{-}C\text{-}N]^{6-}$, and [N-

C-C=N]$^{6-}$. The dimers are linked together by N-N and N-C-C-N groups to form a 3-dimensional network. The metal to hydrazido nitrogen bond distances fall in the range 1.97(4) to 2.19(4) Å, and the metal-diazabutenido nitrogen distances show a more limited range from 2.01(4) to 2.07(3) Å. The hydrazido N-N bond distance is 1.43(5) Å, and the diazabutenido C-C bond distance is 1.59(4) Å and N-C bond distance 1.56(4) Å. The W-W single bond distance is 2.767(2) Å.

The electronic structure calculations indicated the cubic WN was a conductor and might exhibit superconductivity. However, the magnetic susceptibility measurements indicated that the cubic WN exhibited a weak diamagnetic behavior in the temperature range 30-300 K, but did not show any evidence of superconductivity. Moreover, the magnetic susceptibility measurements suggest that W_3N_5 should be an insulator.

References

1. Toth, L. E. *Transition Metal Carbides and Nitrides*, Academic Press, NY, **1971**.
2. Lyutaya, M. D. *Soviet Powder Metall. Metal Cer.* **1979**, 190.
3. Lakhtin, Yu. M.; Kogan, Ya, D.; Borovskaya, T. M.; Solodkin, G. A. *Russ. Metall.* **1979**, *4*, 158.
4. Brese, N. E.; O'Keeffe, M. *Structure and Bonding*, **1992**, *79*, 307.

5. Khirtrova, V. I. *Soviet Phys. Cryst.* **1962**, *6(4)*, 439.

6. Khitrova, V. I.; Pinsker, Z. G. *Sov. Phys.- Crystallogr.* **1962**, *6*, 712.

7. Schönberg, N. *Acta Chemica Scandinavica*, **1954**, *8*, 204.

8. Zhao, Y.; He, S. *Solid State Commun.* **1983**, *45(3)*, 281.

9. Pickett, W. E.; Klein B. M.; Papaconstantopoulos, D. A. *Physica*, **1981**, *107B*, 667.

10. (a) Baxter, D. V.; Chisholm, M. H.; Gama, G. J.; DiStasi, V. F.; Hector, A. L.; Parkin, I. P. *Chem. Mater.* **1996**, *8*, 1222.

(b) Holl, M. M. B.; Wolczanski, P. T.; Proserpio, D.; Bielecki, A.; Zax, D. B. *Chem. Mater.* **1996**, *8*, 2468.

11. Hector, A. L.; Parkin, I. P. *Chem. Mater.* **1995**, *7*, 1728.

12. Close, M. R.; McCarley, R. E. *Inorg. Chem.* **1994**, *33*, 4198.

13. (a) Hoffmann, R. *J. Chem. Phys.* **1963**, *39*, 1397.

(b) Ammeter, J.; Bürgi, H.-B.; Thibeault, J. C.; Hoffmann, R. *J. Am. Chem. Soc.* **1978**, *100*, 3686.

(c) WHangbo, M.-H.; Hoffmann, R. *J. Am. Chem. Soc.* **1978**, *100*, 6093.

14. (a) Clementi, E.; Roetti, C. *At. Data Nucl. Data Tables*, **1974**, *14*, 177.

(b) Baranovskii, V. I.; Nikolskii, A. B. *Tero. Eksp. Khim.* **1967**, *3*, 527.

15. (a) Sheldrick, G. M. *Crystallographic Computing 3*, Eds Sheldrick G. M.; Kruger, C.; Goddard, R., Oxford University Press, 175.

(b) Walker, N.; Stuart, D. *Acta Cryst.* **1983**, *A39*, 158.

(c) Crystal Structure Analysis Package, Molecular Structure Corporation (1985 & 1992).

16. Willens, R. H.; Buehler, E. *Applied Physics Letters*, **1965**, *7(1)*, 95.

17. (a) Moulder, J. F.; Stickle, W. F.; Sobol, P. E.; Bomben, K. D. *Handbook of X-ray Photoelectron Spectroscopy*, Chastain, J. Ed,; Perkin-Elmer Corp.: Eden Prairies, MN, **1992**.

(b) Colton, R. J.; Rabalais, J. W. *Inorg. Chem.* **1976**, *15*, 236.

18. McMillan, W. L. *Phys. Rev.* **1968**, *167*, 331.

CHAPTER 4. SYNTHESIS AND CHARACTERIZATION OF $LnMo_8O_{14}$ CONTAINING Mo_8 BICAPPED OCTAHEDRA (Ln = La, Ce, Pr, Nd, Sm)

A paper to be submitted to Inorganic Chemistry

Zhihong Zhang and Robert E. McCarley

Abstract

A systematic investigation in the Ln_2O_3-MoO_3-Mo (Ln = La, Ce, Pr, Nd, Sm) system has been explored in sealed, evacuated quartz tubes at 1250°C. A new reduced ternary rare-earth molybdenum oxide $LaMo_8O_{14}$ with a novel crystal structure has been discovered. This compound crystallized in the orthorhombic space group *Pbcn* (#60) with crystallographic data: a = 9.197(2) Å, b = 11.128(2) Å, c = 20.006(4) Å, and V = 2048(1) $Å^3$, Z = 8, R = 0.035, and Rw = 0.045. The novel structure contains a 1:1 ratio of cis- to trans-Mo_8 bicapped octahedra, which are arranged alternately along the c-axis of the unit cell. The Mo-Mo bond distances are in the range of 2.590(4) to 2.888(6) Å. The average Mo-Mo bond distance in trans-isomer is 2.703 Å, which is shorter than that found in the cis-isomer (2.748 Å). The Mo-O bond distances are in the range of 1.94(3) to 2.18(2) Å. The M-O bond strength calculations suggest that the cis- and trans-Mo_8 clusters in $LaMo_8O_{14}$ contain 22 and 24 electrons,

respectively. Under these synthetic conditions, the phases containing all cis-Mo_8 bicapped clusters and a 1:1 ratio of cis-Mo_8 to trans-Mo_8 bicapped clusters were found. It is noted that the sizes of the rare-earth cations are critical for the formation of the various phase types. The larger cations (La, Ce, and Pr) aid in the formation of trans-Mo_8 octahedra, and the smaller cations (Nd and Sm) only stabilize the cis-Mo_8 octahedra. A rational explanation for this result arises from the observation that the effective volume of cis-Mo_8 cluster is 3/4th the value of the trans-Mo_8 cluster. The magnetic susceptibility measurements indicate that no effective moment contribution arises from the metal clusters Mo_8, even though the cis-Mo_8 cluster in $LnMo_8O_{14}$ containing all cis-Mo_8 octahedra apparently contains an odd number of electrons (23 e^-). The electrical resistivity measurements and electronic structure calculations indicate that the $LnMo_8O_{14}$ containing all cis-Mo_8 clusters are metallic compounds, and the $LnMo_8O_{14}$ containing a 1:1 ratio of cis- to trans-Mo_8 clusters are semiconducting compounds.

Introduction

Since the discovery of reduced molybdenum oxide, $NaMo_4O_6$,[1] containing trans-edge-shared Mo_6 octahedra, ternary reduced molybdenum oxides have been studied extensively. A variety of structure types with this basic building mode have been

discovered.[2]

Over the past several years, ternary reduced rare-earth molybdenum oxides have caused great interest, because these compounds may possess interesting electrical and magnetic properties. Many compounds have been discovered in this research area by using either high-temperature solid state reactions or electrolysis, and most of them have been structurally characterized.[3-9] One interesting family of reduced rare-earth molybdenum oxides is that of compounds containing Mo_8 bicapped octahedra. The Mo_8 bicapped octahedra could have three structural isomers (cis-, meta-, and trans-), which are shown in Figure 1. This possibility of including the different isomers may lead to an interesting crystal structure chemistry, because different combinations and ratios of these isomers can occur within the same crystal structure.

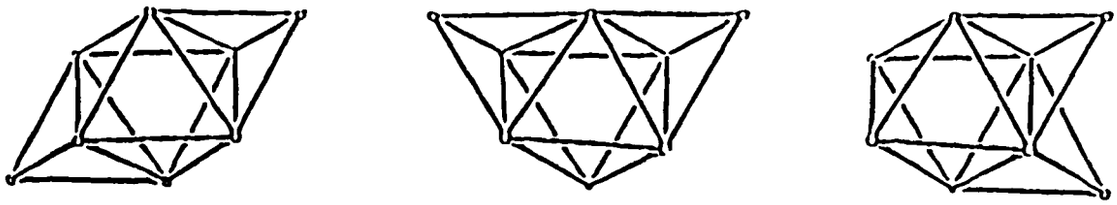

Figure 1. The three structural isomers of Mo_8 bicapped octahedra.

The first compound containing Mo_8 bicapped octahedra was synthesized by electrolysis in 1990.[10] It has a non-stoichiometric formula $LaMo_{7.7}O_{14}$, and contains cis-Mo_8 bicapped octahedra, in which the face capping positions are only 85% occupied by Mo atoms. Subsequently, a stoichiometric compound, $NdMo_8O_{14}$,[11] was discovered, in which the face capping positions are fully occupied. These compounds exhibit paramagentic behavior in the temperature range of 100-300K, and metallic character at room temperature.[12, 13] More recently, compounds $CeMo_8O_{14}$[14] and $PrMo_8O_{14}$,[15] which contain 1:1 and 2:1 ratios of cis- to trans Mo_8 bicapped octahedral clusters, respectively, have been discovered by P. Gougeon and coworkers by performing reactions at extremely high temperatures.

In order to better understand these ternary reduced rare-earth molybdenum compounds containing Mo_8 bicapped octahedra, a systematic study has been explored in the Ln_2O_3-MoO_3-Mo system (Ln = rare-earth). The lanthanum and praseodymium analogues of $CeMo_8O_{14}$ containing a 1:1 ratio of cis- to trans-Mo_8 cluster were discovered at relatively low temperature, and the samarium analogue of $NdMo_8O_{14}$ containing all cis-Mo_8 cluster was found as well. Electronic structure calculations were carried out on the compound $NdMo_8O_{14}$ containing all cis-Mo_8 clusters. The electrical resistivity and magnetic susceptibility were measured on some of these compounds. This paper will present the synthesis, structure, and properties of compounds $LnMo_8O_{14}$ (Ln = La, Ce, Pr, Nd, Sm).

Experimental

Materials

The starting reagents included Ln_2O_3 (Ln = La, Pr, Nd, Sm, and Gd), CeO_2, MoO_3 and Mo powder. Ln_2O_3 and CeO_2 were fired at 900°C for 12 hrs to transform any $Ln_2(CO_3)_3$ impurities to the oxides before use. The Mo powder was reduced with flowing H_2 at 800°C for 6 hrs to remove any surface oxides. MoO_3 was heated in air at 400°C for 4 hours before using. All materials were stored in a desiccator.

Physical Measurements

X-ray powder diffraction

X-ray powder diffraction data were obtained from a Phillips ADP3520 θ-2θ X-ray powder diffractometer using Cu $K\alpha_1$ radiation (λ = 1.54056 Å) at 40 kV and 30 mW. The samples were mounted by pressing the powders into a recessed square in a zero-angle quartz plate (obtained from Gem Dugout).

Magnetic susceptibility

Magnetic susceptibilities were measured with a Quantum Design SQUID magnetosusceptometer. The samples were loaded into a 3 mm inner diameter quartz

tube that had been sealed on the bottom half with a 3 mm outer diameter quartz rod. A 3 mm outer diameter quartz rod was also placed in the top half of the loaded sample tube which was then mounted in an apparatus that allowed evacuation of the sample tube and purging with helium gas. After the system was pumped and purged with helium three times, the upper quartz rod was moved close to the sample under a partial pressure of helium (to facilitate temperature equilibration during measurements). The sample was thus sandwiched between two quartz rods. The tube then was sealed off. This procedure was used to eliminate O_2 contamination, which has an antiferromagnetic transition at ~50 K. The experimental data were corrected for the diamagnetic contribution from the quartz. Measurements on empty quartz tube/rod assemblies, with varying gap sizes, indicated that the diamagnetic contribution from the quartz was related to the size of the gap. Since the signal vs. gap size could be fit by a line, the correction was simply employed by measuring the length of the gap containing the sample.

Electrical resistivity

Electrical resistivity measurements were carried out on a single crystal of $LaMo_8O_{14}$ (1.2 x 1.0 x 0.8 mm^3) and a pressed pellet of $SmMo_8O_{14}$ that had been sintered in an evacuated fused silica ampoule at 1250°C for 48 h. The measurement was based on the van der Pauw four probe method for electrical conductivity. The

basic method employs passage of a constant current through one lead of the sample, while concurrently measuring the potential drop across the other lead at a given temperature. Platinum wire leads were used and attached to the sample via Epo-Tech silver epoxy resin.

Synthetic Procedures

The synthesis of the reduced molybdenum oxides required that the oxygen content be controlled stoichiometrically. Therefore, the reactions were usually carried out in sealed, evacuated silica (~1.0 x 10^{-3} torr) vessels.

In a general procedure, stoichiometric amounts of the starting materials ($25MoO_3$ + 23Mo + $3Ln_2O_3$; Ln = La, Pr, Nd, Sm, and Gd; or $4MoO_3$ + 4Mo + CeO_2) were mixed and thoroughly ground. The mixtures were then loaded into fused silica tubes. The tubes were sealed under dynamic vacuum (~1.0 x 10^{-3} torr). A typical reaction mixture contained 5.667 mmol of MoO_3, 5.212 mmol of Mo, and 0.068 mmol of Ln_2O_3, or 5.112 mmol of MoO_3, 5.212 mmol of Mo, and 1.303 mmol of CeO_2. The reactions were fired at 1250°C for 2 days in a box furnace. Black, powdery products were usually obtained.

Single crystals were obtained by annealing mixtures of the black powdery products and $BaCl_2$ (~10%, used as a flux) in a evacuated (~1.0 x 10^{-3} torr) quartz tube at 1250°C for 5-7 days. Black chunk-like single crystals were usually obtained.

Electronic Structure Calculations

All electronic calculations were of the extended Hückel tight-binding type[16]. The observed lattice parameters of $NdMo_8O_{14}$ and atomic positions were taken from the reported data.[11] Atomic orbital parameters for all atoms, listed in Table 1, and charge iteration parameters for Mo and O were taken from standard sources.[17] DOS curves were evaluated using 8 k-point sets.

Table 1. Atomic Parameters Used in the Extended Hückel Calculations.

atom	orbital	H_{jj}(eV)	ζ_1	C_1	ζ_2	C_2
Mo	5s	-8.77	1.96			
	5p	-5.60	1.90			
	4d	-11.06	4.54	0.5899	1.90	0.5899
O	2s	-32.30	2.28			
	2p	-14.80	2.28			

X-ray Structure Determination

A suitable black crystal with dimensions of 0.10 x 0.10 x 0.06 mm^3 was selected from the reaction product of La_2O_3, Mo, and MoO_3. The crystal was then encased in epoxy resin, and attached to the tip of a glass fiber. All measurements were made on a Rigaku AFC6R diffractometer using graphite monochromated Mo Kα (λ = 0.71069 Å) radiation and a 12 KW rotating anode generator.

Cell constants and an orientation matrix for data collection, obtained from a least-squares refinement using the setting angles of 25 carefully centered reflections in the range $4.0 < 2\theta < 35.0$, corresponded to an orthorhombic cell with dimensions: a = 9.197(2) Å, b = 11.128(2) Å, c = 20.006(4) Å, and V = 2048(1) Å^3. Data were collected at room temperature over the range $4° < 2\theta < 60°$ in the hemisphere ($\pm h$, $+k$, $\pm l$) using the ω - 2θ scan technique. Three standard reflections were monitored every 150 reflections and showed no intensity variation over the collection period. A total of 5372 reflections were collected, of which 2737 were unique ($R_{int} = 0.086$) and 1029 of which were observed with $I > 3.00\sigma(I)$. No Decay correction was applied. First, an empirical absorption correction using the ψ scan technique was applied after the structure solution. After all of the atoms were located and refined isotropically, the ψ scan absorption correction was removed, and an empirical absorption correction using the DIFABS program[18a] was applied which resulted in transmission factors ranging from 0.94 to 1.08. The data were corrected for Lorentz and polarization effects.

The orthorhombic space group was *Pbcn* (#60) was chosen on the basis of systematic absences and intensity statistics. The structure was solved by the SHELXS direct methods[18b] which yielded the positions of the lanthanum and molybdenum and chlorine atoms. Successive Fourier electron difference maps yielded the positions of the oxygen atoms. The structure was then refined by full-matrix least-squares methods

with anisotropic thermal parameters on all La atoms and seven of the eight unique Mo atoms, and isotropic thermal parameters on the remaining one Mo atom and all oxygen atoms. The final cycle of full-matrix least-squares refinement was based on 1029 observed reflections and 136 variable parameters and converged with unweighted and weighted agreement factors of R = 0.035 and Rw = 0.045, respectively. The asymmetric unit was found to be $LaMo_8O_{14}$. All calculations were performed using the TEXSAN[18c] crystallographic software package of Molecular Structure Corporation. The crystallographic data and refinement results are given in Table 2, and the atomic coordinates and equivalent isotropic thermal parameters of non-hydrogen atoms are given in Table 3. The anisotropic thermal parameters are listed in Table 4.

Results and Discussion

Synthesis of $LnMo_8O_{14}$

Most known reduced rare-earth molybdenum oxide compounds containing bicapped Mo_8 clusters were prepared at extremely high temperature (>1800°C). The compound $LaMo_{7.7}O_{14}$ was made at 1080°C using an electrolysis method. However, the starting materials were not in stoichiometric ratio, and the method could not produce a pure powder product.[10] In this work, all compounds $LnMo_8O_{14}$ were prepared at relatively low temperature (1250°C). All of the black powder products

Table 2. Crystallographic data for $LaMo_8O_{14}$

Empirical Formula	$LaMo_8O_{14}$
Formula Weight	1130.42
Crystal Color, Habit	black, chunk
Crystal Size (mm)	0.10 x 0.10 x 0.06
Crystal System	orthorhombic
Space Group	*Pbcn* (#60)
Lattice Parameters	a = 9.197(2) Å
	b = 11.128(2) Å
	c = 20.006(4) Å
	V = 2048(1) Å
Z Value	8
Density(calc.)	7.333 g/cm^3
F_{000}	4040
Diffractometer	Rigaku AFC6R
Radiation	MoKα (λ = 0.71069 Å)
Temperature	23°C
2θ range	4-60°
No. of Reflections Measured	5372
No. of Unique Reflections	2737 (R_{int} = 0.086)
No. of Observations (I>3.00σ(I))	1029
No. of Variables	136
Reflection/Parameter Ratio	7.57
Residuals: R; Rw[a]	0.035; 0.045
Goodness-of-Fit	1.46
Maximum Peak in Final Diff. Map	3.83 e$^-$/Å^3
Minimum Peak in Final Diff. Map	-2.50 e$^-$/Å^3

[a] $R = \Sigma \mid |Fo| - |Fc| \mid / \Sigma |Fo|$; $Rw = [(\Sigma w (|Fo| - |Fc|)^2 / \Sigma w Fo^2)]^{1/2}$.

Table 3. Atomic coordinates and equivalent isotropic thermal parameters ($Å^2$) of the atoms for $LaMo_8O_{14}$.

atom	x	y	z	B(eq)[a]
La(1)	0	0.9794(2)	1/4	0.6(1)
La(2)	0	1/2	1/2	0.5(1)
Mo(1)	0.1211(3)	0.7737(2)	0.4204(1)	0.15(8)
Mo(2)	0.1208(3)	0.2703(2)	0.1675(1)	0.24(7)
Mo(3)	0.1196(6)	0.0120(2)	0.4209(2)	0.37(8)
Mo(4)	0.1211(5)	0.6284(2)	0.2875(2)	0.3(1)
Mo(5)	0.3801(5)	0.6235(2)	0.5435(2)	0.2(1)
Mo(6)	-0.3746(5)	0.8832(2)	0.2065(2)	0.3(1)
Mo(7)	0.1223(5)	0.8752(2)	0.5369(2)	0.2(1)
Mo(8)	-0.3776(5)	0.0032(1)	0.3304(2)	0.12(5)
O(1)	0	0.756(2)	1/4	0.8(4)
O(2)	1/2	0.737(2)	1/4	0.7(4)
O(3)	-0.230(4)	0.010(1)	0.173(2)	1.0(4)
O(4)	0.260(3)	0.004(1)	0.082(1)	0.1(3)
O(5)	0.008(2)	0.741(1)	-0.0012(7)	0.4(3)
O(6)	-0.237(3)	0.887(2)	0.286(1)	0.6(3)
O(7)	-0.270(3)	0.891(2)	0.040(1)	0.5(3)
O(8)	-0.489(2)	0.888(1)	0.118(1)	0.3(3)
O(9)	-0.006(2)	0.896(1)	0.369(1)	0.5(3)
O(10)	-0.258(2)	0.755(1)	0.413(1)	0.4(3)
O(11)	-0.262(2)	0.134(1)	0.039(1)	0.3(3)
O(12)	0.244(3)	0.130(2)	0.213(1)	1.0(4)
O(13)	-0.241(2)	0.764(1)	0.165(2)	0.9(4)
O(14)	0.009(3)	0.134(2)	0.125(1)	1.0(3)
O(15)	0.012(2)	0.634(1)	0.375(1)	0.2(2)

[a] $B_{eq} = 8/3\pi^2(U_{11}(aa^*)^2 + U_{22}(bb^*)^2 + U_{33}(cc^*)^2 + 2U_{12}aa^*bb^*\cos\gamma + 2U_{13}aa^*cc^*\cos\beta + 2U_{23}bb^*cc^*\cos\alpha)$

Table 4. Anisotropic thermal parameters ($Å^2$) of the atoms for $LaMo_8O_{14}$[a,b]

atom	U11	U22	U33	U12	U13	U23
La(1)	0.007(1)	0.0053(7)	0.011(2)	0	-0.001(1)	0
La(2)	0.004(1)	0.0088(8)	0.006(1)	0.0005(7)	0.000(1)	-0.0017(6)
Mo(1)	0.003(1)	0.0016(9)	0.002(1)	0.0000(9)	-0.0001(9)	0.0000(7)
Mo(2)	0.0039(9)	0.0027(7)	0.002(1)	-0.0001(8)	-0.0006(8)	0.0003(6)
Mo(3)	0.004(1)	0.0068(8)	0.003(1)	-0.0008(9)	0.0000(8)	0.0003(8)
Mo(4)	0.005(2)	0.0030(9)	0.002(1)	-0.001(1)	0.001(1)	-0.0004(7)
Mo(5)	0.002(2)	0.0030(9)	0.004(1)	0.002(1)	-0.000(1)	0.0003(7)
Mo(6)	0.005(2)	0.0019(8)	0.002(1)	-0.0013(9)	0.001(1)	-0.0006(8)
Mo(7)	0.001(2)	0.0029(9)	0.004(1)	-0.0001(9)	-0.002(1)	0.0008(7)
Mo(8)	0.0016(6)					
O(1)	0.010(5)					
O(2)	0.009(5)					
O(3)	0.012(5)					
O(4)	0.001(4)					
O(5)	0.005(4)					
O(6)	0.008(4)					
O(7)	0.007(4)					
O(8)	0.004(3)					
O(9)	0.006(3)					
O(10)	0.005(4)					
O(11)	0.004(4)					
O(12)	0.013(5)					
O(13)	0.011(5)					
O(14)	0.013(4)					
O(15)	0.002(3)					

[a]The coefficients U_{ij} of the anisotropic temperature factor expression are defined as $\exp(-2\pi^2(a^{*2}U_{11}h^2 + b^{*2}U_{22}k^2 + c^{*2}U_{33}l^2 + 2a^*b^*U_{12}hk + 2a^*c^*U_{13}hl + 2b^*c^*U_{23}kl))$

[b]Thermal parameters for Mo(8) and all oxygen atoms only refined isotropically.

were examined by X-ray powder diffraction. The results indicated that pure phases were obtained. Under these synthetic conditions, the phases containing all cis-Mo_8 clusters and 1:1 ratio of cis-Mo_8 to trans-Mo_8 were found (see Table 5). However, the phase containing 2:1 ratio of cis-Mo_8 to trans-Mo_8 has not been found under these synthetic conditions. The $PrMo_8O_{14}$ compound containing 2:1 ratio of cis-Mo_8 to trans-Mo_8 was discovered at extremely high temperature (2000K).[15]

Cation effects

This work confirms that the sizes of the rare-earth cations are critical for the formation of the various phase types. Larger cations (La, Ce, and Pr) aid in the formation of trans-Mo_8 bicapped octahedra, and smaller cations (Nd and Sm) stabilize only the cis-Mo_8 bicapped octahedra. This is concluded from the finding that $LaMo_8O_{14}$, $CeMo_8O_{14}$, and $PrMo_8O_{14}$ contain a 1:1 ratio of cis-Mo_8 to trans-Mo_8 octahedra, and $NdMo_8O_{14}$ and $SmMo_8O_{14}$ contain only cis-Mo_8 octahedra. For the rare-earth cations smaller than Sm, no compounds containing Mo_8 bicapped octahedra were found. If one considers the effective volume occupied by the Mo_8 bicapped octahedral cluster, one can show that the effective volume of cis-Mo_8 cluster is only about 3/4 of that of the trans-Mo_8 cluster (see Figure 2). Therefore, the formation of trans-Mo_8 octahedra requires more space, and it can be argued that the larger cations satisfy this requirement by opening up the intercluster space.

Table 5. Compounds prepared in the $LnMo_8O_{14}$ system at 1250°C

Compound	Cluster Type	Ratio	Characterization	Cell Parameters
$LaMoO_{14}$	cis-, trans-	1:1	X-ray single crystal	a = 9.197(2) Å b = 11.128(2) Å c = 20.006(4) Å
$CeMo_8O_{14}$	cis-, trans-	1:1	X-ray powder	
$PrMo_8O_{14}$	cis-, trans-	1:1	X-ray powder	
$NdMo_8O_{14}$	cis-		X-ray single crystal	a = 9.197(2) Å b = 9.996(2) Å c = 11.128(4) Å
$SmMo_8O_{14}$	cis-		X-ray single crystal	a = 9.191(6) Å b = 9.998(3) Å c = 11.139(6) Å
"$EuMo_8O_{14}$"	no bicapped-Mo_8		X-ray powder	
"$GdMo_8O_{14}$"	no bicapped-Mo_8		X-ray powder	
"$DyMo_8O_{14}$"	no bicapped-Mo_8		X-ray powder	

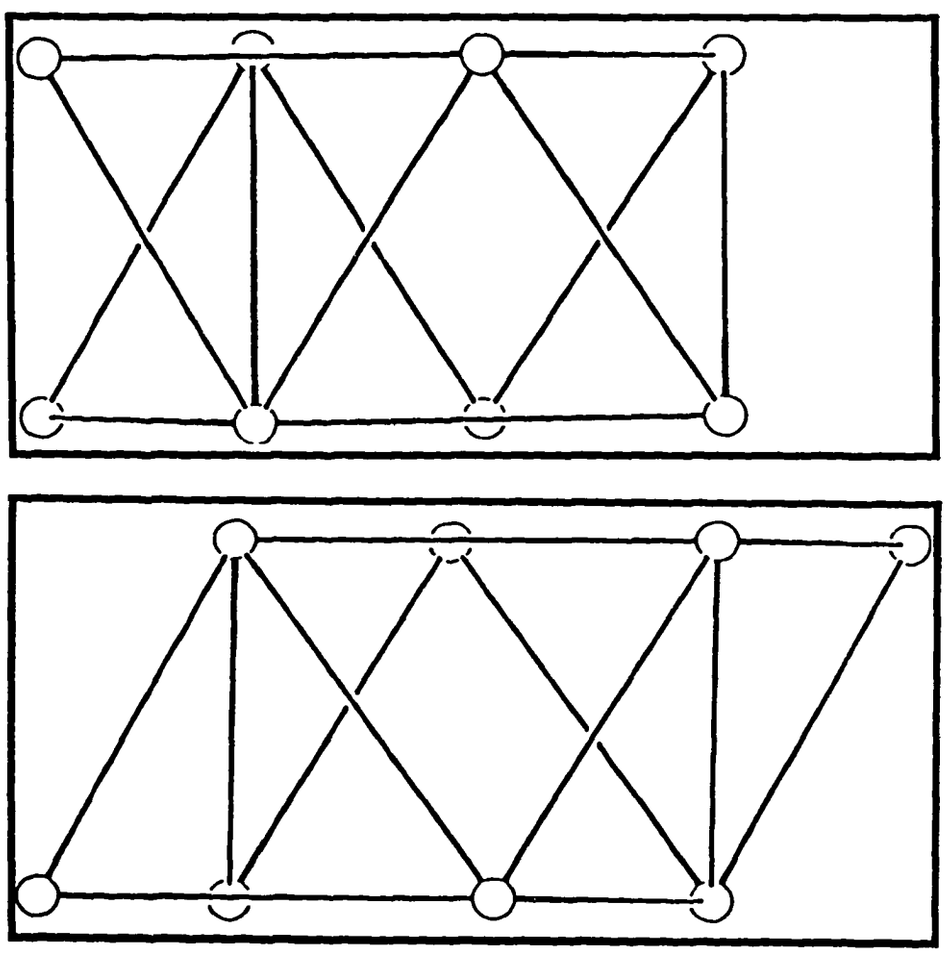

Figure 2. Illustration showing the effective volume differences between the cis- (upper) and trans- (lower) Mo_8 cluster units. By comparison, it is seen that the effective volume of the cis-Mo_8 cluster is 3/4th the value of the trans-Mo_8 cluster.

X-ray powder diffraction

Figure 3 and 4 illustrate the observed X-ray powder diffraction patterns for $SmMo_8O_{14}$ (cis-Mo_8) and $LaMo_8O_{14}$ (cis-Mo : trans-Mo_8 = 1:1), respectively. Their observed versus calculated d-spacings and relative intensities are given in Tables 6, and 7. The X-ray powder patterns of $LnMo_8O_{14}$ phases are quite similar to each other. The differences of their powder patterns are that there is no reflection found in the 2θ range of 20-22° for $LnMo_8O_{14}$ containing all cis-Mo_8, however, a medium strong reflection is found at 2θ 21.36° in the patterns of $LnMo_8O_{14}$ containing a 1:1 ratio of cis-Mo_8 to trans-Mo_8. On the other hand, there is no reflection found in the 2θ range of 58-60° for $LnMo_8O_{14}$ containing 1:1 ratio of cis-Mo_8 to trans-Mo_8, but a medium reflection is found at 2θ 59.44° in the patterns of $LnMo_8O_{14}$ containing all cis-Mo_8. Although a reflection at 2θ 22.71° is found in both types of pattern, the relative intensities of this reflection for $LnMo_8O_{14}$ containing all cis-Mo_8 is 12 times stronger than that for $LnMo_8O_{14}$ containing a 1:1 ratio of cis-Mo_8 to trans-Mo_8. Those differences help one to distinguish the two phases by X-ray powder diffraction.

Since the phase of $LnMo_8O_{14}$ containing 2:1 ratio of cis-Mo_8 to trans-Mo_8 was not observed in our synthetic conditions, the observed powder pattern was not obtained. However, the calculated pattern and d-spacings were obtained based on the published compound $PrMo_8O_{14}$ which was prepared at 2000 K.[15] The calculated XRD powder pattern of $PrMo_8O_{14}$ containing 2:1 ratio of cis- to trans-Mo_8 cluster has

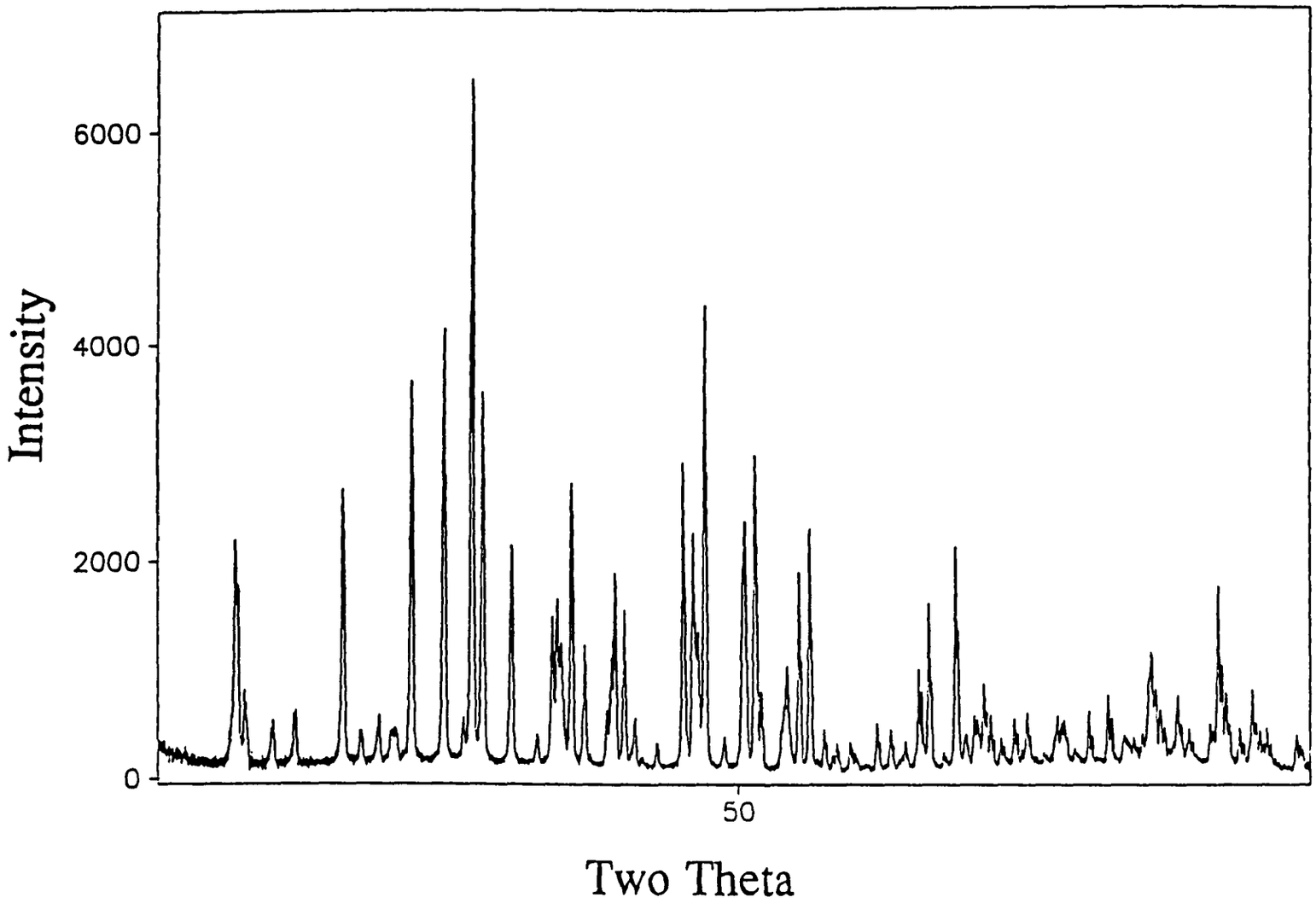

Figure 3. X-ray powder diffraction pattern of $SmMo_8O_{14}$.

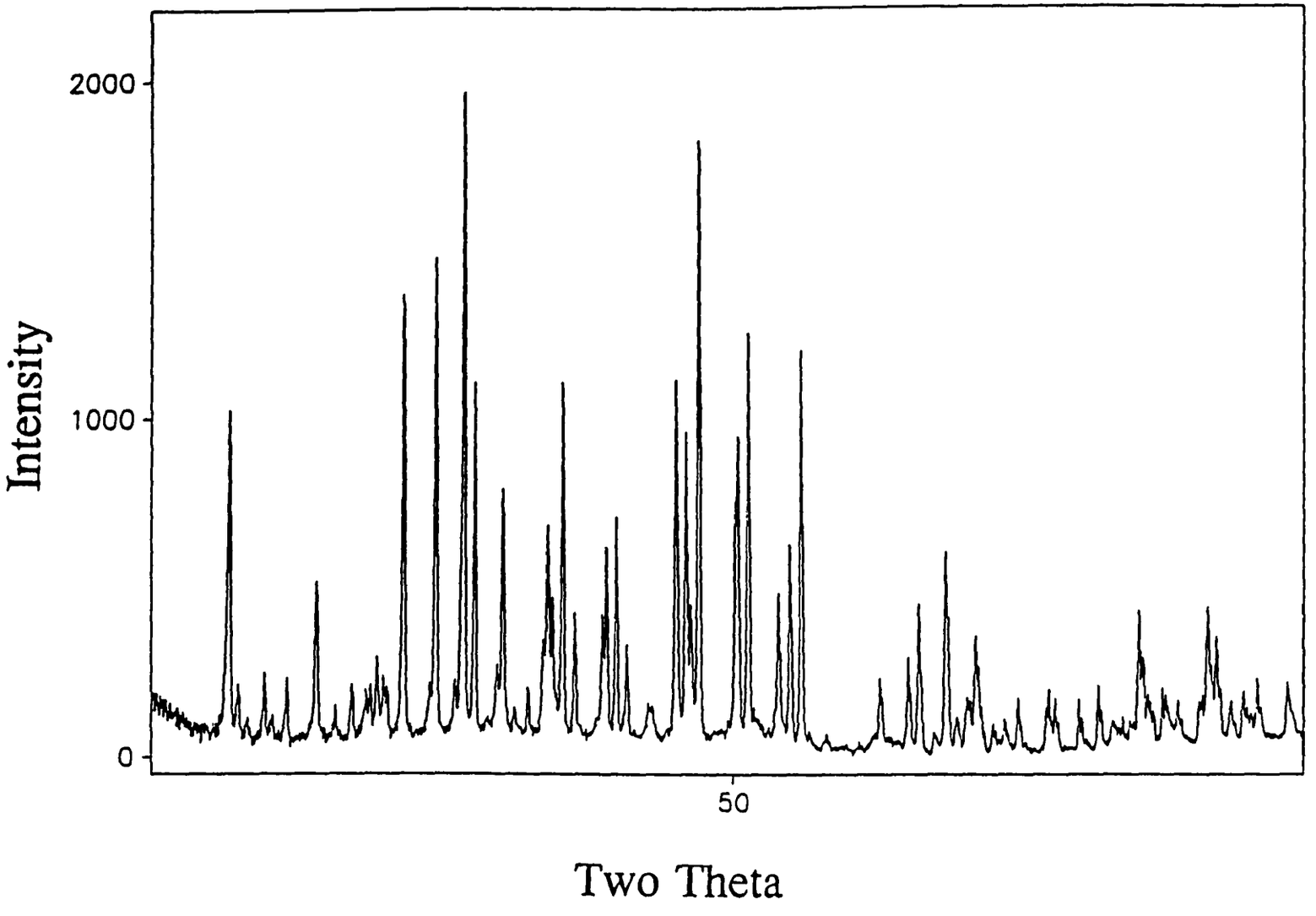

Figure 4. X-ray powder diffraction pattern of $LaMo_8O_{14}$.

Table 6. X-ray powder diffraction data for $LnMo_8O_{14}$ (Ln = Nd, Sm) containing cis-Mo_8 bicapped octahedra

	d_{Nd}		d_{Sm}		
h k l	cal.	obv.	obv.	2θ (cal.)	I (cal.)
1 1 1	5.786	5.793	5.782	15.30	73.7
0 0 2	5.585	5.600	5.586	15.85	23.6
0 2 0	4.992	5.006	4.981	17.75	14.8
2 0 0	4.598	4.600	4.586	19.29	9.5
2 1 1	3.912	3.916	3.909	22.71	49.1
0 2 2	3.722	3.723	3.709	23.89	9.5
2 0 2	3.550	3.543	3.550	25.06	7.4
2 2 0	3.382	3.409	3.387	26.33	4.7
1 1 3	3.262	3.249	3.226	27.32	60.1
1 3 1	3.014	3.010	2.994	29.62	83.6
2 2 2	2.893	2.892	2.885	30.88	5.3
3 1 1	2.834	2.833	2.830	31.54	100.0
2 1 3	2.779	2.771	2.767	32.18	60.4
2 3 1	2.621	2.617	2.619	34.18	38.7
0 4 0	2.496	2.498	2.487	35.95	6.2
0 2 4	2.437	2.429	2.430	36.85	19.9
1 4 0	2.409	2.407	2.398	37.29	26.8
1 3 3	2.396	2.391	2.387	37.51	24.1
2 0 4	2.387			37.65	3.4
1 2 4	2.356	2.349	2.350	38.17	50.2
4 0 0	2.299	2.297	2.289	39.15	17.2
3 3 1	2.210	2.210	2.206	40.79	5.5
2 4 0	2.194		2.185	41.11	13.5
2 3 3	2.184	2.180	2.178	41.31	21.8
2 2 4	2.153	2.147	2.142	41.92	22.0
1 1 5	2.121	2.111	2.116	42.58	10.5
2 4 2	2.042	2.043		44.32	3.4
2 1 5	1.970	1.964	1.960	46.03	48.7
4 2 2	1.956			46.38	3.1
3 4 0	1.936	1.936	1.931	46.90	43.7
3 3 3	1.929		1.921	47.08	7.7
1 5 1	1.922	1.923	1.918	47.24	15.3

Table 6. (continued)

h k l	d_{Nd} cal.	d_{Nd} obv.	d_{Sm} obv.	2θ (cal.)	I (cal.)
3 2 4	1.908	1.905	1.898	47.63	82.6
0 0 6	1.862	1.856		48.88	3.5
1 3 5	1.818	1.816	1.814	50.12	30.1
2 5 1	1.808	1.809	1.803	50.44	35.3
5 1 1	1.786	1.786	1.784	51.11	39.6
3 1 5	1.777	1.776	1.774	51.38	7.7
4 0 4	1.775			51.44	2.3
1 5 3	1.728	1.726		52.93	4.9
2 4 4	1.725			53.04	2.8
2 3 5	1.720	1.716	1.717	53.20	22.8
4 4 0	1.691	1.692	1.689	54.19	25.7
4 2 4	1.672	1.671	1.668	54.85	40.1
2 5 3	1.644	1.644	1.640	55.89	5.8
2 2 6	1.631			56.36	2.4
4 4 2	1.618	1.620	1.615	56.84	4.1
5 3 1	1.593	1.594	1.590	57.82	3.0
1 1 7	1.553	1.548	1.550	59.46	6.6
3 5 3	1.526	1.526	1.521	60.62	7.4
2 6 2	1.507			61.49	2.0
6 1 1	1.501	1.502	1.498	61.74	3.2
5 4 0	1.481	1.482	1.479	62.69	14.5
5 3 3	1.478	1.479		62.84	4.5
1 5 5	1.470			63.21	4.2
5 2 4	1.468	1.468	1.466	63.29	28.2
4 4 4	1.446			64.35	3.2
0 6 4	1.430	1.430	1.427	65.20	53.1
2 5 5	1.416	1.416		65.88	5.0
5 1 5	1.406			66.45	4.8
6 1 3	1.403	1.404	1.402	66.58	6.5
3 1 7	1.401			66.68	2.1
1 7 1	1.398	1.400		66.84	5.2
0 0 8	1.396	1.397	1.395	66.96	18.3
4 2 6	1.390	1.388		67.32	3.1
6 3 1	1.381	1.382	1.379	67.77	6.9

Table 6. (continued)

h k l	d_{Nd} cal.	d_{Nd} obv.	d_{Sm} obv.	2θ (cal.)	I (cal.)
2 6 4	1.365	1.366		68.70	2.1
2 7 1	1.352	1.350	1.348	69.44	9.2
3 5 5	1.339	1.339	1.334	70.22	10.5
1 7 3	1.318			71.51	2.9
6 4 0	1.306			72.27	3.6
6 3 3	1.304	1.304	1.302	72.41	5.2
3 3 7	1.302			72.50	5.4
6 2 4	1.297	1.298	1.296	72.83	6.1
5 5 3	1.272	1.272	1.270	74.57	6.7
6 1 5	1.254	1.254	1.252	75.80	11.7
0 6 6	1.241	1.239	1.238	76.75	3.2
1 8 0	1.237		1.235	77.04	5.5
1 5 7	1.235			77.14	2.2
7 1 3	1.229		1.224	77.59	4.3
3 7 3	1.222			78.17	7.6
1 1 9	1.221	1.220	1.218	78.24	12.0
0 4 8	1.219	1.218	1.216	78.40	6.7
7 3 1	1.215			78.71	6.6
4 6 4	1.214	1.215	1.212	78.76	20.8
6 5 1	1.209	1.210	1.208	79.17	10.1
1 4 8	1.208	1.207	1.205	79.22	8.9
2 5 7	1.203	1.203		79.61	3.7

Table 7. X-ray powder diffraction data for $LnMo_8O_{14}$ (Ln = La, Ce, Pr) containing a 1:1 ratio of cis- and trans-Mo_8 bicapped octahedra

			d_{La}		d_{Ce}	d_{Pr}		
h	k	l	cal.	obv.	obv.	obv.	2θ (cal.)	I (cal.)
1	1	2	5.784	5.840	5.835	5.820	15.31	62.8
0	2	0	5.564	5.577	5.590	5.583	15.91	13.0
0	2	1	5.360	5.364			16.52	3.7
0	0	4	5.002	5.006	5.026	5.021	17.72	15.0
1	1	3	4.857	4.867			18.25	7.3
2	0	0	4.598	4.601	4.611	4.617	19.29	10.8
2	1	1	4.157	4.154	4.116	4.092	21.36	32.8
2	1	2	3.912	3.917	3.924	3.929	22.71	3.9
0	2	4	3.720	3.725	3.723	3.729	23.90	8.2
2	1	3	3.584	3.588	3.572	3.570	24.82	10.3
2	2	0	3.544	3.546	3.543	3.540	25.10	6.1
1	1	5	3.485	3.487	3.472	3.468	25.54	17.3
1	3	1	3.390	3.398			26.26	2.4
2	0	4	3.385	3.392	3.379	3.376	26.30	4.8
1	3	2	3.253	3.254	3.253	3.259	27.39	65.2
1	3	3	3.057	3.059			29.18	9.3
1	1	6	3.017	3.025	3.021	3.021	29.58	69.0
2	2	4	2.892	2.904	2.893	2.895	30.89	6.0
2	3	1	2.857	2.860			31.28	18.8
3	1	2	2.834	2.844	2.840	2.840	31.54	100.0
2	3	2	2.774	2.780	2.775	2.777	32.24	40.6
3	1	3	2.702		2.699	2.696	33.12	2.8
1	1	7	2.651	2.660			33.78	6.5
2	3	3	2.650				33.80	8.1
2	1	6	2.623	2.630	2.626	2.626	34.15	38.1
1	3	5	2.608				34.35	3.3
0	4	3	2.568	2.574			34.91	4.3
0	0	8	2.501	2.507	2.505	2.503	35.88	7.3
0	4	4	2.431	2.436	2.432	2.432	36.94	10.5
1	0	8	2.413	2.418	2.414	2.414	37.23	26.6
1	3	6	2.394	2.399	2.394	2.396	37.53	22.7
2	4	0	2.380				37.76	2.3
3	1	5	2.377				37.81	3.5

Table 7. (continued)

h	k	l	d_{La} cal.	d_{La} obv.	d_{Ce} obv.	d_{Pr} obv.	2θ (cal.)	I (cal.)
1	4	4	2.350	2.355	2.351	2.352	38.26	52.2
4	0	0	2.299	2.304	2.302	2.303	39.15	18.5
2	0	8	2.197	2.202	2.198	2.197	41.05	13.4
2	3	6	2.183	2.187	2.184	2.184	41.33	29.8
2	4	4	2.149	2.154	2.150	2.151	42.00	25.2
1	5	2	2.114	2.119	2.115	2.116	42.73	11.7
3	1	7	2.054	2.058			44.04	2.2
2	2	8	2.043	2.040	2.044	2.041	44.29	4.0
3	3	5	2.035	2.033			44.49	3.6
2	3	7	2.031	2.029			44.57	2.5
2	5	2	1.964	1.968	1.964	1.965	46.17	47.4
4	2	4	1.956				46.39	2.8
3	0	8	1.938	1.942	1.938	1.939	46.84	46.2
1	1	10	1.925	1.928	1.925	1.926	47.16	17.2
3	4	4	1.905	1.909	1.906	1.906	47.70	84.0
1	3	9	1.867				48.73	3.1
1	5	6	1.815	1.819	1.816	1.815	50.23	29.3
2	1	10	1.810	1.814	1.812	1.810	50.37	31.1
5	1	2	1.786	1.792	1.788	1.788	51.11	40.4
4	4	1	1.765	1.770	1.771	1.772	51.74	2.3
2	3	9	1.761				51.86	4.4
2	5	6	1.717	1.720	1.718	1.718	53.30	19.5
4	0	8	1.693	1.697	1.694	1.694	54.14	30.3
4	4	4	1.670	1.672	1.672	1.671	54.91	44.4
5	1	5	1.653				55.56	2.5
4	2	8	1.619		1.622	1.623	56.80	2.4
2	3	11	1.539				60.07	2.7
3	3	10	1.527	1.529	1.528	1.528	60.59	10.3
5	3	5	1.524	1.525		1.523	60.73	2.1
5	0	8	1.482	1.485	1.482	1.483	62.64	14.8
5	4	4	1.467	1.470	1.467	1.468	63.35	28.1
2	1	13	1.447			1.447	64.32	2.8
4	4	8	1.446				64.37	2.7
0	4	12	1.430	1.432	1.429	1.430	65.18	57.6

Table 7. (continued)

h k l	d_{La} cal.	d_{La} obv.	d_{Ce} obv.	d_{Pr} obv.	2θ (cal.)	I (cal.)
2 5 10	1.416	1.417	1.416		65.93	2.0
6 3 1	1.413		1.413		66.06	2.1
6 3 2	1.403	1.404	1.404		66.62	4.1
1 1 14	1.401		1.402		66.71	3.7
3 7 2	1.397	1.399		1.397	66.90	6.7
0 8 0	1.391	1.393	1.390	1.391	67.25	21.0
6 1 6	1.382	1.389	1.384	1.383	67.75	6.2
2 7 6	1.370	1.371	1.369	1.370	68.43	5.7
2 1 14	1.354	1.357	1.355	1.355	69.31	6.9
3 5 10	1.338	1.341	1.339	1.339	70.26	10.9
6 0 8	1.307	1.306	1.306	1.305	72.23	3.9
6 3 6	1.304	1.302			72.42	6.9
6 4 4	1.297	1.299	1.298	1.296	72.89	7.1
5 3 10	1.272	1.274	1.272	1.270	74.54	8.9
6 5 2	1.252	1.255	1.254	1.253	75.90	11.4
1 0 16	1.239	1.241	1.240	1.239	76.87	6.5
1 7 10	1.233		1.230	1.230	77.29	5.1
3 3 14	1.223	1.226	1.223	1.223	78.08	9.4
1 9 2	1.216	1.216	1.216	1.215	78.58	3.4
4 4 12	1.214	1.213	1.211	1.212	78.73	15.9
6 1 10	1.210	1.209	1.208		79.11	8.6
1 8 8	1.205	1.203	1.202	1.205	79.46	7.4

shown that two medium intensity reflections occur at 2θ 24.04° and 26.86°, which are not observed in the other two phases. Also a medium intensity reflection at 2θ 21.71° is observed in this pattern, but is not observed in the pattern of $LnMo_8O_{14}$ containing all cis-bicapped Mo_8 clusters. Table 8 gives the calculated d-spacings, 2θ values, and relative intensities of $PrMo_8O_{14}$ containing a 2:1 ratio of cis- to trans-Mo_8 bicapped octahedra. The calculated X-ray powder patterns of $NdMo_8O_{14}$, $LaMo_8O_{14}$, and $PrMo_8O_{14}$ in the 2θ range of 20-30° are shown in Figure 5.

Table 8. The calculated X-ray powder diffraction data for $PrMo_8O_{14}$ containing a 2:1 ratio of cis- to trans-Mo_8 bicapped octahedra

2θ	d	h k l	I
15.31	5.784	1 1 3	57.7
15.93	5.557	0 2 0	14.0
16.21	5.464	0 2 1	5.3
17.19	5.152	1 1 4	3.6
17.72	5.002	0 0 6	15.3
19.27	4.602	2 0 0	10.6
20.87	4.252	2 1 0	4.0
21.71	4.091	2 1 2	26.3
21.73	4.087	1 1 6	2.9
22.70	3.913	2 1 3	3.6
23.91	3.718	0 2 6	8.4
24.04	3.699	2 1 4	12.1
25.10	3.544	2 2 0	6.7

Table 8. (continued)

2θ	d	h k l	I
25.28	3.520	2 2 1	0.5
26.29	3.387	2 0 6	5.4
26.59	3.350	1 3 2	5.1
26.86	3.316	1 1 8	15.4
27.42	3.250	1 3 3	60.8
28.54	3.124	1 3 4	8.9
29.58	3.017	1 1 9	68.1
30.89	2.892	2 2 6	5.7
30.96	2.886	2 3 0	1.8
31.52	2.836	3 1 3	100.0
31.54	2.834	2 3 2	15.2
31.56	2.832	1 3 6	1.6
32.26	2.773	2 3 3	38.9
32.37	2.764	1 1 10	6.9
32.52	2.751	3 1 4	2.7
33.23	2.693	2 3 4	9.0
34.14	2.624	2 1 9	37.3
35.57	2.521	0 4 5	5.1
35.87	2.501	0 0 12	6.8
36.98	2.429	0 4 6	11.0
37.22	2.413	1 0 12	26.3
37.55	2.393	1 3 9	21.9
37.79	2.378	2 4 0	1.8
37.91	2.371	2 4 1	1.9
38.29	2.348	1 4 6	50.4
38.54	2.334	3 3 2	0.4
38.74	2.322	3 1 8	2.8
39.12	2.301	4 0 0	17.7
39.85	2.260	1 4 7	2.0
41.04	2.197	2 0 12	13.7
41.34	2.182	2 3 9	27.7
42.03	2.148	2 4 6	23.2

Table 8. (continued)

2θ	d	h k l	I
42.78	2.112	1 5 3	10.0
42.90	2.106	3 1 10	2.2
43.47	2.080	2 3 10	1.5
44.29	2.043	2 2 12	3.8
45.32	1.999	3 3 8	4.2
46.21	1.963	2 5 3	47.2
46.37	1.956	4 2 6	2.7
46.58	1.948	3 4 5	2.0
46.82	1.938	3 0 12	44.7
47.16	1.926	1 1 15	16.8
47.46	1.914	2 1 14	1.6
47.72	1.904	3 4 6	80.5
48.58	1.872	1 5 8	2.6
49.02	1.857	3 3 10	1.5
49.03	1.856	3 4 7	2.2
49.24	1.849	0 6 1	2.3
50.11	1.819	1 3 14	3.3
50.27	1.813	1 5 9	26.4
50.36	1.810	2 1 15	30.5
51.06	1.787	3 5 2	2.6
51.07	1.786	5 1 3	40.0
51.52	1.772	4 4 0	1.6
51.62	1.769	4 4 1	2.4
52.11	1.754	1 5 10	1.9
52.22	1.750	3 5 4	1.8
53.09	1.723	2 4 12	1.9
53.18	1.721	2 3 14	3.7
53.34	1.716	2 5 9	19.0
54.11	1.693	4 0 12	29.2
54.92	1.670	4 4 6	42.2
56.23	1.634	5 1 8	2.0
56.79	1.620	4 2 12	2.5

Table 8. (continued)

2θ	d	h k l	I
58.65	1.573	2 3 16	2.3
59.33	1.556	1 7 2	2.0
60.38	1.531	1 7 4	2.7
60.59	1.527	3 3 15	9.5
61.38	1.509	5 3 8	2.1
62.61	1.482	5 0 12	14.7
63.29	1.468	1 5 15	2.2
63.34	1.467	5 4 6	27.8
63.54	1.463	2 5 14	2.1
64.38	1.446	4 4 12	2.4
64.43	1.445	5 3 10	1.6
65.20	1.430	0 4 18	54.8
65.96	1.415	2 1 20	2.5
66.15	1.411	5 5 2	2.0
66.58	1.403	6 3 3	3.8
66.71	1.401	1 1 21	3.7
66.96	1.396	3 7 3	4.8
67.34	1.389	0 8 0	18.7
67.70	1.383	6 1 9	6.2
68.50	1.369	2 7 9	4.9
69.30	1.355	2 1 21	6.8

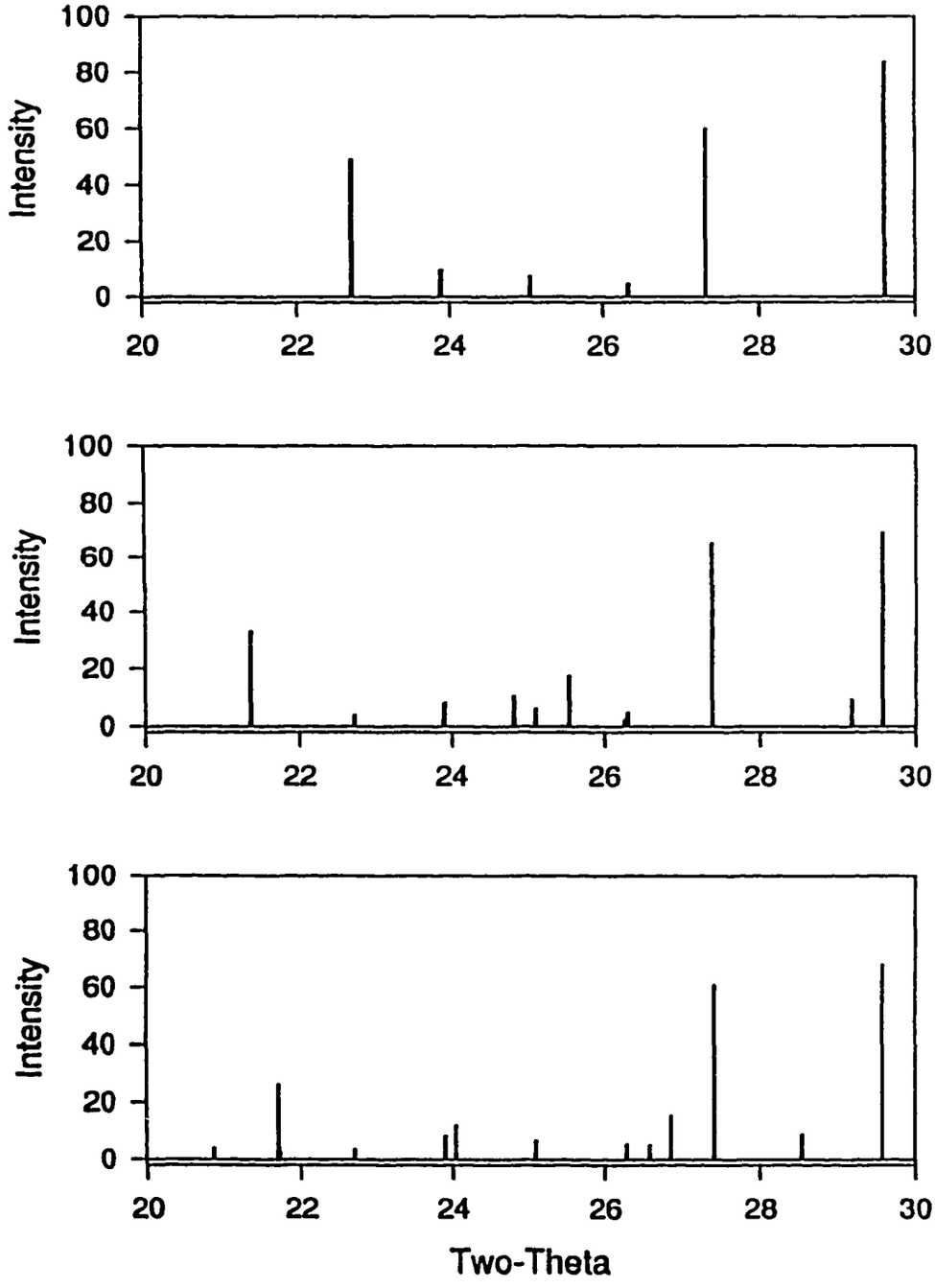

Figure 5. The calculated X-ray powder diffraction patterns of (a) $NdMo_8O_{14}$ containing all cis-Mo_8 octahedra, (b) $LaMo_8O_{14}$ containing a 1:1 ratio of cis- to trans-Mo_8 octahedra, and (c) $PrMo_8O_{14}$ containing a 2:1 ratio of cis- to trans-Mo_8 octahedra in the 2θ range of 20-30°.

Structure of $LnMo_8O_{14}$ (Ln = La, Ce, Pr)

The structures of $LaMo_8O_{14}$, $CeMo_8O_{14}$ and $PrMo_8O_{14}$ are characterized by the coexistence of cis- and trans-bicapped Mo_8 clusters with 1:1 ratio. The two isomers are extended along the c axis in alternating fashion (Figure 6). The ordering of the two isomers causes the c axis of the unit cell to be two times longer than the b axis of the unit cell of $LnMo_8O_{14}$ containing all cis-Mo_8 clusters, but the other two axes are almost identical. The Mo_8 clusters and the O atoms are arranged in layers parallel to the bc plane as shown in Figure 7. The oxygen atoms form a close packing in the sequence of ABAC, where, in the A layers, some of the O atoms are missing or replaced by Ln cations, while the B and C layers are fully occupied by oxygen atoms.

The structures of cis- and trans-bicapped Mo_8 octahedra and their oxygen environments are shown in Figures 8 and 9. The perfect cis-Mo_8O_{24} and trans-Mo_8O_{24} cluster units should have C_{2v} and D_{3d} symmetries, respectively. However, due to the structure distortions, their symmetries are lowered to C_2 and C_i, respectively.

The Mo-Mo and Mo-O bond distances for trans-Mo_8O_{24} and cis-Mo_8O_{24} clusters in $LaMo_8O_{14}$ compound are given in Tables 9 and 10, respectively. The Mo-Mo bond distances are in the range of 2.590(4) to 2.888(6) Å. The average Mo-Mo bond distance in the trans-isomer is 2.703 Å, which is shorter than that found in the cis-isomer (2.748 Å). This result indicates that the metal-metal bonds in the trans-isomer

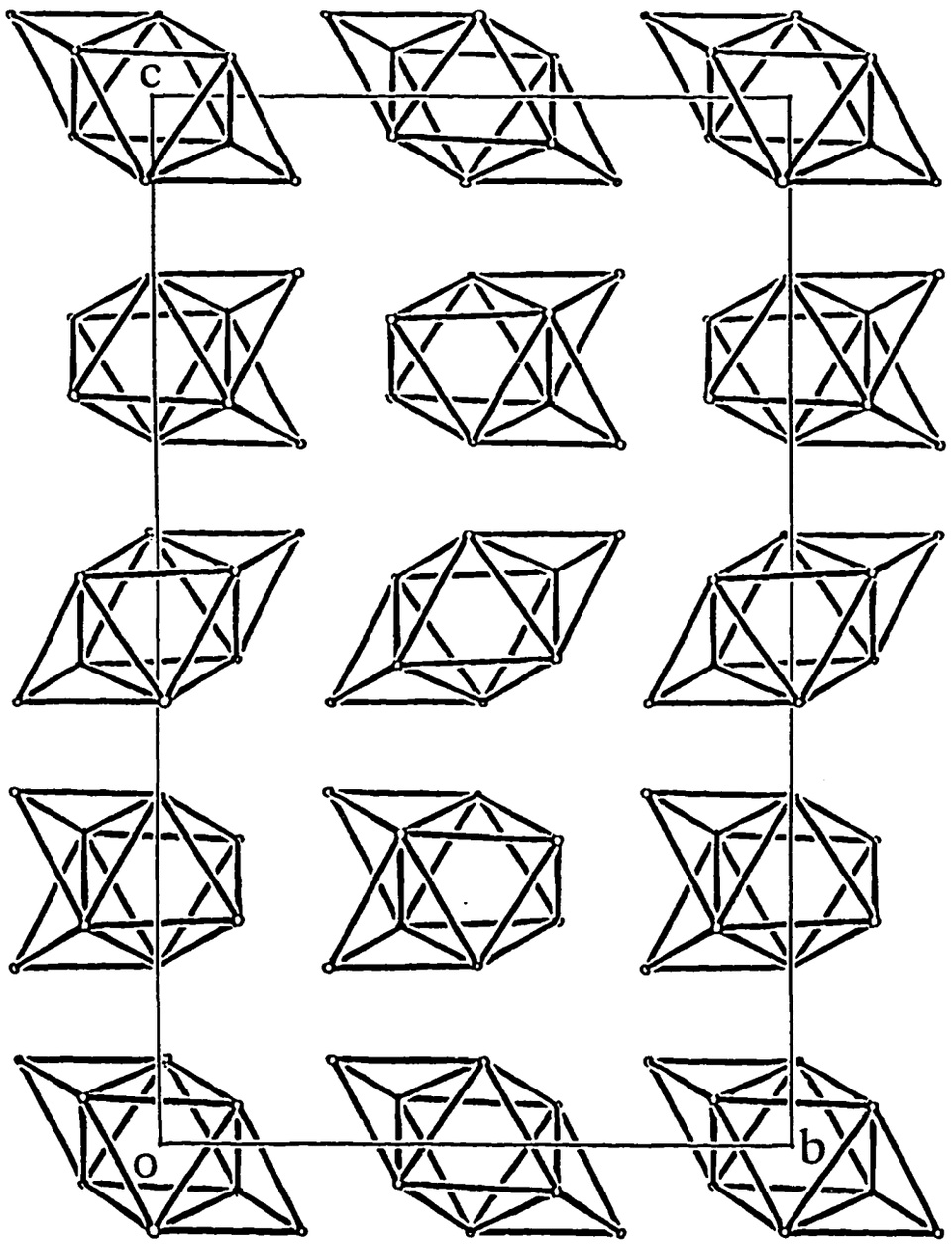

Figure 6. The packing diagram of the cis- and trans-Mo_8 bicapped octahedra in $LaMo_8O_{14}$, viewed down the a axis.

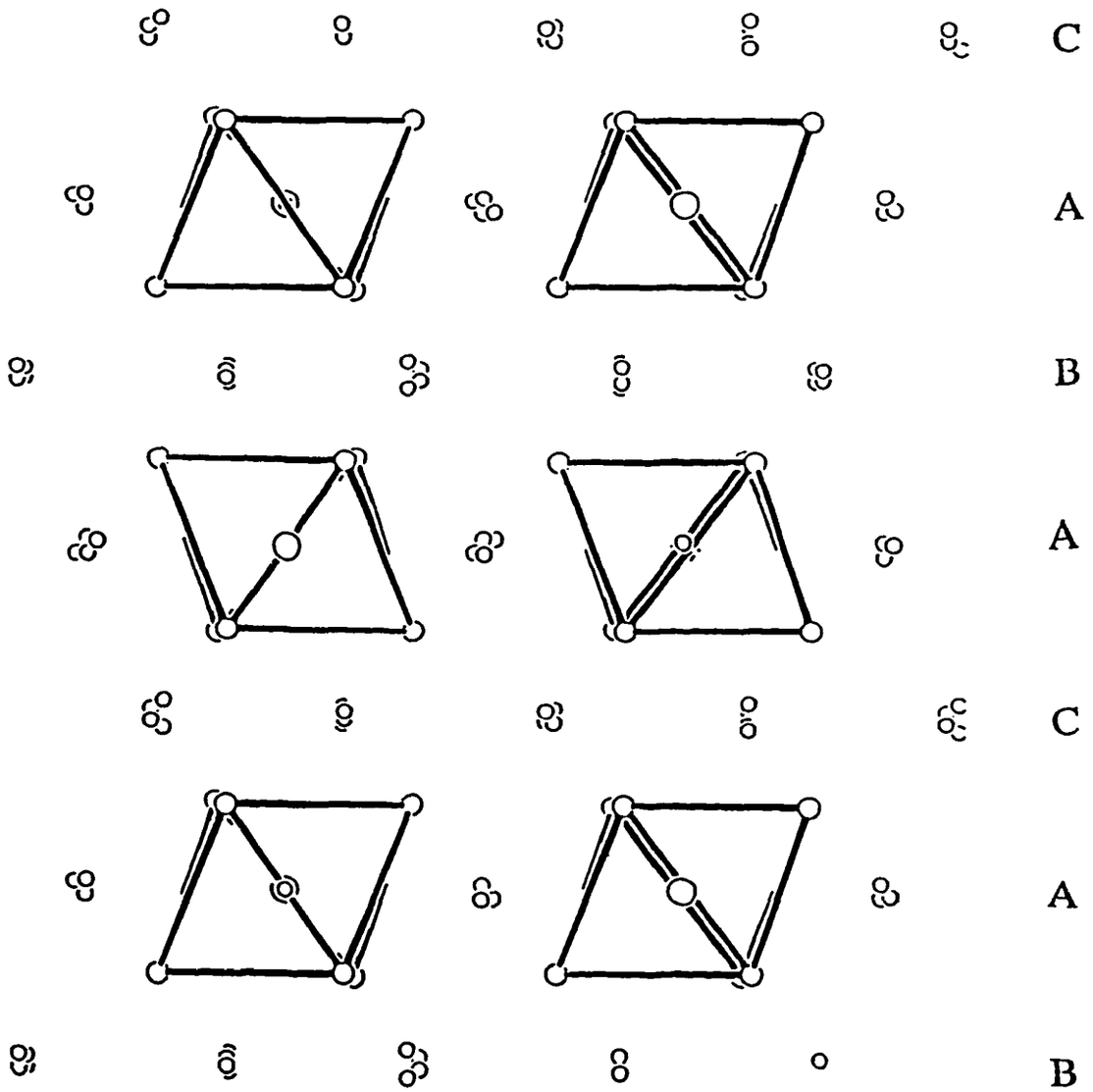

Figure 7. The arrangement of Mo_8 clusters (medium open circles), La cations (large open circles), and O atoms (small open circles) parallel to the bc plane.

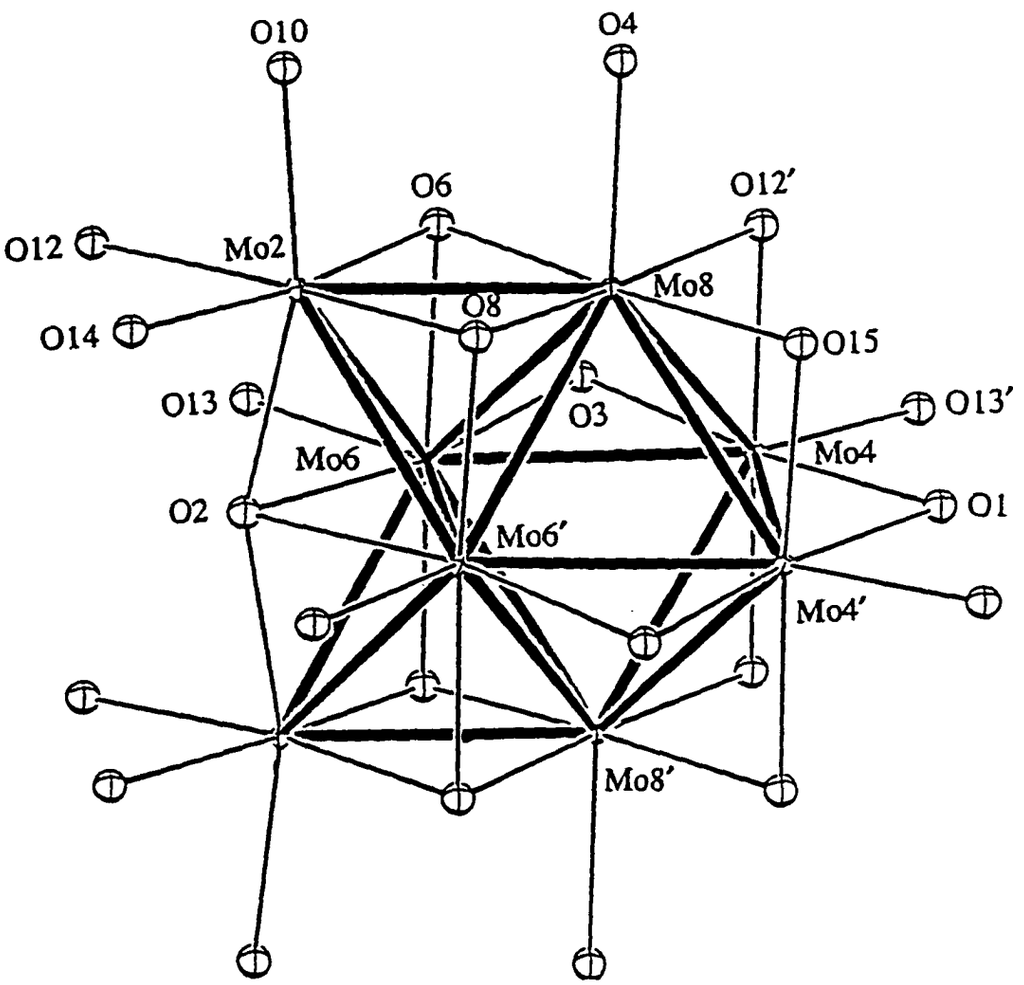

Figure 8. The cis-Mo_8O_{24} cluster unit.

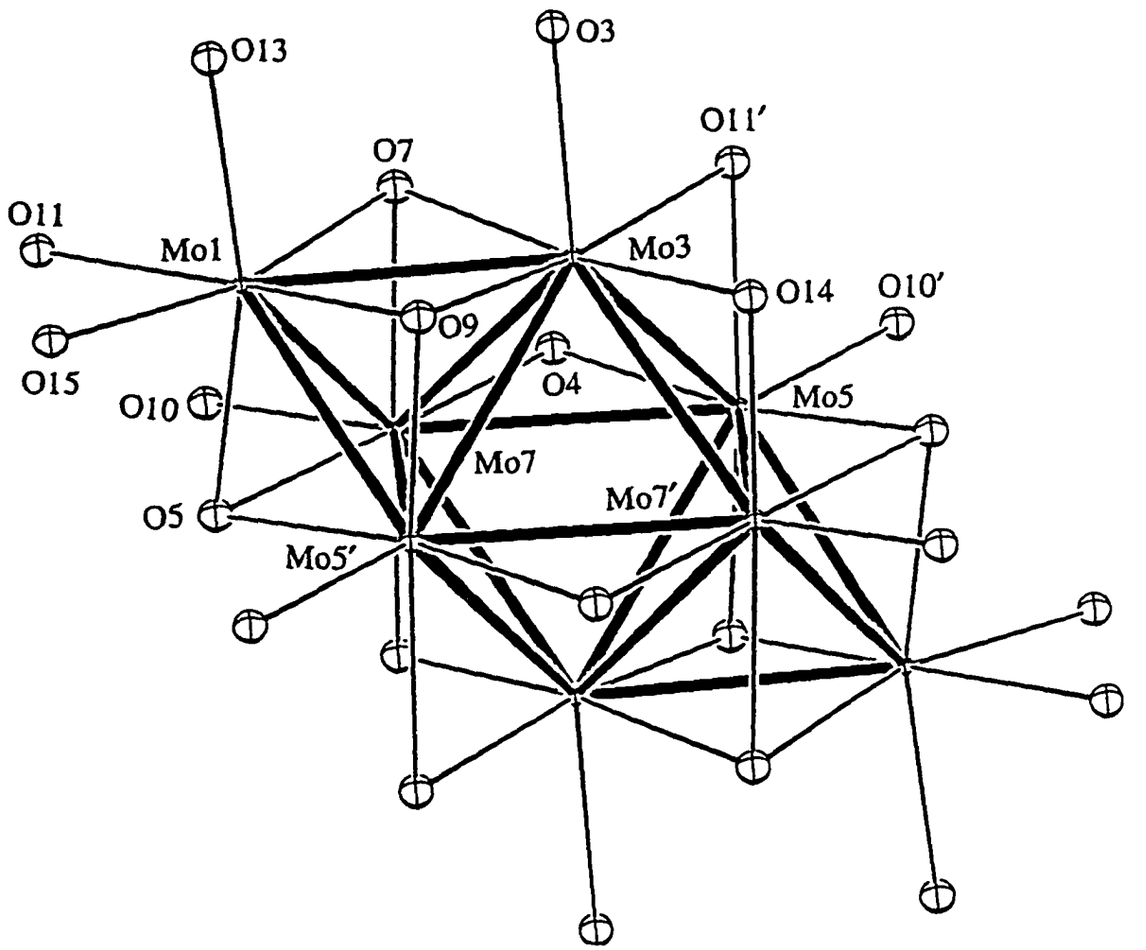

Figure 9. The trans-Mo_8O_{24} cluster unit.

Table 9. Bond distances (Å) for the trans-Mo_8O_{24} cluster in $LaMo_8O_{14}$

atom	atom	distance	atom	atom	distance
Mo(1)	Mo(3)	2.651(3)	Mo(1)	Mo(5)	2.597(4)
Mo(1)	Mo(7)	2.590(4)	Mo(3)	Mo(5)	2.763(6)
Mo(3)	Mo'(5)	2.748(6)	Mo(3)	Mo(7)	2.775(6)
Mo(3)	Mo'(7)	2.690(6)	Mo(5)	Mo(7)	2.766(3)
Mo(5)	Mo'(7)	2.747(8)	Mo(1)	O(5)	2.04(2)
Mo(1)	O(7)	2.05(2)	Mo(1)	O(9)	2.07(2)
Mo(1)	O(11)	2.06(2)	Mo(1)	O(13)	2.04(3)
Mo(1)	O(15)	2.07(2)	Mo(3)	O(3)	2.13(3)
Mo(3)	O(7)	2.08(2)	Mo(3)	O(9)	2.02(2)
Mo(3)	O(11)	2.05(2)	Mo(3)	O(14)	2.02(2)
Mo(5)	O(4)	2.06(2)	Mo(5)	O(5)	2.03(2)
Mo(5)	O(9)	2.05(2)	Mo(5)	O(10)	2.04(2)
Mo(5)	O(11)	2.11(2)	Mo(7)	O(4)	2.06(2)
Mo(7)	O(5)	2.04(2)	Mo(7)	O(7)	2.06(2)
Mo(7)	O(10)	2.08(2)	Mo(7)	O(14)	2.05(2)

Table 10. Bond distances (Å) for the cis-Mo_8O_{24} cluster in $LaMo_8O_{14}$

atom	atom	distance	atom	atom	distance
Mo(2)	Mo(6)	2.705(5)	Mo(2)	Mo'(6)	2.816(4)
Mo(2)	Mo(8)	2.591(3)	Mo(4)	Mo'(4)	2.685(9)
Mo(4)	Mo(6)	2.731(3)	Mo(4)	Mo(8)	2.738(6)
Mo(4)	Mo'(8)	2.774(6)	Mo(6)	Mo'(6)	2.888(9)
Mo(6)	Mo(8)	2.742(6)	Mo(6)	Mo'(8)	2.814(6)
Mo(1)	Mo(4)	3.113(4)	Mo(2)	Mo(7)	3.074(4)
Mo(2)	O(2)	2.025(5)	Mo(2)	O(6)	2.06(2)
Mo(2)	O(8)	2.04(2)	Mo(2)	O(10)	1.97(2)
Mo(2)	O(12)	2.13(2)	Mo(2)	O(14)	2.02(2)
Mo(4)	O(1)	1.95(2)	Mo(4)	O(3)	2.06(3)
Mo(4)	O(12)	1.94(3)	Mo(4)	O(13)	2.10(2)
Mo(4)	O(15)	2.01(2)	Mo(6)	O(2)	2.18(2)
Mo(6)	O(3)	2.06(3)	Mo(6)	O(6)	2.04(2)
Mo(6)	O(8)	2.06(2)	Mo(6)	O(13)	1.99(2)
Mo(8)	O(4)	2.06(3)	Mo(8)	O(6)	2.03(2)

are stronger than the bonds in the cis-isomer, and thus the trans-isomer may contain more electrons than the cis-isomer. Within the trans-isomer, the average Mo-Mo bond distance involving the capping metal atoms is much shorter than that between atoms composing the octahedron, which are 2.613 Å and 2.748 Å, respectively. The intercluster Mo-Mo bond distances are in the range 3.074(4)-3.113(4) Å. The Mo-O bond distances are in the range of 1.94(3) to 2.18(2) Å. The average Mo-O bond distance in trans-isomer is 2.06. While the average Mo-O bond distance in cis-isomer is 2.04 Å.

Each lanthanum cation is coordinated by ten oxygen atoms. Figure 10 shows the coordination spheres of the lanthanum cations. The La1 cation is sitting on a two-fold axis, and the La2 cation is sitting on an inversion center. The average La-O bond length is 2.67(2) Å. Table 11 lists the La-O bond distances.

Table 11. La-O bond distances (Å) in $LaMo_8O_{14}$

atom	atom	distance	atom	atom	distance
La(1)	O(1)	2.49(2)	La(1)	O(2)	2.86(2)
La(1)	O(3)	2.64(3)	La(1)	O(6)	2.52(2)
La(1)	O(9)	2.56(2)	La(1)	O(12)	2.90(2)
La(2)	O(4)	2.75(3)	La(2)	O(5)	2.68(2)
La(2)	O(7)	2.57(2)	La(2)	O(8)	2.67(2)
La(2)	O(11)	2.76(2)			

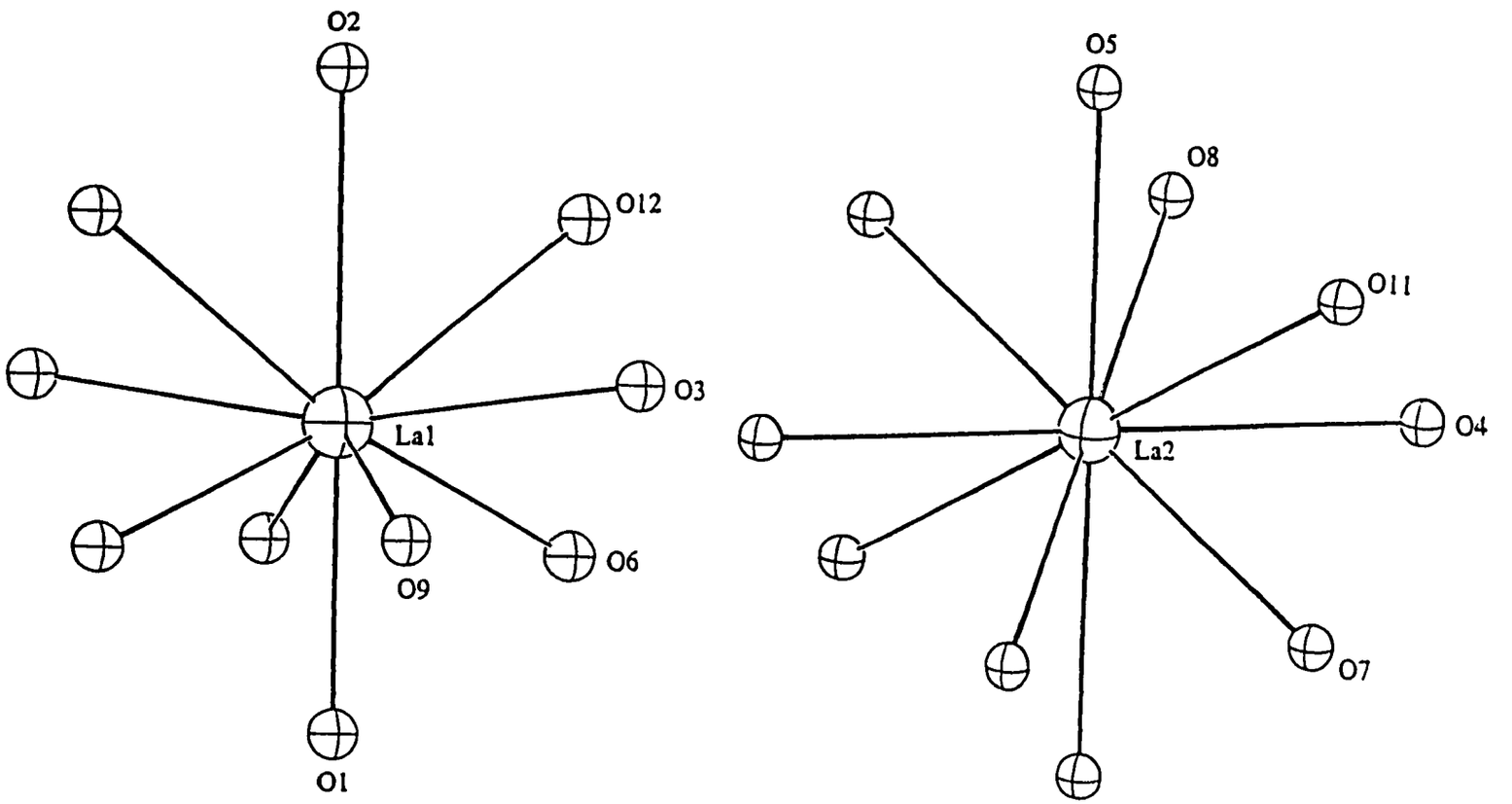

Figure 10. The coordination environments of the La cations in $LaMo_8O_{14}$.

Bond length-bond order relations

The application of bond length-bond order relationships has provided valuable insights into the structure, bonding, oxidation states, and electron counting of the reduced molybdenum oxide compounds. For calculation of M-O bond strengths in metal oxides, the most reliable empirical relationship between bond strengths and bond distances has been developed by Brown and Wu.[19] The relationship is given in equation 2

$$s(M\text{-}O) = [d(M\text{-}O)/d_1(M\text{-}O)]^{-n} \qquad (2)$$

where s(M-O) is the bond strength of M-O bond in valence units (v.u); d(M-O) is the observed M-O bond distance (Å), and d_1(M-O) is the M-O single bond distance (Å); n is an exponential parameter having a value characteristic of each metal atom. For molybdenum, the best d_1(M-O) and n values are 1.882 and 6.0, respectively.

The Mo-O bond strength calculation results on $LaMo_8O_{14}$, containing 1:1 ratio of cis-Mo_8 to trans-Mo_8 clusters, and $NdMo_8O_{14}$, containing all cis-Mo_8 clusters, are given in Table 12. Based on the Mo-O bond strength sums, the number of metal centered electrons (MCE)[20] of Mo_8 clusters were calculated.

The number of MCE indicates that the cis-Mo_8 clusters in $LaMo_8O_{14}$ contains 22 electrons, and the trans-Mo_8 clusters in $LaMo_8O_{14}$ contains 24 electrons. The cis-Mo_8 cluster in $NdMo_8O_{14}$ should contain 23 electrons based on the formula. The

Table 12. Mo-O bond strength sums and cluster electron counting for $LaMo_8O_{14}$ and $NdMo_8O_{14}$

	$LaMo_8O_{14}$		$NdMo_8O_{14}$
	cis-Mo_8	trans-Mo_8	cis-Mo_8
$\Sigma[\Sigma s(Mo_n\text{-}O)]^a$	25.94	24.68	25.42
MCE^b	22.06	23.32	22.58

$^a s(Mo_n\text{-}O) = [d(Mo_n\text{-}O)/1.882]^{-6.0}$

$^b MCE = 48 - \Sigma[\Sigma s(Mo_n\text{-}O)]$

calculated MCE of the cis-Mo_8 cluster in $NdMo_8O_{14}$ is very consistent with 23.

Magnetic properties of $LnMo_8O_{14}$ containing a 1:1 ratio of cis- to trans-Mo_8 bicapped octahedra

The molar magnetic susceptibilities of $LnMo_8O_{14}$ (Ln = La, Ce, and Pr) as a function of temperature are shown in Figure 11, 12, and 13.

The susceptibility data in the 100-300 K range were fitted to a modified Curie-Weiss relation, $\chi = C/(T - \theta) + \chi_o$, where C, θ, and χ_o refer to the Curie constant, the Weiss temperature, and temperature independent susceptibility, respectively. The results of nonlinear fitting of the observed data are given in Table 13.

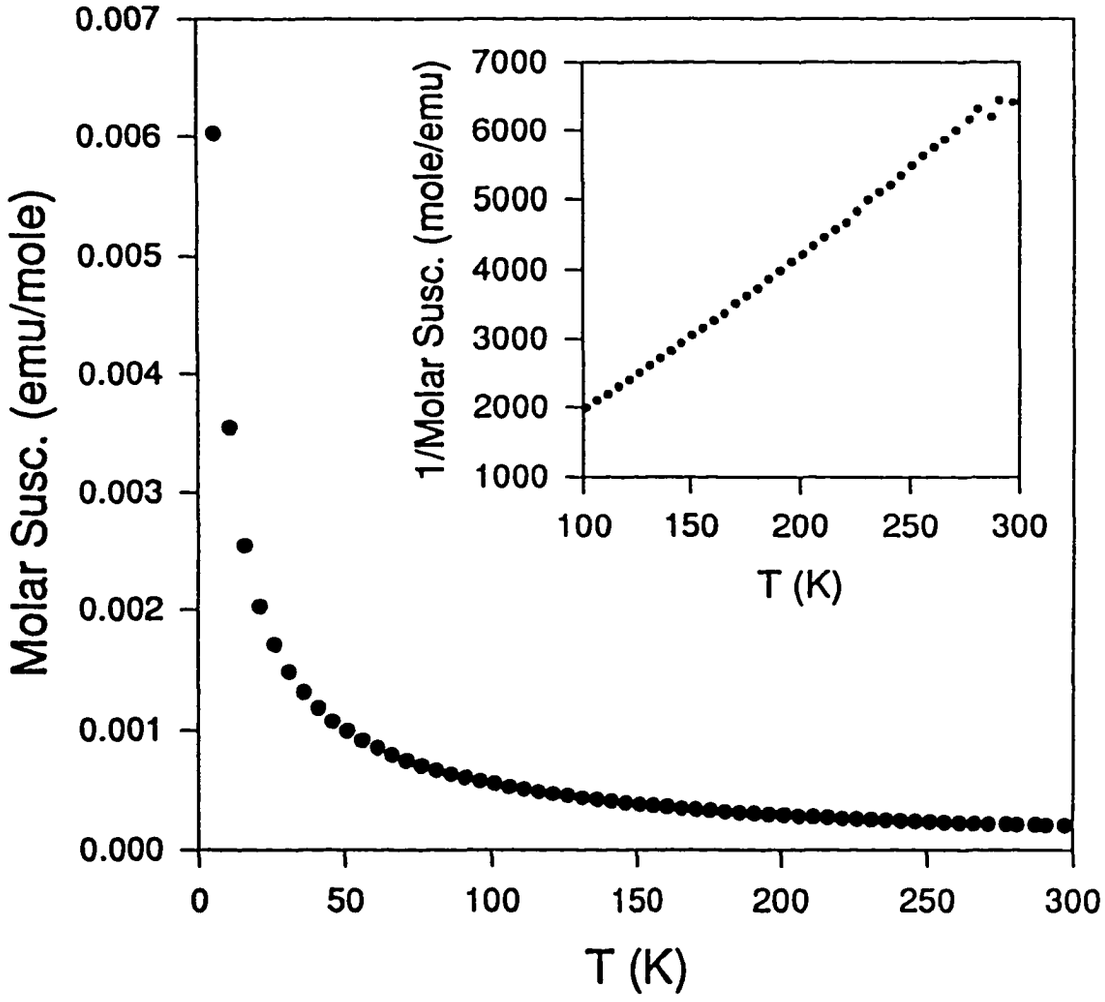

Figure 11. The molar magnetic susceptibility of $LaMo_8O_{14}$ as a function of temperature and reciprocal susceptibility vs. temperature (inset)

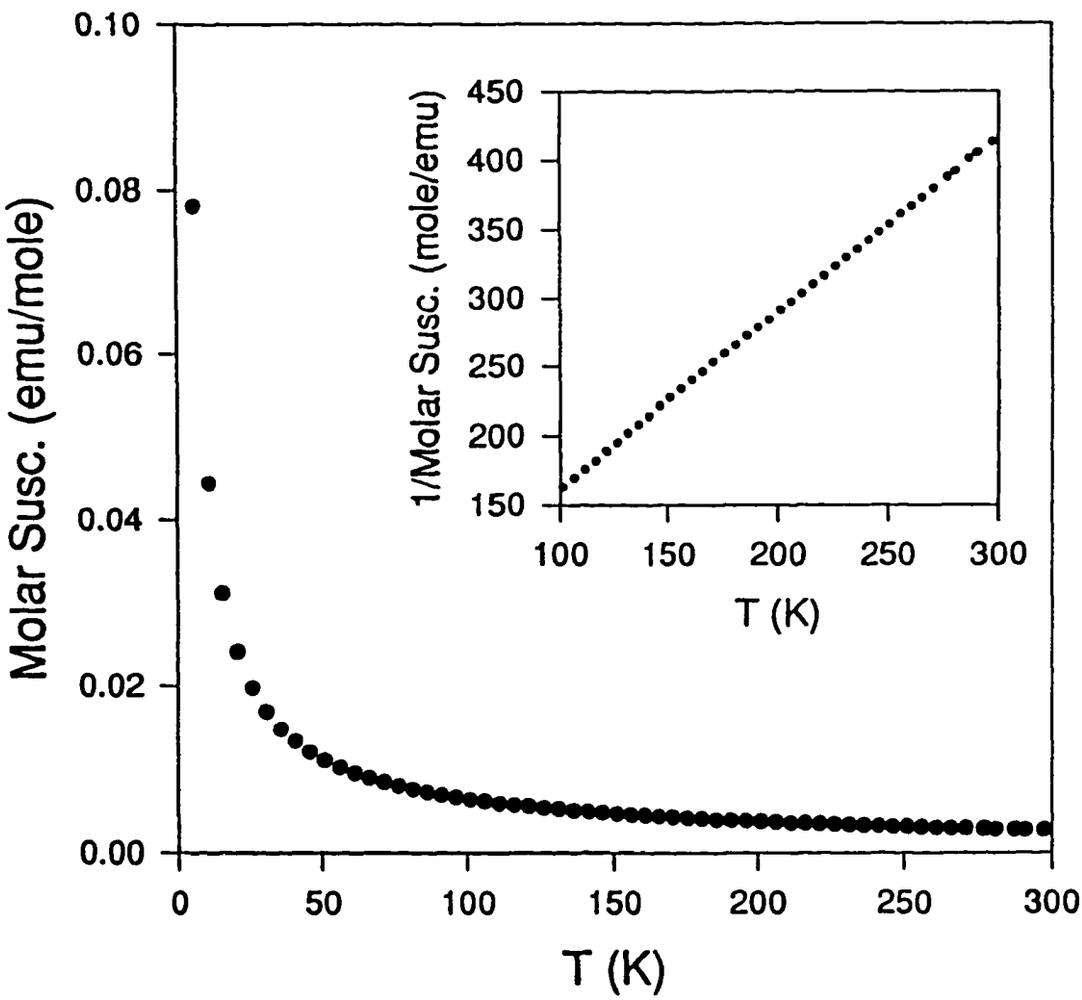

Figure 12. The molar magnetic susceptibility of $CeMo_8O_{14}$ as a function of temperature and reciprocal susceptibility vs. temperature (inset).

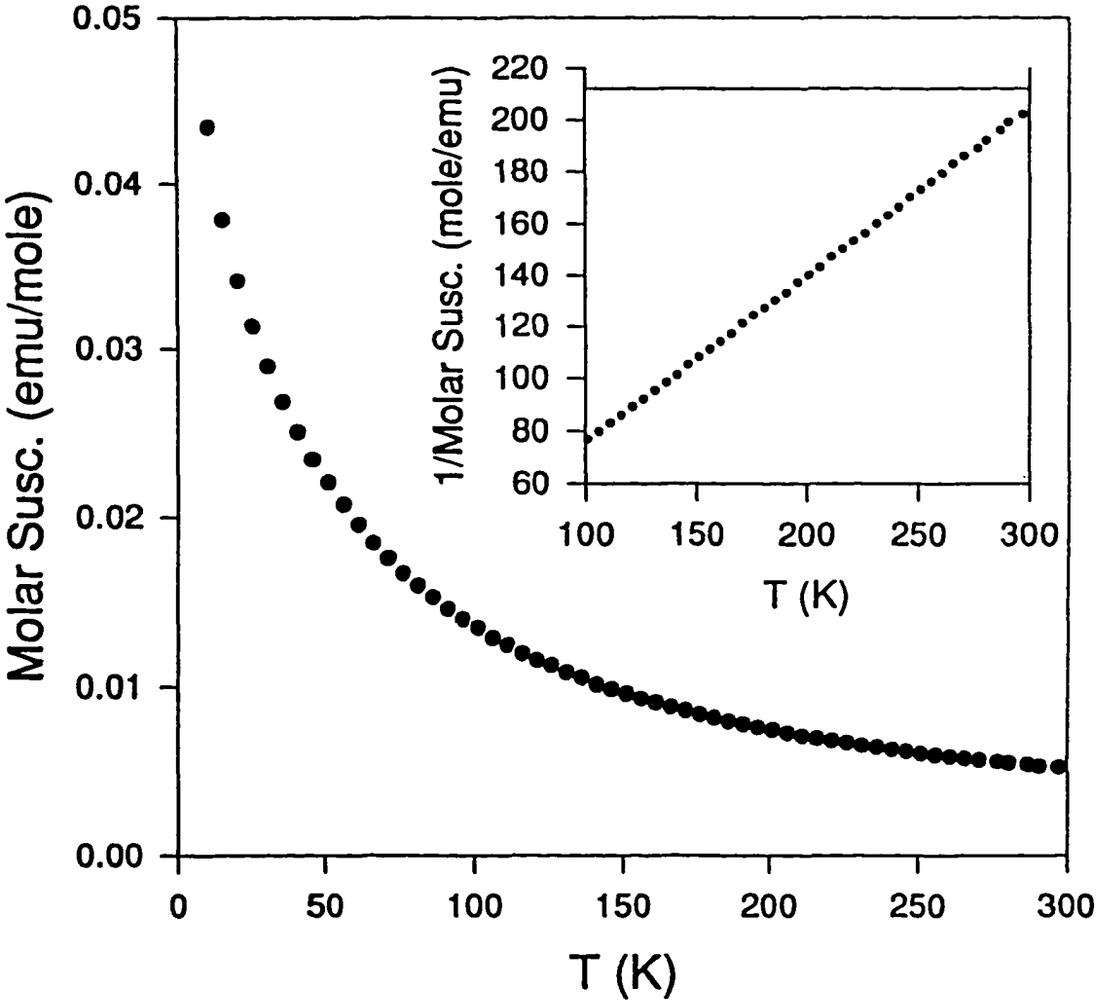

Figure 13. The molar magnetic susceptibility of $PrMo_8O_{14}$ as a function of temperature and reciprocal susceptibility vs. temperature (inset).

Table 13. Parameters derived from the non-linear fitting results of observed magnetic data for $LnMo_8O_{14}$ (Ln = La, Ce, Pr) containing a 1:1 ratio of cis- to trans-Mo_8 octahedra

Compound	C(emu·K/mole)	θ(K)	χ_o(emu/mole)	μ(BM)
$LaMo_8O_{14}$	0.042	21.8	4.54×10^{-5}	0.58
$CeMo_8O_{14}$	0.79	-27.2	1.50×10^{-4}	2.52
$PrMo_8O_{14}$	1.55	-16.4	2.94×10^{-4}	3.52

$LaMo_8O_{14}$. A small effective moment (0.58 BM) in the temperature range 100-300 K was observed for $LaMo_8O_{14}$. By measuring the susceptibility of La_2O_3 which was used in the synthesis of $LaMo_8O_{14}$, a small moment (0.68 BM) was also observed (see Appendix C). Since La^{3+} and O^{2-} are diamagnetic, the observed moment in La_2O_3 must be from impurities. Therefore, the small moment observed in $LaMo_8O_{14}$ may also be from the impurities introduced during the synthesis.

$CeMo_8O_{14}$. The effective magnetic moment of $CeMo_8O_{14}$ is 2.52 BM, which is almost identical to the calculated moment of Ce^{3+} (2.54 BM).[21]

$PrMo_8O_{14}$. The effective magnetic moment of $PrMo_8O_{14}$ is 3.52 BM, which also is almost identical to the calculated moment of Pr^{3+} (3.58 BM).[21]

Based on the facts discussed above, there is no contribution to the observed moment from either the cis- or trans-bicapped Mo_8 clusters, and all the electrons within the clusters are evidently paired. This conclusion is consistent with the bond length-bond order calculation results, which indicate that the cis-Mo_8 cluster contains 22 electrons, and the trans-Mo_8 cluster contains 24 electrons in $LaMo_8O_{14}$ containing a 1:1 ratio of cis- to trans-bicapped Mo_8 clusters.

Magnetic properties of $LnMo_8O_{14}$ containing all cis-Mo_8 bicapped octahedra

The molar magnetic susceptibilities of $LnMo_8O_{14}$ (Ln = Nd and Sm) as a function of temperature are shown in Figures 14 and 15. The susceptibility data in the 100-300 K range were fitted to a modified Curie-Weiss relation, $\chi = C/(T - \theta) + \chi_o$. The results of nonlinear fitting of the observed data are given in Table 14.

Table 14. The non-linear fitting results of observed magnetic data for $LnMo_8O_{14}$ (Ln = Nd and Sm) containing all cis-Mo_8 octahedra

Compound	C(emu·K/mole)	θ(K)	χ_o(emu/mole)	μ(BM)
$NdMo_8O_{14}$	1.30	-14.4	1.20×10^{-3}	3.23
$SmMo_8O_{14}$	0.11	-55.9	1.16×10^{-3}	0.92

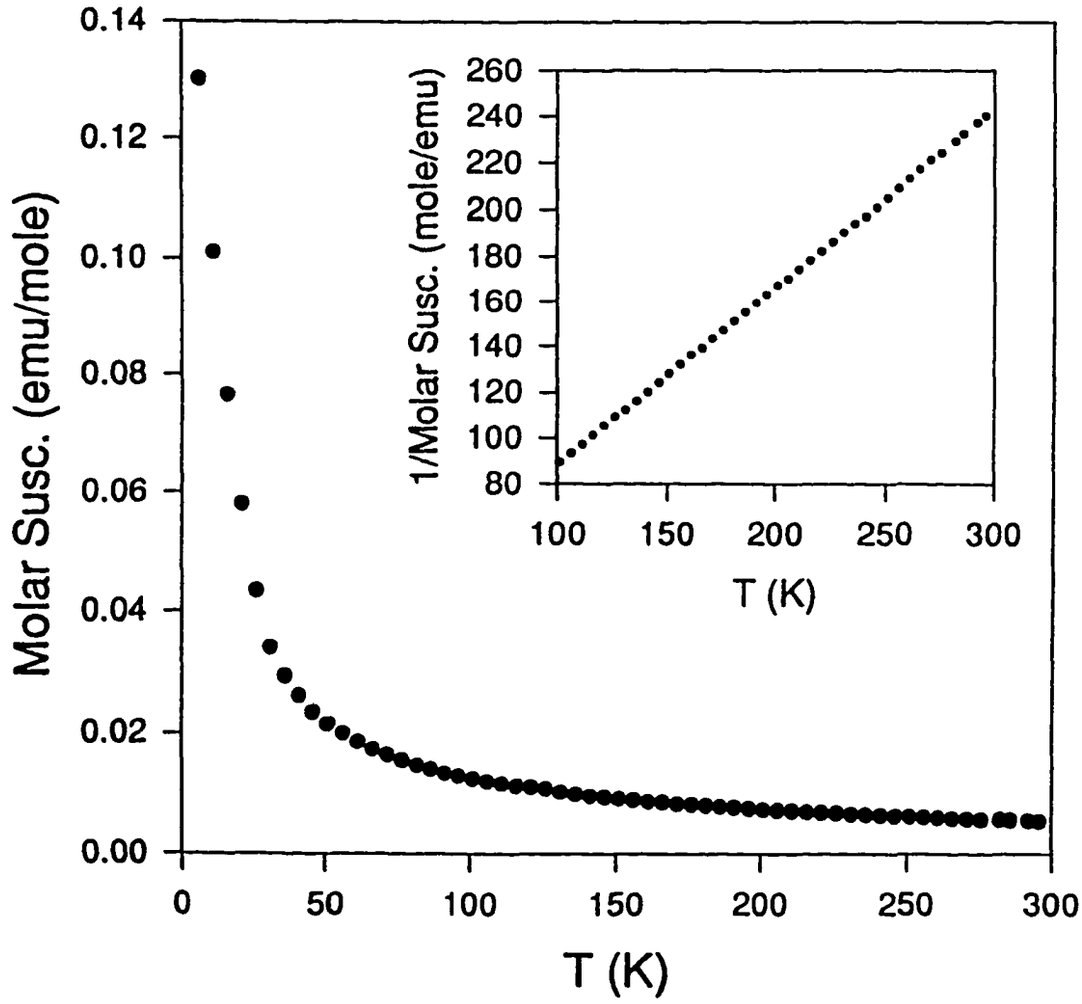

Figure 14. The molar magnetic susceptibility of $NdMo_8O_{14}$ as a function of temperature and reciprocal susceptibility vs. temperature (inset).

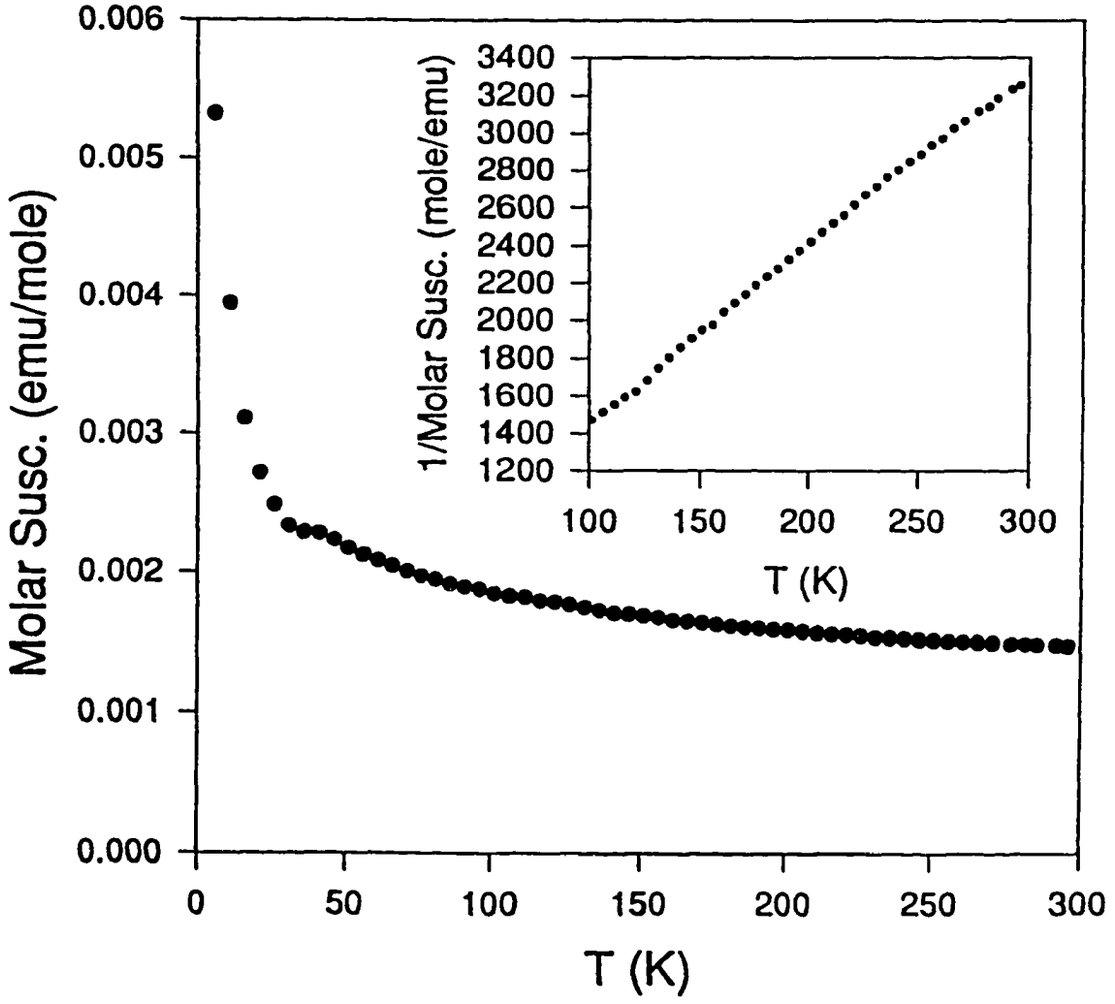

Figure 15. The molar magnetic susceptibility of $SmMo_8O_{14}$ as a function of temperature and reciprocal susceptibility vs. temperature (inset).

$NdMo_8O_{14}$. The effective magnetic moment for $NdMo_8O_{14}$ containing all cis-bicapped Mo_8 clusters is 3.25 BM. Since the cis-Mo_8 clusters in $LnMo_8O_{14}$ containing all cis-bicapped Mo clusters are formally 23-electron clusters, the clusters might be expected to make a contribution to the observed magnetic moment. However, by comparison to the calculated magnetic moment of Nd^{3+} (3.62 BM),[21] and the observed moment of neodynium oxide Nd_2O_3 (3.52 BM),[22] it appears that there is no magnetic moment contribution from the 23-electron clusters. The electrical resistivity measurements have shown metallic character for $NdMo_8O_{14}$,[13] indicating that the unpaired electrons in the cis-Mo_8 clusters must be delocalized between the metal clusters. The paramagnetism from the conduction electrons in a material, which is also called Pauli paramagnetism,[23] is independent of temperature. Therefore, there is no effective magnetic moment contribution from the delocalized electrons, and the effective magnetic moment essentially arises from the rare-earth cations.

$SmMo_8O_{14}$. The effective magnetic moment for $SmMo_8O_{14}$ containing all cis-bicapped Mo_8 clusters is 0.92 BM. Again, a comparison to the calculated magnetic moment of Sm^{3+} (0.85 BM),[21] and the observed moment for samarium oxide Sm_2O_3 (0.92 BM)[22] indicates that there is no contribution to the observed moment from the 23-electron clusters.

In fact, by comparison of the χ_o terms of $LnMo_8O_{14}$, it was found that the magnitudes of χ_o for $LnMo_8O_{14}$ containing all cis-Mo_8 clusters are 4-25 times more

than that of $LnMo_8O_{14}$ containing 1:1 ratio of cis- to trans-Mo_8 clusters. This result indicates that a substantial contribution to the temperature independent susceptibility arises from the conducting electrons.

Electrical properties of $LnMo_8O_{14}$

The $LnMo_8O_{14}$ compounds have long intercluster distances, for example, 3.074(4) - 3.113(4) Å in $LaMo_8O_{14}$ containing a 1:1 ratio of cis- to trans-Mo_8 octahedra, therefore, the electrical resistivities might be expected to exhibit insulating or semiconducting behaviors. However, a measurement on $NdMo_8O_{14}$ containing all cis-Mo_8 octahedra indicated a metallic behavior which was characterized by a decreasing resistivity ratio as the temperature decreased.[13]

In this work, an electrical resistivity measurement was made on a $LaMo_8O_{14}$ single crystal (1.2 x 1 x 0.8 mm^3). The results are shown in Figure 16. The resistivity decreases with an increase in temperature, which is a typical semiconducting behavior.

Therefore, it can be concluded that the $LnMo_8O_{14}$ compounds containing all cis-Mo_8 octahedra are metallic, and $LnMo_8O_{14}$ compounds containing a 1:1 ratio of cis- to trans-Mo_8 octahedra are semiconducting. This conclusion is consistent with the results of the magnetic susceptibility measurements. The unpaired electrons in the cis-Mo_8 clusters of $LnMo_8O_{14}$ containing all cis-Mo_8 octahedra are delocalized, and have

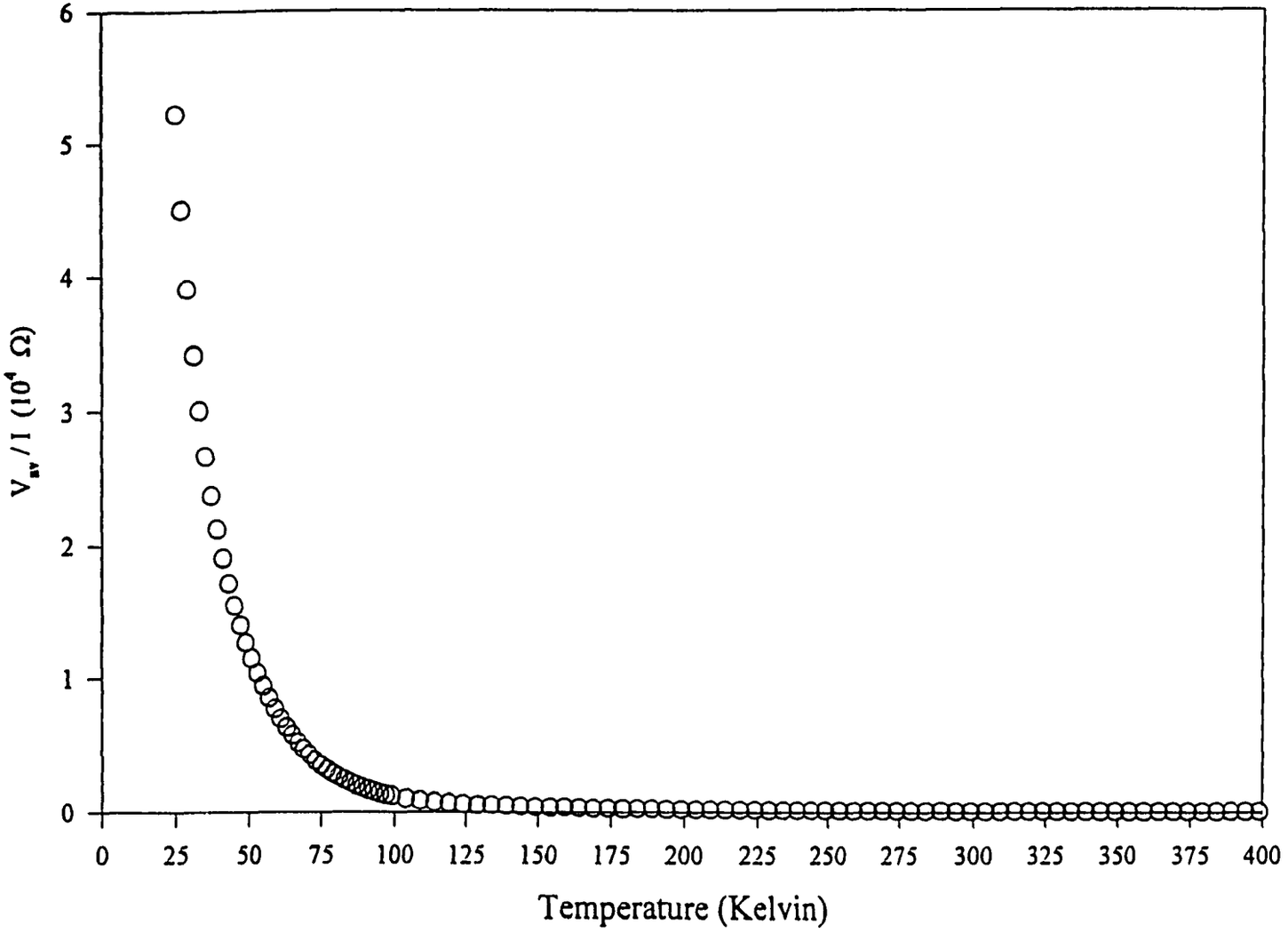

Figure 16. The electrical resistivity of $LaMo_8O_{14}$ as a function of temperature.

no contribution to the effective magnetic moment. However, all of the electrons are paired and localized in the Mo_8 clusters of $LnMo_8O_{14}$ containing a 1:1 ratio of cis- to trans-Mo_8 octahedra, and the materials are semiconductors.

Electronic structure calculations

The electrical resistivity measurements have shown that $LaMo_8O_{14}$ exhibits semiconducting and $NdMoO_{14}$ shows metallic behavior. It would be interesting to know the electronic structures of these compounds to better understand the physical properties. Due to the calculation limitations, the calculation could only be carried out on the compound $NdMoO_{14}$, which has a relatively smaller unit cell than $LaMo_8O_{14}$.

The total DOS curve (Figure 17) for $NdMo_8O_{14}$ containing all cis-Mo_8 bicapped octahedra was obtained by sampling 8 k-point sets in the Brillouin zone. It is seen that the Fermi level falls near a peak in the total DOS, which indicates that the $NdMo_8O_{14}$ compound is a conductor. This result is consistent with the resistivity measurements of $NdMo_8O_{14}$ by C. Carlson.[13] The resistivity measurements of $NdMo_8O_{14}$ indicated that the $NdMo_8O_{14}$ exhibited metallic character.

J. Martin and coworkers calculated the band structure of $NdMo_8O_{14}$ containing cis-Mo_8 bicapped octahedra based on one layer from the reported structure.[24] Their results show 11 low-lying d bands below the Fermi level that could accommodate 22 electrons. The Fermi level falls in a narrow band which is half occupied by the "23rd"

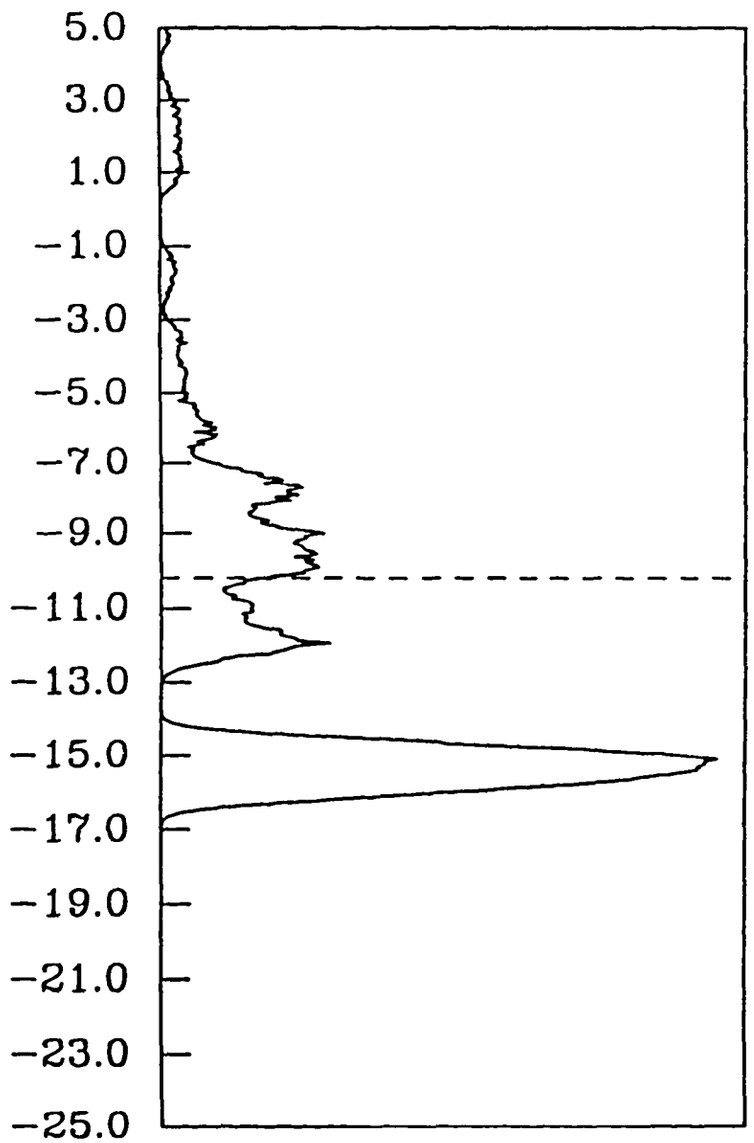

Figure 17. The total DOS curve for $NdMo_8O_{14}$. The Fermi level at -10.19 eV is noted by a dashed line.

electron. This result suggests that the "23 rd" electron be localized and $NdMo_8O_{14}$ be a semiconductor, which is not consistent with resistivity measurements of $NdMo_8O_{14}$.

Conclusions

A new ternary rare-earth reduced molybdenum oxide $LaMo_8O_{14}$ with a novel crystal structure was discovered by synthesis at 1250°C in a sealed, evacuated quartz tube. The novel structure contains a 1:1 ratio of cis- to trans-Mo_8 bicapped octahedra, which are arranged alternately along the c-axis of the unit cell. The Mo-Mo bond distances are in the range of 2.590(4) to 2.888(6) Å. The average Mo-Mo bond distance in trans-isomer is 2.703 Å, which is shorter than that found in the cis-isomer (2.748 Å). The Mo-O bond distances are in the range of 1.94(3) to 2.18(2) Å. The M-O bond strength calculations indicate that the cis- and trans-Mo_8 clusters in $LaMo_8O_{14}$ contain 22 and 24 electrons, respectively.

A systematic investigation in the Ln_2O_3-MoO_3-Mo (Ln = La, Ce, Pr, Nd, Sm, Gd, and Dy) system was explored at 1250°C in sealed, evacuated quartz tubes. Under these synthetic conditions, the phases containing all cis-Mo_8 bicapped clusters and a 1:1 ratio of cis-Mo_8 to trans-Mo_8 bicapped clusters were found. However, the phase containing a 2:1 ratio of cis- to trans-Mo_8 bicapped octahedra was not observed. It

was interesting to note that the sizes of the rare-earth cations are critical for the formation of the various phase types. The larger cations (La, Ce, and Pr) aid in the formation of trans-Mo_8 octahedra, and the smaller cations (Nd and Sm) only stabilize the cis-Mo_8 octahedra. For the rare-earth cations smaller than Sm (Gd and Dy), no compounds containing Mo_8 bicapped octahedra were found. A rational explanation for this result arises from the observation that the effective volume of cis-Mo_8 cluster is 3/4th the value of the trans-Mo_8 cluster.

The magnetic susceptibility measurements indicated that no effective moment contribution arose from the metal clusters Mo_8, even though the cis-Mo_8 cluster in $LnMo_8O_{14}$ containing all cis-Mo_8 octahedra should contain an odd number of electrons (23). The electrical resistivity measurements and electronic structure calculations indicate that the $LnMo_8O_{14}$ containing all cis-Mo_8 clusters are metallic compounds, and the $LnMo_8O_{14}$ containing a 1:1 ratio of cis- to trans-Mo_8 clusters are semiconducting compounds.

References

1. Torardi, C. C.; McCarley, R. E. *J. Am. Chem. Soc.* **1979**, *101*, 3963.

2. Schimek, G. L. *Ph. D. Dissertation*, Iowa State University, **1993**.

3. Torardi, C. C.; Fecketter, C.; McCarroll, W. H.; DiSalvo, F. J. *J. of Solid State Chem.* **1985**, *60*, 332.

4. Moni, A.; Subramanian, M. A.; Clearfield, A.; DiSalvo, F. J.; McCarroll, W. H. *J. of Solid State Chem.* **1987**, *66*, 136.

5. Gougeon, P.; Gall, P.; McCarley, R. E. *Acta Cryst.* **1991**, *C47*, 1585.

6. (a) Gougeon, P.; Gall, P.; Sergent, M. *Acta Cryst.* **1991**, *C47*, 421.
(b) Gougeon, P.; Gall, P. *Acta Cryst.* **1994**, *C50*, 1183.

7. Gougeon, P.; Gall, P.; McCarley, R. E. *Acta Cryst.* **1991**, *C47*, 2026.

8. (a) Gall, P.; Gougeon, P. *Acta Cryst.* **1992**, *C48*, 1915.
(b) Gall, P.; Gougeon, P. *Acta Cryst.* **1993**, *C49*, 659.

9. Gall, P.; Toupet, L.; Gougeon, P. *Acta Cryst.* **1993**, *C49*, 1580.

10. Leligny, H.; Ledesert, M.; Labbe, Ph.; Raveau, B.; McCarroll, W. H. *J. of Solid State Chem.* **1990**, *87*, 35.

11. Gougeon, P.; McCarley, R. E. *Acta Cryst.* **1991**, *C47*, 241.

12. Ramanujachary, K. V.; Jones, E. B.; Greenblatt, M.; McCarroll, W. H. *J. Solid State Chem.* **1995**, *117*, 261.

13. Carlson, C. D. *Ph. D. Dissertation*, Iowa State University, **1989**.

14. Kerihuel, G.; Gougeon, P. *Acta Cryst.* **1995**, *C51*, 787.

15. Kerihuel, G.; Gougeon, P. *Acta Cryst.* **1995**, *C51*, 1475.

16. (a) Hoffmann, R. *J. Chem. Phys.* **1963**, *39*, 1397.

(b) Ammeter, J.; Bürgi, H.-B.; Thibeault, J. C.; Hoffmann, R. *J. Am. Chem. Soc.* **1978**, *100*, 3686.

(c) Whangbo, M.-H.; Hoffmann, R. *J. Am. Chem. Soc.* **1978**, *100*, 6093.

17. (a) Clementi, E.; Roetti, C. *At. Data Nucl. Data Tables*, **1974**, *14*, 177.

(b) Baranovskii, V. I.; Nikolskii, A. B. *Tero. Eksp. Khim.* **1967**, *3*, 527.

18. (a) Walker, N.; Stuart, D. *Acta Cryst.* **1983**, *A39*, 158.

(b) Sheldrick, G. M. *Crystallographic Computing 3*, Eds Sheldrick G. M.; Kruger, C.; Goddard, R., Oxford University Press, 175.

(c) Crystal Structure Analysis Package, Molecular Structure Corporation (1985 & 1992).

19. Brown, I. D.; Wu, K. K. *Acta Cryst.* **1976**, *B32*, 1957.

20. McCarley, R. E. *Polyhedron*, **1986**, *5*, 51.

21. Greenwood, N. N.; Earnshaw, A. *Chemistry of The Elements*, Pergammon Press, New York, **1990**, 1443.

22. Zhang, Z. *Ph. D. Dissertation*, Iowa State University, **1997**, Appendix C.

23. Steger, J. J. *Solid State Chemistry and Physics*, Weller, P. F. Ed.,Marcel Dekker, Inc.,New York, **1973**, 340.

24. Private communications with J. Martin.

GENERAL CONCLUSIONS

The goal of this dissertation has been to develop the chemistry of Group VI metal (Mo, W) nitrides and oxides.

When compared to their oxides, much less information is known about the Group VI nitrides. This lack of information stems from the chemical instability of Group VI metal nitrides with respect to N_2 and N-saturated elements at high temperatures. Therefore, "turning down the heat" has become an important synthetic strategy to produce Group VI metal nitrides. One focus of this dissertation was to prepare tungsten nitrides via molecular precursors at relatively low temperatures.

$WNCl_3$, which contains a tetrameric nitride core W_4N_4, represents a potential intermediate to the desired product WN_x ($x \geq 1$). It is soluble in acetonitrile and forms an acetonitrile adduct $[WNCl_3 \cdot NCCH_3]_4$. The $[WNCl_3 \cdot NCCH_3]_4$ complex consists of a W_4N_4 tetrameric core as well. Substitution of chloride by nitride and azide has been accomplished by either solid state reactions or solution reactions at low temperatures. Several new nitrides and carbide nitrides have been prepared and characterized. However, attempts to remove chlorine by reduction reaction, using reducing reagents such as hexamethyldisilane, tributyltin hydride, tin and zinc metal, were not successful.

An interesting compound $WN(N_3)_3$ was prepared from the reaction of $WNCl_3$ and

NaN_3 in acetonitrile at room temperature. It may have a similar tetrameric structure to $[WNCl_3 \cdot NCCH_3]_4$. Due to the extremely explosive nature, this compound could not be isolated from the acetonitrile solution in a large yield. Thermal decomposition of this compound in 1,2-dichlorobenzene at reflux was attempted, however, the azide did not decompose completely.

A bulk solid phase of tungsten nitride W_3N_5 was prepared through a solid state reaction between $WNCl_3$ and Zn_3N_2 in sealed Pyrex tubes at 400 °C. The XPS study indicated that the oxidation state of tungsten in this amorphous phase was +5. Therefore, each tungsten atom in this W_3N_5 compound possesses one single d-electron. The magnetic susceptibility measurements indicated that W_3N_5 exhibited diamagnetic property in the temperature range 6-300 K. This result suggest that the single electron possessed by the tungsten atom in W_3N_5 be used for W-W bond formation.

By heating W_3N_5 at 600°C in sealed quartz tubes, a cubic tungsten mononitride phase (WN) with rock salt structure (a = 4.171 Å) was obtained. Similarly, by heating W_3N_5 at 800 °C in sealed quartz tubes the hexagonal WN phase and tungsten metal were obtained. At the same time, a few golden crystals were also obtained, which were grown via a chemical transport reaction. The structure of the golden compound $W_2N_2(C_2N_2)$ consists of W_2 dimers, hydrazido ligands N_2^{4-}, and 1,4-diazabutenido ligands represented by three resonance structures, $[N\text{-}C{=}C\text{-}N]^{6-}$, $[N{=}C\text{-}C\text{-}N]^{6-}$, and $[N\text{-}C\text{-}C{=}N]^{6-}$. The dimers are linked together by μ^2, η^2 N-N and N-C-C-N groups to

form a 3-dimensional network. The metal to hydrazido nitrogen bond distances fall in the range 1.97(4) to 2.19(4) Å, and the metal-diazabutenido nitrogen distances show a more limited range from 2.01(4) to 2.07(3) Å. The hydrazido N-N bond distance is 1.43(5) Å, and the diazabutenido C-C bond distance is 1.59(4) Å and N-C bond distance 1.56(4) Å. The W-W single bond distance is 2.767(2) Å.

The electronic structure calculations indicated that the cubic WN with NaCl structure was a conductor and might exhibit superconductivity because the high density of states at the Fermi level. However, the magnetic susceptibility measurements indicated that the cubic WN was basically diamagnetic above 6 K, but did not show any evidence that this cubic WN phase was a superconductor.

The reduced ternary molybdenum oxides have been extensively explored since the discovery of the $NaMo_4O_6$ compound containing trans-edge-shared Mo_6 octahedra. Many compounds with interesting structures and properties have been found.

A new reduced ternary rare-earth molybdenum oxide $LaMo_8O_{14}$ containing Mo_8 bicapped octahedra was discovered at 1250°C in a sealed, evacuated quartz tube. The novel structure contains a 1:1 ratio of cis- to trans-Mo_8 bicapped octahedra, which are arranged alternately along the c-axis of the unit cell. The Mo-Mo bond distances are in the range of 2.590(4) to 2.888(6) Å. The average Mo-Mo bond distance in the trans-isomer is 2.703 Å, which is shorter than that found in the cis-isomer (2.748 Å). The Mo-O bond distances are in the range of 1.94(3) to 2.18(2) Å. The Mo-O bond

strength calculations indicate that the cis- and trans-Mo_8 clusters in $LaMo_8O_{14}$ contain 22 and 24 electrons, respectively.

A systematic investigation in the Ln_2O_3-MoO_3-Mo (Ln = La, Ce, Pr, Nd, Sm) system was explored at 1250°C in sealed, evacuated quartz tubes. Under these synthetic conditions, only the phases containing all cis-Mo_8 bicapped clusters, and a 1:1 ratio of cis-Mo_8 to trans-Mo_8 bicapped clusters, were found. However, the phase containing a 2:1 ratio of cis- to trans-Mo_8 bicapped octahedra was not observed. It was noteworthy that the sizes of the rare-earth cations were critical for the formation of the various phase types. The larger cations (La, Ce, and Pr) aided in the formation of trans-Mo_8 octahedra, and the smaller cations (Nd and Sm) only stabilized the cis-Mo_8 octahedra. A rational explanation for this result arises from the observation that the effective volume of cis-Mo_8 cluster is 3/4th the value of the trans-Mo_8 cluster. The magnetic susceptibility measurements indicate that no effective moment contribution arises from the metal clusters Mo_8, even though the cis-Mo_8 cluster in $LnMo_8O_{14}$ containing all cis-Mo_8 octahedra should contain an odd number of electrons (23 e^-). The electrical resistivity measurements and electronic structure calculations indicate that the $LnMo_8O_{14}$ containing all cis-Mo_8 clusters are metallic compounds, and the $LnMo_8O_{14}$ containing a 1:1 ratio of cis- to trans-Mo_8 clusters are semiconducting compounds.

APPENDIX A. PHYSICAL CONSTANTS

Table A-1. Values of physical constants involved in this dissertation[a]

Quantity	Symbol	Value	Units
Planck constant	h	6.6260755(40)	10^{-34} J s
Bohr magneton	μ_B	9.2740154(31)	10^{-24} J T^{-1}
Avogadro constant	N_A	6.0221367(36)	10^{23} mol^{-1}
Boltzmann constant	k	1.380658(12)	10^{-23} J K^{-1}

[a] Alberty, R. A.; Silbey, R. J. *Physical Chemistry*, 1st Ed. John Wiley & Sons, Inc. New York, **1992.**

APPENDIX B. CORE-DIAMAGNETIC SUSCEPTIBILITIES

Table B-1. Selected core-diamagnetic susceptibilities[a]

Ion	Susceptibility	
	-1.0×10^{-6} emu/g	-1.0×10^{-4} emu/mol
Ag^{+}	24	25.89
Cd^{2+}	22	24.73
Ce^{3+}	20	28.02
Ce^{4+}	17	23.82
Cl^{-}	26	9.23
CN^{-}	18	4.68
Cu^{+}	12	7.63
Cu^{2+}	11	6.99
Dy^{3+}	19	30.88
Er^{3+}	18	30.11
Eu^{2+}	22	33.43
Eu^{3+}	20	30.39
F^{-}	11	2.09
Fe^{2+}	13	7.26
Fe^{3+}	10	5.58
Gd^{3+}	20	31.45
Hf^{4+}	16	28.56
Hg^{2+}	37	74.22

Table B-1. (continued)

Ho^{3+}	19	31.34
O^{2-}	12	1.92
OH^-	12	2.04
La^{3+}	20	27.78
Lu^{3+}	17	29.74
Mo^{2+}	31	29.74
Mo^{3+}	23	22.07
Mo^{4+}	17	16.31
Mo^{5+}	12	11.51
Mo^{6+}	7	67.16
Nd^{3+}	20	28.85
NH_4^+	11.5	1.73
Pr^{3+}	20	28.18
Pr^{4+}	17	23.95
Sc^{3+}	6	2.70
Sm^{2+}	23	34.59
Sm^{3+}	20	30.08
Sn^{2+}	20	23.74
Sn^{4+}	16	18.99
Sr^{2+}	15	13.14
Ta^{5+}	14	25.33
Tb^{3+}	19	30.20
Tb^{4+}	17	27.02
Te^{2-}	70	89.32
Te^{4+}	14	17.86

Table B-1. (continued)

Te^{6+}	12	15.31
Th^{4+}	23	53.37
Ti^{3+}	9	4.31
Ti^{4+}	5	2.40
Tl^{+}	34	69.49
Tl^{3+}	31	63.35
Tm^{3+}	18	30.41
V^{2+}	15	7.64
V^{3+}	10	5.09
V^{4+}	7	3.57
V^{5+}	4	2.04
W^{2+}	41	75.38
W^{3+}	36	66.19
W^{4+}	23	42.29
W^{5+}	19	34.93
W^{6+}	13	23.90
Y^{3+}	12	10.67
Yb^{2+}	20	34.61
Yb^{3+}	18	31.15

[a] Mulay, L. N.; Boudreaux, E. A. *Theory and applications of molecular diamagnetism*, New York: Wiley, **1976**.

APPENDIX C. MAGNETIC PROPERTIES OF Ln_2O_3

The molar magnetic susceptibilities of Ln_2O_3 (Ln = La, Pr, Nd, and Sm) as a function of temperature are shown in the following Figures. The susceptibility data in the 100-300 K range were fit to a modified Curie-Weiss relationship, $\chi = C/(T - \theta) + \chi_o$, where C, θ, and χ_o refer to the Curie constant, the Weiss temperature, and temperature independent susceptibility.

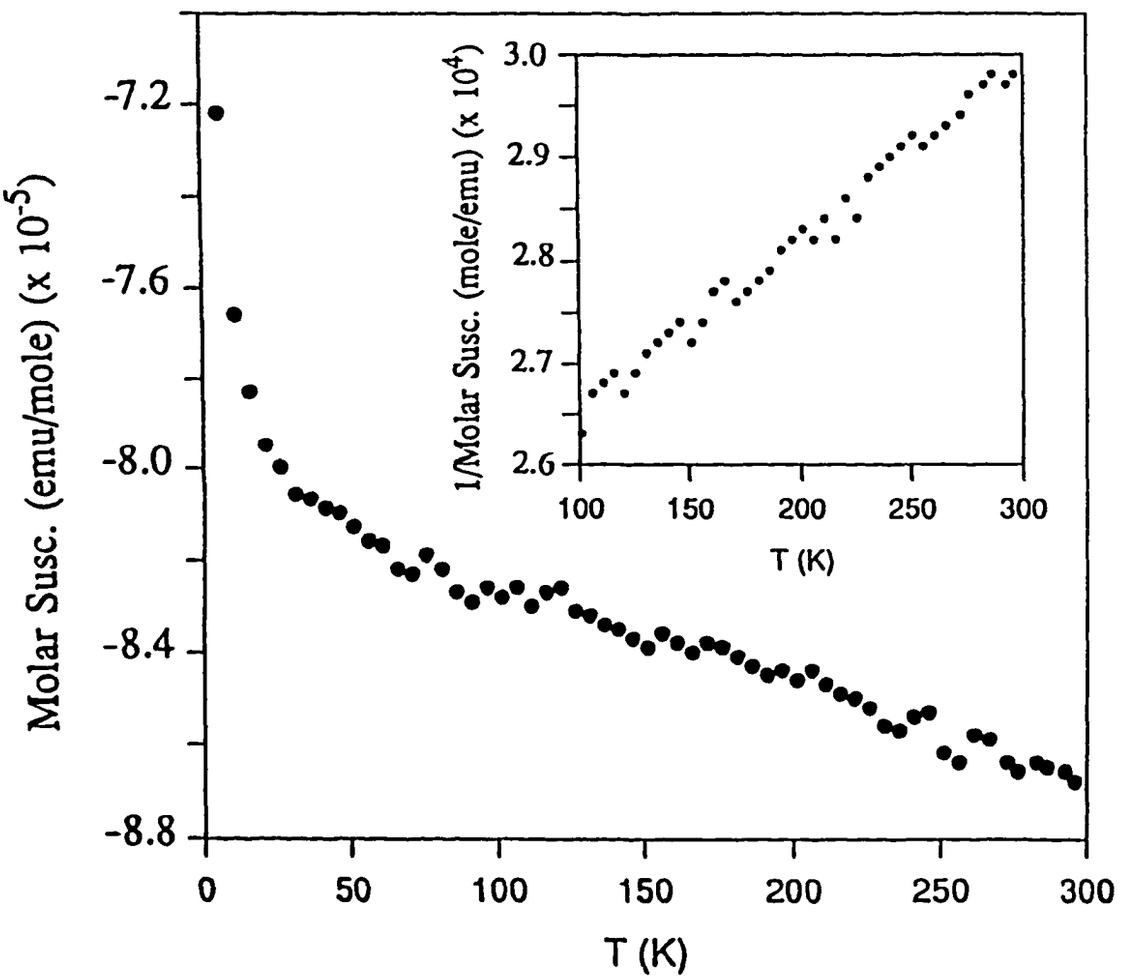

Figure C-1. The molar magnetic susceptibility of La_2O_3 as a function of temperature and reciprocal susceptibility vs. temperature (inset).
Curie = 0.059, Weiss = -39.1, χ_o = -1.2 x 10^{-4}, and μ = 0.69.

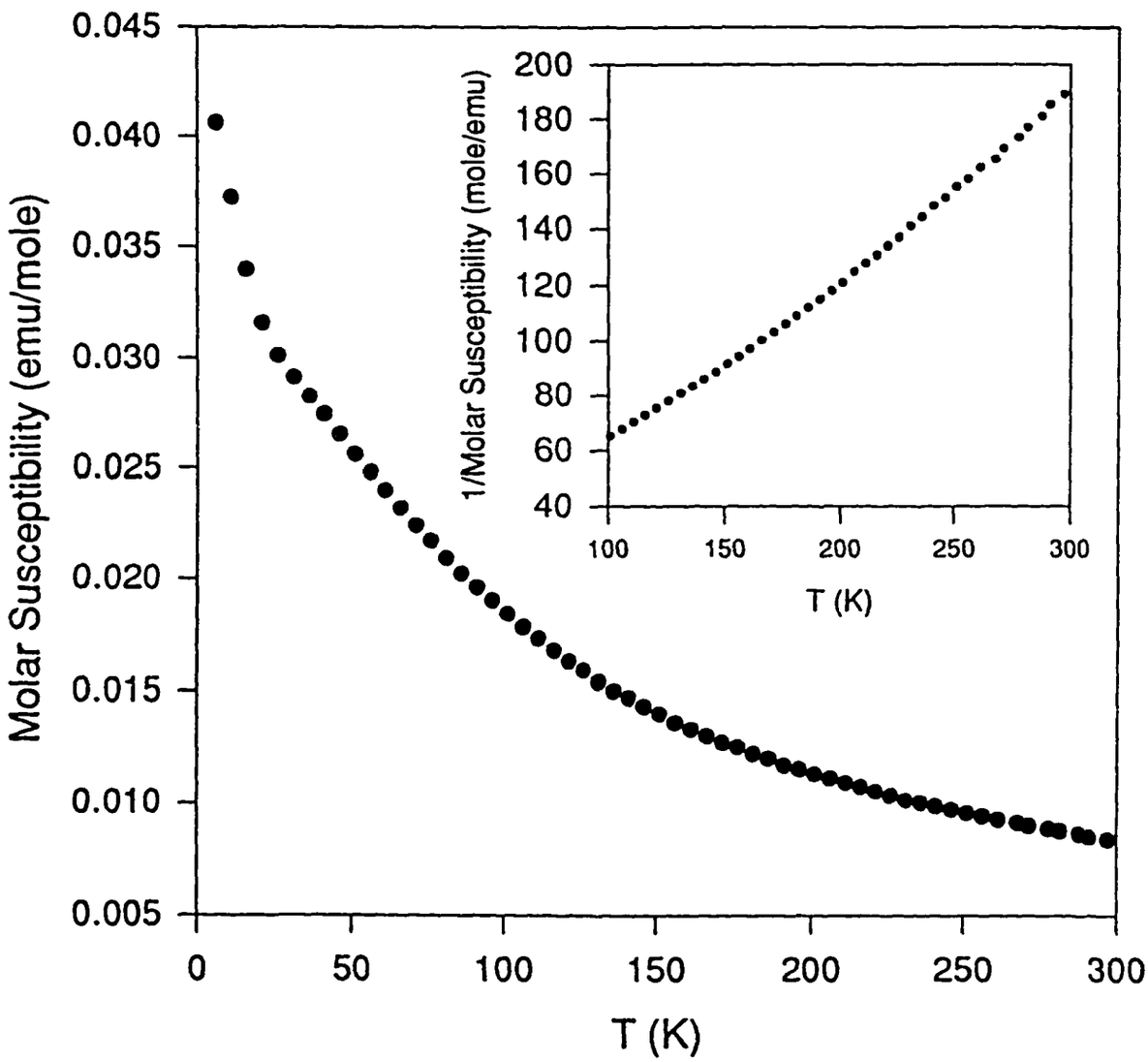

Figure C-2. The molar magnetic susceptibility of Pr_2O_3 as a function of temperature and reciprocal susceptibility vs. temperature (inset).
Curie = 1.59, Weiss = -2.7, χ_o = 3.04 x 10^{-3}, and μ = 3.57.

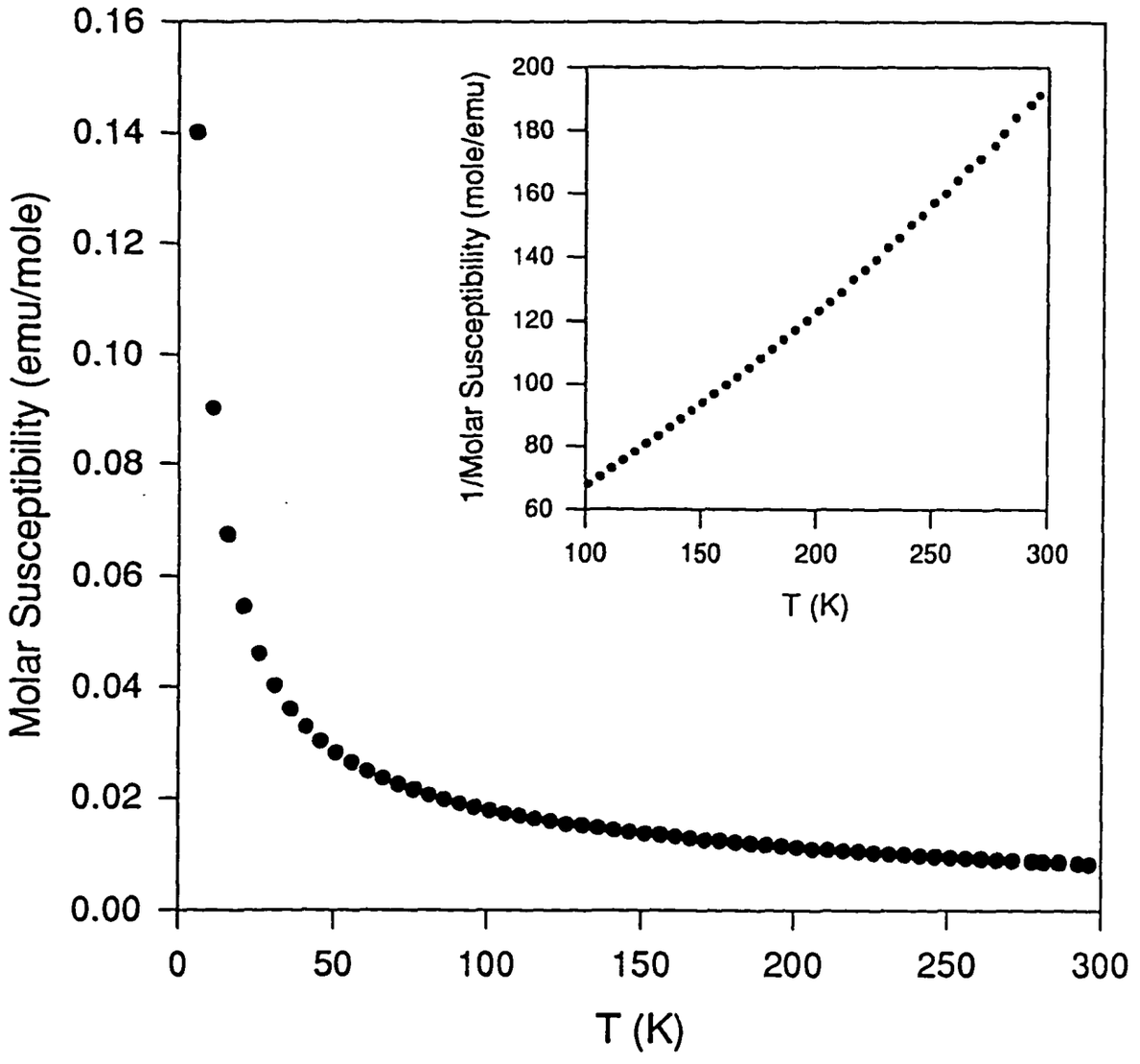

Figure C-3. The molar magnetic susceptibility of Nd_2O_3 as a function of temperature and reciprocal susceptibility vs. temperature (inset).

Curie = 1.59, Weiss = -0.51, χ_o = 2.83 x 10^{-3}, and μ = 3.57.

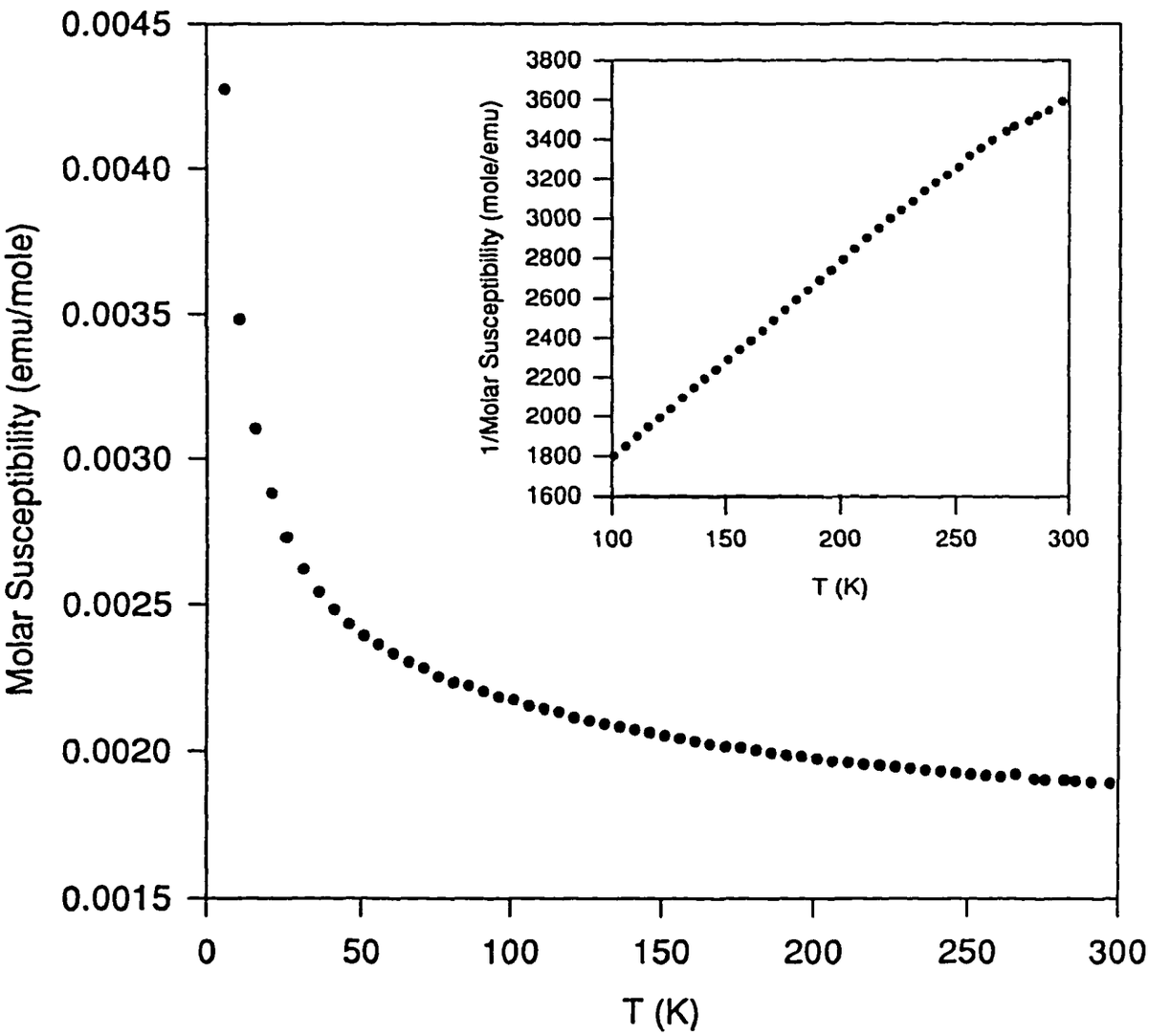

Figure C-4. The molar magnetic susceptibility of Sm_2O_3 as a function of temperature and reciprocal susceptibility vs. temperature (inset).
Curie = 0.11, Weiss = -92.5, χ_o = 1.16 x 10^{-3}, and μ = 0.94

APPENDIX D. $[WNCl_3 \cdot NCCH_2CH_3]_4$

X-ray structure determination

The single crystals of $[WNCl_3 \cdot NCCH_2CH_3]_4$ were obtained by dissolving $[WNCl_3 \cdot NCCH_2CH_3]_4$ in 1,1-dichloromethane and standing at room temperature for two weeks. A suitable deep orange single crystal with dimensions 0.20 x 0.10 x 0.10 mm^3 was selected from material still in contact with the mother solution. The crystal was then encased in epoxy resin while in a glove bag under a nitrogen flow, attached to the tip of a glass fiber, and immediately delivered to the diffractometer with low temperature equipments. All measurements were made on a Rigaku AFC6R diffractometer using graphite monochromated Mo Kα (λ = 0.71069 Å) radiation and a 12 kW rotating anode generator.

Cell constants and an orientation matrix for data collection were obtained from a least-squares refinement using the setting angles of 25 carefully centered reflections in the range $4.0 < 2\theta < 35.0$, and corresponded to a triclinic cell with dimensions: a = 8.875(2) Å, b = 10.220(2) Å, c = 10.311(2) Å, α = 110.76(1)°, β = 92.36(1)°, γ = 89.56(1)°, and V = 873.7(3) $Å^3$. The data were collected at -60 °C using the ω-2θ scan technique over the range $4° < 2\theta < 50°$ in the hemisphere ($\pm h$, $+k$, $\pm l$). Three standard reflections were monitored every 150 reflections and showed no intensity variation over the collection period. A total of 3283 reflections were collected, of

which 3092 were unique (R_{int} = 0.024) and 2644 of which were observed with $I > 3.00\sigma(I)$. No Decay correction was applied. With an absorption coefficient for Mo Kα radiation of μ = 140.7 cm^{-1}, an empirical absorption correction using the ψ scan technique was applied after the structure solution. The data were corrected for Lorentz and polarization effects.

The triclinic space group was $P\bar{1}$ (#2) was chosen on the basis of systematic absences and intensity statistics. The structure was solved by the SHELXS direct methods which yielded the positions of the tungsten atoms. Successive Fourier electron difference maps yielded the positions of the chlorine, nitrogen and carbon atoms. The structure was then refined by full-matrix least-squares methods with anisotropic thermal parameters on all non-hydrogen atoms. The final cycle of full-matrix least-squares refinement was based on 2644 observed reflections and 163 variable parameters and converged with unweighted and weighted agreement factors of R = 0.023 and Rw = 0.031, respectively. The asymmetric unit was found to be $[WNCl_3 \cdot NCCH_2CH_3]_2$. All calculations were performed using the TEXSAN crystallographic software package of Molecular Structure Corporation. The crystallographic data and refinement results are given in Table D-1, and the positional parameters and isotropic equivalent temperature factors are given in Table D-2. The anisotropic temperature factors are listed in Table D-3.

Table D-1. Crystallographic data for $[WNCl_3 \cdot NCCH_2CH_3]_4$

Empirical Formula	$C_{12}Cl_{12}H_{20}N_8W_4$
Formula Weight	1437.18
Crystal Size	0.20 x 0.10 x 0.10 mm^3
Crystal System	triclinic
Space Group	P1 (#2)
Lattice Parameters	a = 8.875(2) Å
	b = 10.311(2) Å
	c = 10.220(2) Å
	α = 110.76(1)°
	β = 92.36(1)°
	γ = 89.56(1)°
Volume	873.7(3) $Å^3$
Z Value	1
Calculated Density	2.731 g/cm^3
F_{000}	648.00
μ(MoKα)	140.74 cm^{-1}
Diffractometer	Rigaku AFC6R
Radiation	MoKα (λ = 0.71069Å)
Temperature	-60.0 °C
Two-theta Range	0-50°
Scan Mode	ω-2θ
No. of Reflections Collected	3283
No. Observations (I > 3.00σ(I))	2644
No. Variables	163
Max Shift/error in Final Cycle	0.00
Goodness of Fit[a]	2.56
Max. and Min. Peaks in the Final Diff. Map	0.86, -1.55 $e^-/Å^3$
Residuals[b]	R = 0.023, Rw = 0.031

[a] Goodness of Fit = $[\Sigma\omega\{|F_o| - |F_c|\}^2/\{N_{obs} - N_{parameters}\}]^{1/2}$

[b] $R = \Sigma \; | \; |Fo| - |Fc| \; | \; / \; \Sigma \; |Fo|$; $Rw = [(\Sigma \; w \; (|Fo| - |Fc|)^2 \; / \; \Sigma \; w \; Fo^2 \;)]^{1/2}$.

Table D-2. Atomic coordinates and equivalent isotropic thermal parameters ($Å^2$) of the non-hydrogen atoms for $[WNCl_3 \cdot NCCH_2CH_3]_4$

atom	x	y	z	B_{eq} [a]
W(1)	0.35810(4)	-0.75580(3)	0.56381(3)	1.293(8)
W(2)	0.70306(4)	-0.88754(3)	0.70801(3)	1.275(7)
Cl(1)	0.5359(3)	-0.6904(2)	0.4407(2)	2.42(5)
Cl(2)	0.8675(3)	-0.8488(3)	0.5590(3)	2.61(5)
Cl(3)	0.2348(3)	-0.7890(3)	0.7749(2)	2.44(5)
Cl(4)	0.7751(3)	-0.6930(2)	0.8979(3)	2.96(5)
Cl(5)	0.1703(3)	-0.6206(2)	0.5202(3)	2.78(5)
Cl(6)	0.5806(3)	-0.9850(2)	0.8504(2)	2.22(5)
N(1)	0.3181(8)	-0.9123(7)	0.4385(7)	1.6(2)
N(2)	0.5461(7)	-0.8260(7)	0.6493(7)	1.6(1)
N(3)	0.4478(9)	-0.5518(7)	0.7428(8)	2.3(2)
N(4)	0.9178(9)	-0.9910(8)	0.7740(8)	2.5(2)
C(1)	0.511(1)	-0.4606(10)	0.8177(10)	2.1(2)
C(2)	1.025(1)	-1.042(1)	0.7908(10)	2.5(2)
C(3)	0.591(1)	-0.339(1)	0.916(1)	3.2(2)
C(4)	1.165(1)	-1.113(1)	0.813(1)	3.1(2)
C(5)	0.749(1)	-0.326(1)	0.869(1)	3.7(3)
C(6)	1.144(1)	-1.270(1)	0.765(1)	3.6(3)

[a] $B_{eq} = 8/3\pi^2(U_{11}(aa^*)^2 + U_{22}(bb^*)^2 + U_{33}(cc^*)^2 + 2U_{12}aa^*bb^*\cos\gamma + 2U_{13}aa^*cc^*\cos\beta + 2U_{23}bb^*cc^*\cos\alpha)$

Table D-3. Anisotropic thermal parameters[a] ($Å^2$) of the non-hydrogen atoms for $[WNCl_3 \cdot NCCH_2CH_3]_4$

Atom	U_{11}	U_{22}	U_{33}	U_{12}	U_{13}	U_{23}
W(1)	0.0162(2)	0.0170(2)	0.0157(2)	-0.0013(1)	-0.0009(1)	-0.0058(1)
W(2)	0.0152(2)	0.0165(2)	0.0169(2)	-0.0022(1)	0.0002(1)	-0.0064(1)
Cl(1)	0.033(1)	0.032(1)	0.034(1)	0.006(1)	0.002(1)	-0.019(1)
Cl(2)	0.023(1)	0.038(1)	0.046(1)	0.003(1)	0.003(1)	-0.025(1)
Cl(3)	0.025(1)	0.024(1)	0.043(1)	0.0026(9)	0.006(1)	-0.011(1)
Cl(4)	0.044(2)	0.033(1)	0.027(1)	-0.013(1)	0.005(1)	-0.002(1)
Cl(5)	0.030(1)	0.042(1)	0.032(1)	-0.007(1)	-0.011(1)	-0.012(1)
Cl(6)	0.032(1)	0.025(1)	0.032(1)	0.0046(10)	0.0002(10)	-0.016(1)
N(1)	0.019(4)	0.019(4)	0.023(4)	-0.004(3)	0.001(3)	-0.008(3)
N(2)	0.014(4)	0.028(4)	0.019(3)	0.001(3)	-0.002(3)	-0.010(3)
N(3)	0.035(5)	0.032(5)	0.016(4)	-0.007(4)	0.001(4)	-0.006(4)
N(4)	0.023(4)	0.033(5)	0.035(5)	-0.004(4)	-0.004(4)	-0.010(4)
C(1)	0.025(5)	0.023(5)	0.034(5)	0.003(4)	-0.005(4)	-0.014(4)
C(2)	0.024(5)	0.023(5)	0.043(6)	-0.004(4)	-0.004(5)	-0.008(5)
C(3)	0.041(6)	0.040(7)	0.033(6)	-0.002(5)	0.014(5)	-0.001(5)
C(4)	0.028(6)	0.046(7)	0.039(6)	-0.011(5)	-0.012(5)	-0.012(5)
C(5)	0.039(7)	0.043(7)	0.057(7)	0.001(5)	0.019(6)	-0.015(6)
C(6)	0.036(6)	0.064(8)	0.046(7)	0.006(6)	-0.010(5)	-0.028(6)

[a]The coefficients U_{ij} of the anisotropic temperature factor expression are defined as $\exp(-2\pi^2(a^{*2}U_{11}h^2 + b^{*2}U_{22}k^2 + c^{*2}U_{33}l^2 + 2a^*b^*U_{12}hk + 2a^*c^*U_{13}hl + 2b^*c^*U_{23}kl))$

Description of structure

$[WNCl_3 \cdot NCCH_2CH_3]_4$ crystallizes in the triclinic space group $P\bar{1}$ with one $[WNCl_3 \cdot NCCH_2CH_3]_4$ molecule per unit cell. There are no free solvent molecules in the unit cell. An ORTEP diagram of the unit cell is shown in Figure D-1. The molecular structure of $[WNCl_3 \cdot NCCH_3CH_3]_4$ (Figure D-2), which is similar to the molecular structure of $[WNCl_3 \cdot NCCH_3]_4$, consists of a W_4N_4 tetramer core. The selected bond distances and angles for $[WNCl_3 \cdot NCCH_2CH_3]_4$ are listed in Tables D-4 and D-5, respectively.

Table D-4. Selected bond distances (Å) in $[WNCl_3 \cdot NCCH_2CH_3]_4$

atom	atom	distance	atom	atom	distance
W(1)	Cl(1)	2.304(2)	W(1)	Cl(3)	2.315(2)
W(1)	Cl(5)	2.294(2)	W(1)	N(1)	1.696(7)
W(1)	N(2)	2.093(6)	W(1)	N(3)	2.362(7)
W(2)	Cl(2)	2.288(2)	W(2)	Cl(4)	2.315(2)
W(2)	Cl(6)	2.344(2)	W(2)	N(1)	2.080(7)
W(2)	N(2)	1.700(6)	W(2)	N(4)	2.366(7)
N(3)	C(1)	1.12(1)	N(4)	C(2)	1.12(1)
C(1)	C(3)	1.47(1)	C(2)	C(4)	1.49(1)
C(3)	C(5)	1.52(1)	C(4)	C(6)	1.53(1)

Table D-5. Selected bond angles (°) in $[WNCl_3 \cdot NCCH_2CH_3]_4$

atom	atom	atom	angle	atom	atom	atom	angle
Cl(1)	W(1)	Cl(3)	161.80(8)	Cl(1)	W(1)	Cl(5)	94.86(9)
Cl(1)	W(1)	N(1)	96.0(3)	Cl(1)	W(1)	N(2)	83.5(2)
Cl(1)	W(1)	N(3)	81.3(2)	Cl(3)	W(1)	Cl(5)	93.75(9)
Cl(3)	W(1)	N(1)	97.9(3)	Cl(3)	W(1)	N(2)	83.7(2)
Cl(3)	W(1)	N(3)	83.3(2)	Cl(5)	W(1)	N(1)	101.1(2)
Cl(5)	W(1)	N(2)	163.6(2)	Cl(5)	W(1)	N(3)	86.4(2)
N(1)	W(1)	N(2)	94.7(3)	N(1)	W(1)	N(3)	171.7(3)
N(2)	W(1)	N(3)	77.3(3)	Cl(2)	W(2)	Cl(4)	95.04(10)
Cl(2)	W(2)	Cl(6)	162.85(8)	Cl(2)	W(2)	N(1)	86.0(2)
Cl(2)	W(2)	N(2)	97.2(2)	Cl(2)	W(2)	N(4)	82.3(2)
Cl(4)	W(2)	Cl(6)	92.15(9)	Cl(4)	W(2)	N(1)	164.4(2)
Cl(4)	W(2)	N(2)	100.0(2)	Cl(4)	W(2)	N(4)	84.8(2)
Cl(6)	W(2)	N(1)	83.0(2)	Cl(6)	W(2)	N(2)	96.8(2)
Cl(6)	W(2)	N(4)	82.9(2)	N(1)	W(2)	N(2)	95.2(3)
N(1)	W(2)	N(4)	80.0(3)	N(2)	W(2)	N(4)	175.2(3)
W(1)	N(1)	W(2)	172.4(4)	W(1)	N(2)	W(2)	176.2(4)
W(1)	N(3)	C(1)	169.4(8)	W(2)	N(4)	C(2)	172.3(8)
N(3)	C(1)	C(3)	178.7(10)	N(4)	C(2)	C(4)	179(1)
C(1)	C(3)	C(5)	111.6(9)	C(2)	C(4)	C(6)	111.6(8)

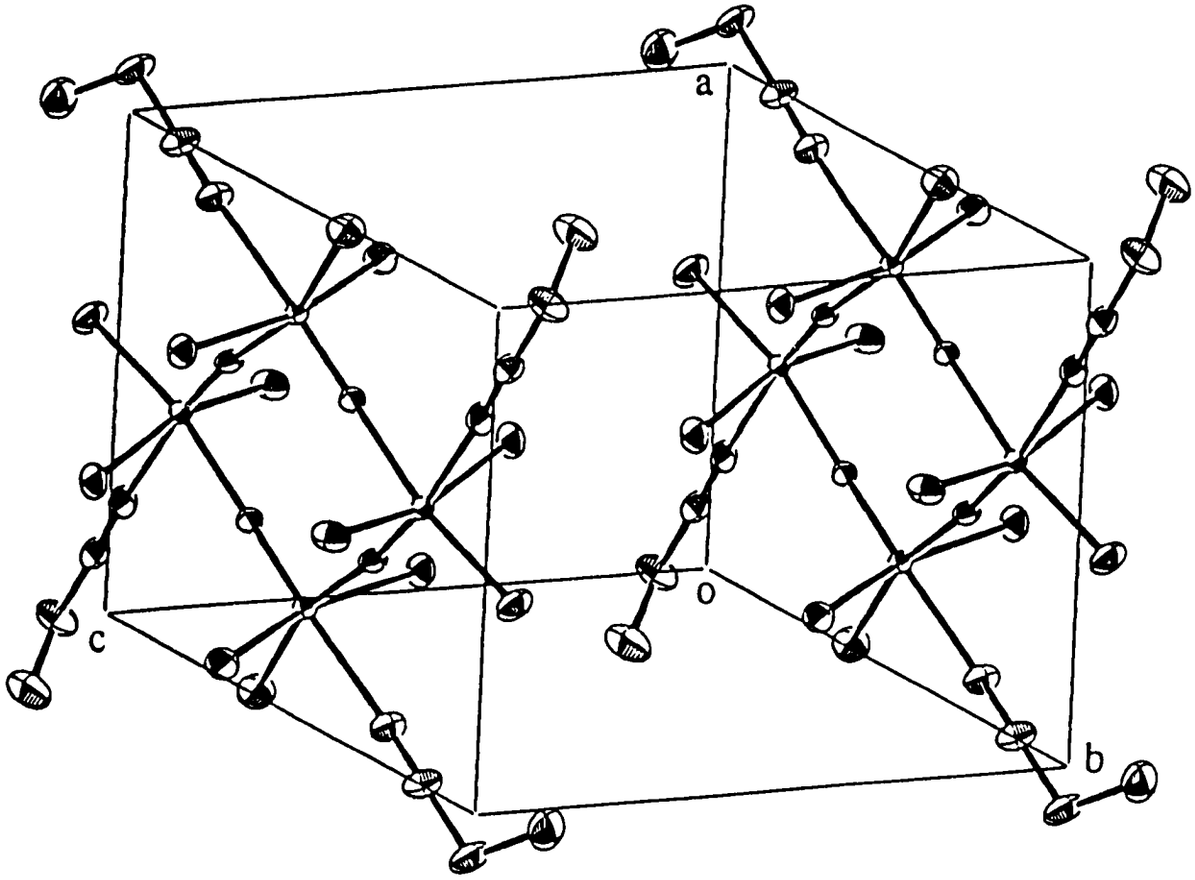

Figure D-1. An ORTEP diagram of the unit cell for $[WNCl_3 \cdot NCCH_2CH_3]_4$.

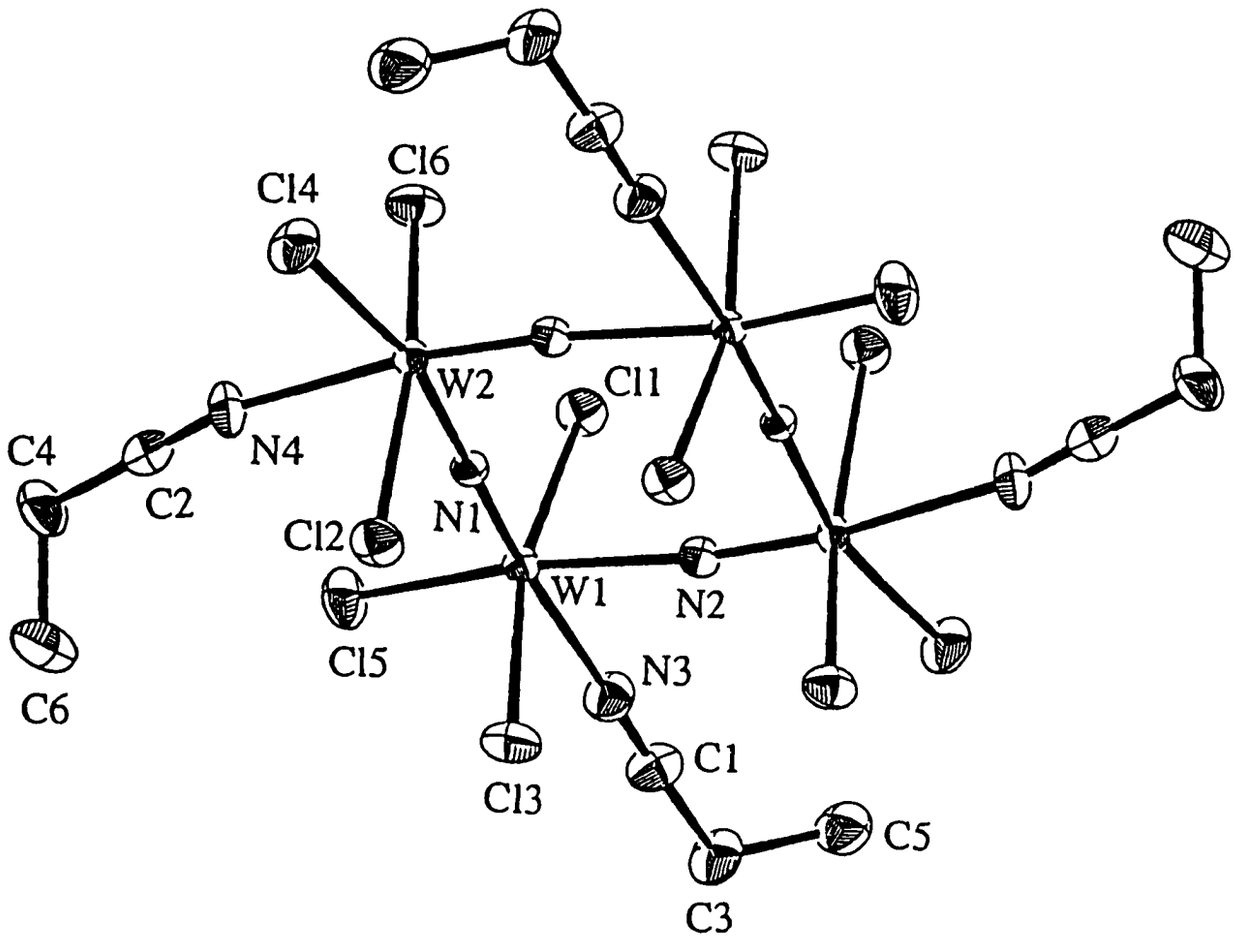

Figure D-2. The molecular structure of $[WNCl_3 \cdot NCCH_2CH_3]_4$.

REFERENCES

1. (a) Yih, S. W. H.; Wang, C. T. *Tungsten: Sources, Metallurgy, Properties, and Applications*, Plenum Press, New York, **1979**.

   (b) Swift, R. A. ed.; *Research of Chrome-Moly Steels*, American Society of Mechanical Engineers, New Yok, **1984**.

2. Deaton, J. C.; Solomon, E. I.; Durfor, C. N.; Wetherbee, P. J.; Burgess, B. K.; Jacobs, D. B. *Biocjem. Biophys. Res. Commun.* **1984**, *121*, 1042.

3. Stein, A.; Keller, S. W.; Mallouk, T. E. *Science*, **1993**, *259*, 1558.

4. (a) Draganjac, M.; Rauchfuss, T. B. *Angew. Chem. Int. Ed. Engl.* **1985**, *24*, 742.

   (b) Böttcher, P. *Angew. Chem. Int. Ed. Engl.* **1988**, *27*, 759.

   (c) Rouxel, J. *Acc. Chem. Res.* **1992**, *25*, 328.

   (d) Dhingra, S.; Kanatzidis, M. G. *Science*, **1992**, *258*, 1769.

5. Nenoff, T. M.; Harrison, W. T. A.; Gier, T. E.; Stucky, G. D. *J. Am. Chem. Soc.* **1991**, *113*, 378.

6. Jacobson, A. J. *Solid State Chemistry Compounds*, Cheetham, A. K.; Day, P. Eds. Claredon Press, **1992**, 182.

7. (a) Baxter, D. V.; Chisholm, M. H.; Gama, G. J.; DiStasi, V. F.; Hector, A. L.; Parkin, I. P. *Chem. Mater.* **1996**, *8*, 1222.

(b) Holl, M. M. B.; Wolczanski, P. T.; Proserpio, D.; Bielecki, A.; Zax, D. B. *Chem. Mater.* **1996**, *8*, 2468.

8. (a) Vennos, D. A.; Badding, M. E.; DiSalvo, F. J. *Inorg. Chem.* **1990**, *29*, 4059.
(b) Elder, S. H.; Doerrer, L. H.; DiSalvo, F. J.; Parise, J. B.; Guyomard, D; Tarascon, J. M. *Chem. Mater.* **1992**, *4*, 928.
9. (a) Jacobs, H.; Niewa R. *Eur. J. Solid State Inorg. Chem.* **1994**, *31*, 105.
(b) Rauch, P. E.; DiSalvo, F. J.; Brese, N. E.; Partin, D. E.; O'Keeffe, M. *J. Solid State Chem.* **1994**, *110*, 162.
10. Subramanya Herle, P.; Hegde, M. S.; Vasanthacharya, N. Y.; Gopalakrishnan,J.; Subbanna, G. N. *J. Solid State Chem.* **1994**, *112*, 208.
11. Bem, D. S.; Olsen, H. P.; zur Loye, H. *Chem. Mater.* **1995**, *7*, 1824.
12. Subramanya Herle, P.; Vasanthacharya, N. Y.; Hegde, M. S.; Gopalakrishnan, J. *J. Alloys Comp.* **1995**, *217*, 22.
13. Bem, D. S.; Lampe-önnerud, C. M.; Olsen, H. P.; zur Loye, H. *Inorg. Chem.* **1996**, *36*, 581.
14. (a) Niewa, R.; Jacobs H. *J. Alloys Comp.* **1996**, *233*, 61.
(b) Niewa, R.; Jacobs H. *J. Alloys Comp.* **1996**, *234*, 171.
15. Lyutaya, M. D. *Soviet Powder Metall. Metal Cer.* **1979**, 190.
16. Lakhtin, Yu. M.; Kogan, Ya, D.; Borovskaya, T. M.; Solodkin, G. A. *Russ. Metall.* **1979**, *4*, 158.

17. Toth, L. E. *Transition Metal Carbides and Nitrides*, Academic Press, NY, **1971.**

18. Brese, N. E.; O'Keeffe, M. *Structure and Bonding*, **1992**, *79*, 307.

19. Khirtrova, V. I. *Soviet Phys. Cryst.* **1962**, *6(4)*, 439.

20. Fix, R. M.; Gordon, R. G.; Hoffman, D. M. *J. Am. Chem. Soc.* **1990**, *112*, 7833.

21. Schönberg, N. *Acta Chemica Scandinavica*, **1954**, *8*, 204.

22. Hector, A. L.; Parkin, I. P. *Chem. Mater.* **1995**, *7*, 1728.

23. Torardi, C. C.; McCarley, R. E. *J. Am. Chem. Soc.* **1979**, *101*, 3963.

24. Schimek, G. L. *Ph. D. Dissertation*, Iowa State University, 1993.

25. Gall, P.; Gougeon, P. *Acta Cryst.* **1992**, *C48*, 1915.

26. Torardi, C. C.; Fecketter, C.; McCarroll, W. H.; DiSalvo, F. J. *J. of Solid State Chem.* **1985**, *60*, 332.

27. Moni, A.; Subramanian, M. A.; Clearfield, A.; DiSalvo, F. J.; McCarroll, W. H. *J. of Solid State Chem.* **1987**, *66*, 136.

28. Gougeon, P.; Gall, P.; McCarley, R. E. *Acta Cryst.* **1991**, *C47*, 1585.

29. (a) Gougeon, P.; Gall, P.; Sergent, M. *Acta Cryst.* **1991**, *C47*, 421.
(b) Gougeon, P.; Gall, P. *Acta Cryst.* **1994**, *C50*, 1183.

30. Gougeon, P.; Gall, P.; McCarley, R. E. *Acta Cryst.* **1991**, *C47*, 2026.

31. Gall, P.; Gougeon, P. *Acta Cryst.* **1993**, *C49*, 659.

32. Gall, P.; Toupet, L.; Gougeon, P. *Acta Cryst.* **1993**, *C49*, 1580.

33. Leligny, H.; Ledesert, M.; Labbe, Ph.; Raveau, B.; McCarroll, W. H. *J. of Solid State Chem.* **1990**, *87*, 35.

34. Gougeon, P.; McCarley, R. E. *Acta Cryst.* **1991**, *C47*, 241.

35. Ramanujachary, K. V.; Jones, E. B.; Greenblatt, M.; McCarroll, W. H. *J. Solid State Chem.* **1995**, *117*, 261.

36. Carlson, C. D. *Ph. D. Dissertation*, Iowa State University, **1989**.

37. Kerihuel, G.; Gougeon, P. *Acta Cryst.* **1995**, *C51*, 787.

38. Kerihuel, G.; Gougeon, P. *Acta Cryst.* **1995**, *C51*, 1475.

ACKNOWLEDGMENTS

I would like to express my sincere appreciation and thanks to Dr. Robert E. McCarley for his guidance and instruction during my graduate years at Iowa State University. Our discussions were always fruitful and motivating. His encouragement and patience helped me to overcome many difficult times in the past five years. Thanks, Doc.

I would also like to thank the past and present members of the McCarley group (George L. Schimek, Xiaobing Xie, and Cahit J. Eylem). Special appreciation goes to Shane J. Hilsenbeck for his generous assistance in many ways.

This research would not have been possible without the aid of the following people and their expertise:

Dr. Robert Jacobson for X-ray crystallography

James Anderegg for X-ray photoelectron spectroscopy

Jerome Ostenson for magnetic susceptibility measurements

Dr. Gordon Miller for EHMO calculations

I would like to thank my family for the support and love they have shown me through telephone and letters from thousands miles away at the other part of the earth. I would also like to thank the many friends I have gained during these years in Ames.

You will always be in my thoughts and memories.

Finally, I am extremely grateful for the love and support of my beautiful wife, Songyan Deng. I will always remember her encouragement, patience and faith during our days in Ames.

This work was performed at the Ames Laboratory under Contract No. W-7405-Eng-82 with the U. S. Department of Energy. The United States government has assigned the DOE Report number IS-T 1829 to this thesis.